SYNTHESIS AND CHARACTERIZATION OF MANGANESE (IV) OXIDE – MULTIWALLED CARBON NANO TUBES (MWCNT) COMPOSITE VIA SOLID-STATE TECHNIQUE

VICNESWARAN ARUMUGAM

DISSERTATION SUBMITTED IN PARTIAL FULLFILMENT OF THE REQUIREMENTS FOR THE DEGREE OF MASTER OF ENGINEERING

FACULTY OF ENGINEERING

UNIVERSITY OF MALAYA

KUALA LUMPUR

2013

UNIVERSITY OF MALAYA

ORIGINAL LITERARY WORK DECLARATION

Name of candidate: VICNESWARAN ARUMUGAM

Registration / Matric No: KGH 060007

Name of Degree: MASTER OF ENGINEERING

Title of Dissertation ("this Work"):

SYNTHESIS AND CHARACTERIZATION OF MANGANESE (IV) OXIDE – MULTIWALLED CARBON NANO TUBES (MWCNT) COMPOSITE VIA SOLID-STATE TECHNIQUE

Field of Study: NANOMATERIAL COMPOSITE

I do solemnly and sincerely declare that:
(1) I am the sole author / writer of this work;
(2) This work is original;
(3) Any use of any work in which copyright exists was done by way of fair dealing and for permitted purposes and any excerpt or extract from, or reference to or reproduction of any copyright work has been disclosed expressly and sufficiently and the title of the work and its authorship have been acknowledged in this work;
(4) I do not have any actual knowledge nor do I ought reasonably to know that the making of this work constitutes an infringement of any copyright work;
(5) I hereby assign all and every rights in the copyright to this work to the University of Malaya ("UM"), who henceforth shall be owner of the copyright in this work and that any reproduction or use in any form or by any means whatsoever is prohibited without the written consent of the UM having been first had and obtained;
(6) I am fully aware that if in the course of making this work I have infringed any Copyright whether intentionally or otherwise, I may be subject to legal action or any other action as may be determined by UM.

Candidate's Signature: **Date:**

Subscribed and solemnly declared before;

Witness's Signature: **Date:**

Name:

Designation:

ABSTRACT

In this study, γ-MnO$_2$ (Manganese (IV) Oxide), was hydro thermally synthesized with multi-walled carbon nano tubes (MWCNT) in various mole fractions via solid state technique.

FESEM and TEM studies show that the MnO$_2$ layer has covered the surface of the MWCNT while retaining the original structure of the MWCNT during the triturate process. In TEM, the diameter of the MWCNT was found varied from 8 nm to 40 nm. The MWCNT / MnO$_2$ composite diameter however, varied from 30 nm to 120 nm. In XRD analysis based on Sherrer's calculation, higher mole fraction of MnO$_2$ in the composite increases the crystallite size of MnO$_2$ from 60.71 nm to 91.07 nm. The presence of MnO$_2$ was observed at four distinct peaks (angle 2θ = 28.5^o, 37.2^o, 56.5^o and 59.7^o) at planes (110), (101), (211) and (220) respectively. MWCNTs were observed at angle 2θ = 25.8^o and 43°, at planes (002) and (100) respectively. The EDX study shows the presence of Mn, O, C in the composite with various weight percentage due to the difference in the composite composition. The impurities such as Al, Si and Fe were found, with less than 5 wt.%. TGA / DTG study shows the thermal stability of the composite increases with higher presence of MnO$_2$. This condition prevents the composite from being easily oxidized and loses weight at higher temperatures. The highest weight loss of the composite was calculated at 45% and the lowest weight loss was calculated at 13 % from the initial weight of the composite. The presence of MnO$_2$ layer over MWCNT has proven to reduce the oxidization of MWCNT. Thus, MnO$_2$ increases the thermal stability of the MWCNT in this composite.

ABSTRAK

Dalam kajian ini, γ-MnO$_2$ (Mangan (IV) Oksida) telah disintesis menerusi kaedah hydrotermal dengan tiub karbon nano berdinding multi (MWCNT) dalam komposisi mol yang berbeza menerusi kaedah keadaan pepejal.

Penelitian menerusi FESEM and TEM memunjukkan lapisan MnO$_2$ telah menyelaputi MWCNT tanpa mengubah struktur asal karbon tersebut semasa process pengilingan. Hasil penelitian menerusi TEM menunjukkan diameter MWCNT didapati berada di antara 8 nm hingga 40 nm. Komposit MWCNT / MnO$_2$ pula menunjukkan saiz di antara 30 nm dan 120 nm. Hasil daripada analisis XRD menerusi kiraan Sherrer's pula, saiz kristalogi komposit yang mengandungi kandungan MnO$_2$ yang tertinggi didapati berada dalam lingkungan 60.71 nm hingga 91.07 nm. Kehadiran MnO$_2$ telah dibukti menerusi kehadiran empat puncak yang jelas pada sudut 2θ = 28.5^o, 37.2^o, 56.5^o and 59.7^o, pada lapisan kristalogi (110), (101), (211) dan (220). MWCNT pula menunjukkan puncaknya pada sudut 2θ = 25.8^o and 43°, pada lapisan kristalogi (002) dan (100). Kehadiran Mn, O dan C dalam komposit didapati dalam peratusan yang berbeza diantara sampel disebabkan oleh perbezaan komposisi bahan dalam komposit. Selain itu, bahan asing lain seperti Al, Si and Fe juga ditemui dalam kuantiti yang kurang daripada 5% daripada berat sampel tersebut. Kajian menerusi TGA / DTG pula menunjukkan kestabilan terma yang semakin meningkat bagi komposit yang mengandungi lebih banyak kandungan MnO$_2$. Sampel yang mengandungi lebih banyak MWCNT pula menunjukkan peratus kehilangan berat yang tertinggi, iaitu 45%, di mana, sampel yang mengandungi lebih banyak MnO$_2$ pula menunjukkan peratus kehilangan berat terendah, pada 13% sahaja. Kehadiran lapisan MnO$_2$ pada permukaan MWCNT mengurangkan kadar pengoksidaan permukaan MWCNT dan terbukti dapat meningkatkan kestabilan terma komposit MWCNT / MnO$_2$.

ACKNOWLEDGEMENT

First and foremost, I would like to express my sincere gratitude to my advisor Prof. Dr. Rafie Johan, for the outstanding support of my M.Eng dissertation, for his patience, motivation, enthusiasm, and immense knowledge in the field. His guidance helped me in all the time of research and writing of this thesis. I could not have imagined having a better advisor and mentor for my M.Eng study.

Besides my advisor, I would like to thank my wife, Ms. Subashini Supramaniam, who is a candidate for the M.Eng program as well in UM, for giving me the motivation and aspiration to further and complete my studies in engineering. Not forgetting, our son, Thevesh, has been my backbone of motivating for the successful completion of my work.

My sincere thanks also goes to my mother, Madam Gowri Sankar, my late father, Mr. Arumugam Govindasamy, my in laws, Mr. & Mrs. Pon. Supramaniam and my siblings for supporting me spiritually and blessing me for continuous success in my studies.

Last but not least, I would like to thank the rest of the team, the lab technicians, my lab mates in the University Malaya and my fellow friends for guiding and supporting me throughout my research. I would also like to forward my special thanks to the UM board for granting me semester exemptions a couple of times during the course, as I lost my dad during this precious period, which has placed me in a difficult position. Their kind understanding and support has guided me to pull through the hardship.

TABLE OF CONTENTS

LIST OF FIGURES

LIST OF TABLES

LIST OF SYMBOLS

GPa	Giga Pascal
Θ	Bragg angle
N	number of crystallites
η	number of point reflections
β	half-width of the broadened line
λ	wavelength
δ	disorientation angle
E	Young's modulus
μ	Poisson's ratio
A	weighted mean atomic weight
r	distance
v	frequency
k	wave vector of elastic
T_c	polymer's crystallization temperature
T_m	melting point
ε	the wavelength-dependent molar absorptivity coefficient
b	path length
c	velocity of light in a vacuum
Å	Angstrom
R	reflection
n_f	refractive index
h	Planck's constant
ν	frequency
E	electronic energy

LIST OF ABBREVIATIONS

MnO_2 Manganese (IV) Oxide / Manganese Dioxide

SWCNT   Single walled carbon nano tubes

MWCNT   Multi walled carbon nano tubes

IS   Impedance Spectroscopy

TGA   Thermogravimetry analysis

XRD   X-Ray Diffraction

EDX   Energy Dispersive X-ray Spectroscopy (EDX)

UV-Vis   UV – Visible Spectrophotometer

FESEM   Field Emission – Scanning Electron Microscope

SEM   Scanning Electron Microscope

TEM   Transmission electron microscope

CNTs   Carbon nanotubes

nm   Nanometers

A   Absorbance

wt%   Weight percentage

CHAPTER ONE

INTRODUCTION

1.1   Background

Nano composites in mechanical terms are different from conventional composite materials. It is a multiphase solid material where one of the phases has one, two or three dimensions of less than 100 nanometers (nm), or structures having nano-scale repeat distances between the different phases which constitute the nano composite material (Ajayan *et al*, 2003). This gives nano composites exceptionally high surface area to volume ratio of the reinforcing phase and / or high aspect ratio.

The reinforcing geometry can be made up as in the form of particles (eg. minerals such as Mn, Zn,), fibers (eg. carbon nano tubes) or sheets (eg. exfoliated clay stacks). The matrix material properties are significantly affected in the vicinity of the reinforcement. This large amount of reinforcement surface area means that a relatively small amount of nano scale reinforcement can have an observable effect on the macro scale properties of the nano composite. For example, adding carbon nanotubes are dramatically increases the electrical capacitance, conductivity and thermal conductivity of certain composites (Jun, 2009). This approach, yields other possibilities on application of multiwall carbon nanotubes (MWCNT) / manganese dioxide (MnO_2) as supercapacitors (Jun, 2009) and superconductors (Wei, 2010). Similarly, other kinds of nano particulates may result in enhanced optical properties, dielectric properties, heat resistance or mechanical properties such as stiffness, strength and resistance to wear and damage. In general, the nano reinforcement is dispersed into the matrix during processing. The percentage by weight (called mass fraction) of the nano particulates introduced can remain very low (on the order of 0.5% to 5%) due to the low filler percolation threshold, especially for the most commonly used non-spherical, high

aspect ratio fillers (e.g. nanometer-thin platelets, such as clays, or nanometer-diameter cylinders, such as carbon nanotubes).

Manganese (IV) oxide (MnO_2) also known as manganese dioxide, is the inorganic compound with the formula MnO_2 from rutile mineral group. The low cost and naturally abundance of MnO_2, coupled with the environment friendliness, with potentially as good super capacitance and conductor when mixed with other elements has made it a very promising material used as a composite material.

Multi walled carbon nano tubes (MWCNT) was discovered by Iijima in 1991(Iijima, 1991). Since then, carbon nano tubes attracted much attention of many world class researchers. CNTs can be conceptualized as seamless hollow tubes rolled up from two-dimensional graphene sheets with diameters in the nanometer range of 2 nm – 20 nm and lengths usually on the micron scale (Iijima, 1991). Depending on the number of tube walls, CNTs can be classified into single-walled carbon nanotubes (SWCNTs) and MWCNTs.

In this study, different mole fractions of MWCNT and MnO_2 were triturated @ solid state technique, to produce nano composite and were characterized via FESEM, EDX, TEM, XRD and TGA. Their interesting mechanical and thermal properties were studied to co-relate to their current applications in nano electronics and nano composites (Kilbride *et al*., 2002; Poncharal, 1999; Baughman *et al*., 2002). The MWCNT / MnO_2 composites have been used as supercapacitors and are known to have increased electrical conductivity of MnO_2 (Jun, 2009).

1.2 Important Research Problem

The main objective of this study is to produce MWCNT / MnO_2 nano composites via solid technique (trituration process). Currently, many other techniques such as physical mixing (Pinero, 2005), thermal decomposition (Fan, 2006), ball milling (Zhou, 2006), electro-deposition (Lee, 2005), sonochemical synthesis (Kawaoka, 2004), sol–gel (Hibino, 2004) and redox reaction (Wu, 2004) are utilized for the production of such composites.

There are advantages and disadvantages among the processes for the mass production of MWCNT / MnO_2. Among the major problem commonly faced by these production methods are the higher production costs and quality of the nano composites produced. Although the requirement for the deposition of MnO_2 on MWCNT may defer for based on specific application, simple process such as trituration may be used for specific thermal stability properties, which is proven via this method. It is observed that the thermal stability of the MWCNT / MnO_2 composite increases with the addition of more mole fraction of MnO_2. The TGA results shows only 8% weight loss for the composite with higher MnO_2 content with lesser MWCNT. This reveals a potential application of these composite as a protection layer from oxidization.

This research can be taken to another step to study the electrical properties of the composites for potential use as super capacitors / super conductance application (Juan, 2006). This will further strengthen this research for a low cost production of MWCNT / MnO_2 nano composite for various applications.

1.3   Research Objectives

The objectives of this research are as mention below:

1. To produce MWCNT / MnO_2 nano composite via solid state technique.

2. To investigate the mechanical and thermal effect of various mole fraction of MWCNT / MnO_2 composite.

3. To proceeds with the characterization study of the MWCNT / MnO_2 composite using analytical methods such as FESEM, EDX, TEM, XRD and TGA.

1.4   Scope of thesis

Chapter one

Chapter one gives a general introduction as well as the aim of this study. It also described the research objectives and the scope of the thesis.

Chapter Two

Chapter two will be focused on literature review, which gives a detailed overlook on the area of study, previous works, methodology, results and applications, which will be the fundamentals of this research.

Chapter Three

Chapter three will be focused on the methodology of the research for characterization, analytical tools / equipment and materials used to carry out the analysis.

Chapter Four

Chapter four presents the results of the analysis and the discussion on the results obtained.

Chapter Five

Chapter Five gives the conclusion based on the outcome gained and some recommendation for future studies.

CHAPTER TWO

LITERATURE REVIEW

2.1 Composite

Composite materials are in general referred to a combination of two or more constituent materials, either naturally occurring or engineered through research, with significantly different in chemical and physical properties, to produce composite material with properties that cannot be achieved by any of the components acting alone. The composition however will have a distinct interface separating the components at the macroscopic and microscopic level, within the finished structure.

Composites however, not new for human kind as the earliest signs of composites were found dated back to 6000 B.C. "*Wattle*" and "*Daub*" is some of the earliest known composites which were used as a construction material for house in Central Europe (Pritchett, 2001) "*Wattle*" is a woven lattice of wooden strips and "*Daub*" is a sticky material usually made of clay, soil, sand, straw or animal dung. It is still an important construction material in many parts of the world, as it is a low impact sustainable building technique in modern cities and also for the restoration of historical buildings.

A simple scheme for the classification of composite materials is shown in Figure 2.1. There are typically three main divisions; particle reinforced, fiber reinforced and structural composites. Particle reinforced composites are divided into two subcategories; large particle and dispersion strengthened composites. The distinction between these is based upon reinforcement mechanism. The term 'large' is used to indicate the particle − matrix interactions which cannot be treated at atomic or

molecular level. Concrete is an example of large particle composite, being composed of cement (as matrix), sand and gravel (the particulates). Dispersion strengthened composites is referring to hardening of metal or metal alloys by uniform dispersion of several volume percent of fine particles which is normally the oxide materials. The dispersed phase may be metallic or non-metallic. A typical example of such reinforcement is the addition of 3 vol% of thoria (ThO_2) to nickel alloys to significantly increase the high temperature strength (William, 1994).
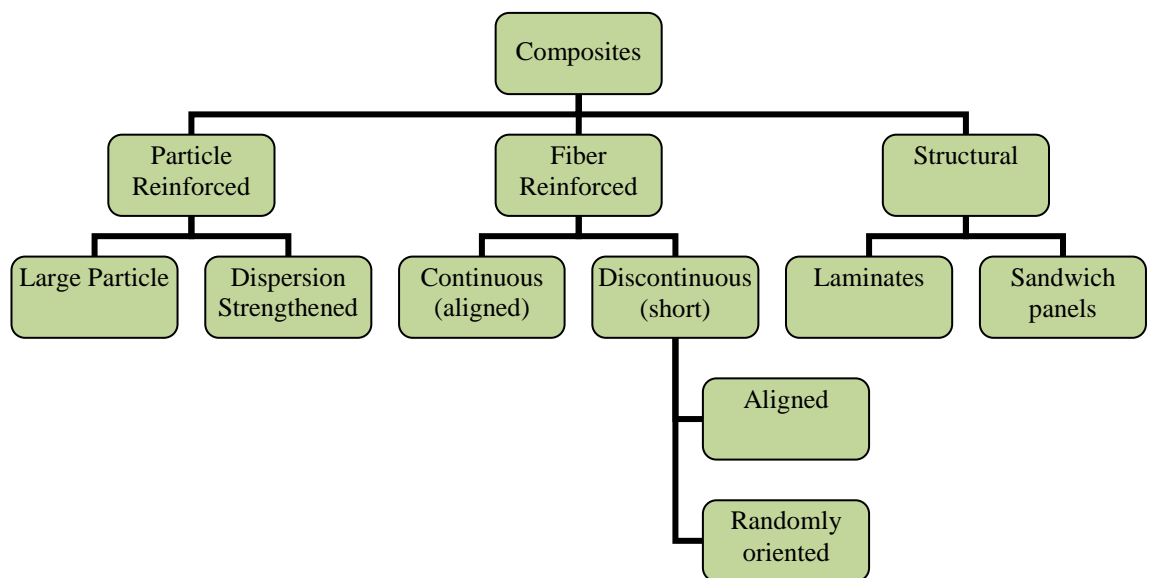
Figure 2.1: Classification of composite material (William, 1994)

Fiber reinforced composites are the most technologically important composite as it dispersed phase is in the form of fiber. Normally, these types of composites have high strength or / and stiffness. The orientation and the length of the fiber however have influence on the properties of the composites formed. Shorter fiber reinforced composites in general does not produce a significant improvement in strength. Fiber reinforced composites can be divided into two sub categories, such as continuous (aligned) and discontinuous (short). The continuous fiber composites reflect better reinforcement efficiency and properties compared to discontinuous composites. The

discontinuous randomly oriented reinforced composites can be categories into fiber-glass reinforced composites, fiber reinforced plastic matrix composites, metal matrix – fiber composites and hybrid composites. Fiber-glass composites consist of glass fibers normally contained in a plastic matrix. The glass fibers are chosen as they are economical to make and easily drawn into high strength fibers from molten state. The typical example of fiber glass reinforced composite used in wind turbine is shown below (Figure 2.2).

Figure 2.2: Fibre-glass reinforced wind turbine blades (Nano, 2012)

Structural composites are normally composed of both homogenous and composite material which the properties depends on the constituent materials as well as the geometrical designs of the various structural elements. There are two types of commonly found structural composites in the market, which is laminar composite and sandwich panel. Typical examples of sandwich panel are including roofs, floors, building walls and also on air craft body. Figure 2.3 illustrate the honeycomb sandwich panel.
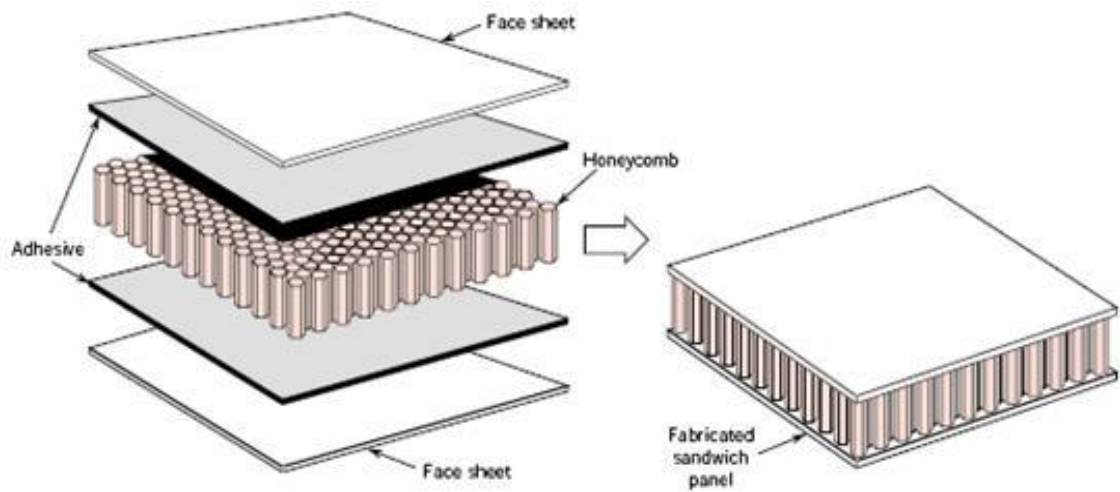
Figure 2.3: Typical honeycomb composite layout

(Donald, 2003)

Modern day composites are used widely in high performance and extreme environment such as automobile, aerospace and military applications. Ceramics for example, are widely used by high performance carmakers for the fabrication of ceramic-coated brake pads to withstand high temperatures for high speed braking. Similarly, some of the parts exposed to high temperatures, such as the windscreens and missiles are also coated with ceramics and contribute further to aerospace and military industries. Household items are not an exception from composites. Bathtub, which is made of reinforced fiberglass, is a type of composite as well. Similarly, imitated granites, marble and sinks are also some other examples of composites. The availability of affordable composites in the market has become a perquisite in our lives. This has dramatically driven many researchers and scientists from various institutions to venture further into new composite materials to seek for advancement in this field. Some of the most talked about frontier, which promises new advancement in materials, are nano composite materials.

2.2 Nano composites

Nano composites in mechanical terms are different from conventional composite materials. The definition itself has broadened significantly to encompass a large variety of systems such as zero dimensional and one dimensional material such as (Mo_3Se_3-) n with chains and clusters, two-dimensional material such as clays or fibers such as carbon nano tubes (CNT) either as single walled carbon nano tubes (SWCNT) or multi walled carbon nano tubes (MWCNT), metal oxides such as MnO_2, metal phosphates, three-dimensional material such as zeolites and amorphous materials, made of distinctly dissimilar components and mixed at the nanometer scale. This creates exceptionally high surface area to volume ratio of the reinforcing phase and / or high aspect ratio. The matrix material properties are significantly affected in the vicinity of the reinforcement. This large amount of reinforcement surface area means that a relatively small amount of nano scale reinforcement can have an observable effect on the macro scale properties of the nano composite. For example, adding carbon nanotubes dramatically increases the electrical and thermal conductivity of a composite. Other kinds of nano particulates may result in enhanced optical properties, dielectric properties, heat resistance or mechanical properties such as stiffness, strength and resistance to wear and damage. In general, the nano reinforcement is dispersed into the matrix during processing. The percentage by weight (called mass fraction) of the nano particulates introduced can remain very low (on the order of 0.5% to 5%) due to the low filler percolation threshold, especially for the most commonly used non-spherical, high aspect ratio fillers (e.g. nanometer-thin platelets, such as clays, or nanometer-diameter cylinders, such as carbon nanotubes).

There are three types on matrix nano composites available. Firstly, it is the group of composites with ceramic being the main component, which is normally from

the oxides group such as oxides, nitrides, borides, silicides etc. with the second component being from metal group, such as Ni, Ru, Zn, etc. (Pirlot *et al*, 2002).

The second type of matrix nano composite is metal matrix nano composites. Metal matrix nano composites can be defined as reinforced metal matrix composites. This kind of composites can be classified as continuous and non-continuous reinforced materials. One of the important nano composites is a carbon nanotube metal matrix composite (CNT-MMC) which is emerging new materials that are being developed to take advantage of the high tensile strength and electrical conductivity of carbon nanotube materials. Critical to the realization of CNT-MMC possessing optimal properties in these areas are the development of synthetic techniques that are (a) economically producible, (b) provide for a homogeneous dispersion of nanotubes in the metallic matrix, and (c) lead to strong interfacial adhesion between the metallic matrix and the carbon nanotubes. In addition to carbon nanotube metal matrix composites, boron nitride reinforced metal matrix composites and carbon nitride metal matrix composites are the new research areas on metal matrix nano composites. The third kind of nano composite is the energetic nano composite, generally as a hybrid sol–gel with silica base, which, when combined with metal oxides and nano-scale aluminum powder, can form *s*uper thermite materials.

Experimental work has generally shown that virtually all types and classes of nano composite materials lead to new and improved properties when compared to their macro composite counterparts. Therefore, nano composites promise new applications in many fields such as mechanically reinforced lightweight components, non-linear optics, battery cathodes and ions, nano-wires, sensors, ultra / super capacitors, super conductors and other systems.

This rapidly expanding field is generating many exciting new materials with novel properties. The latter can derive by combining properties from the parent constituents into a single material. There is also the possibility of new properties which are unknown in the parent constituent materials. Multi walled carbon nano tubes (MWCNT) / MnO_2 nano composites are a good example of such interest.

2.2.1 Manganese (IV) Oxides

Manganese (IV) oxide (MnO_2) also known as manganese dioxide, is the inorganic compound with the formula MnO_2 from rutile mineral group. Normally, it is found together with Fe_2O_3 and Al_2O_3 and formed under highly oxidizing conditions in manganese-bearing hydrothermal deposits and rocks; in bogs and lakes, under shallow marine conditions; commonly an alteration product of manganite (Mineral, 2005). The low cost and naturally abundance of MnO_2, coupled with the environment friendliness, with potentially as good super capacitance and conductor when mixed with other elements has made it a very promising material used as a composite material. It is also one of the preferred composite materials due to its ion exchange, molecular adsorption, catalytic, electrochemical, and magnetic properties. It is widely used as catalysts and molecular-sieves and especially as electrode materials in Li/MnO_2 batteries because of its energetic compatibility in a reversible lithium electrochemical system.

It is in blackish brown in colour originated from mineral pyrolusite, as shown in Figure 2.4, is the main ore of manganese and a component of manganese nodules. It has specific gravity of 5.026 m/s^2 and melting point of 1539^oC. MnO_2 is insoluble in water and inert to most acids except when heated. The density of MnO_2 is 5.026 g/cm^3 and

molecular weight is 86.94 g/mole (Chandra, 1999). Figure 2.5 shows the molecule bonding of MnO_2 (O=Mn=O).

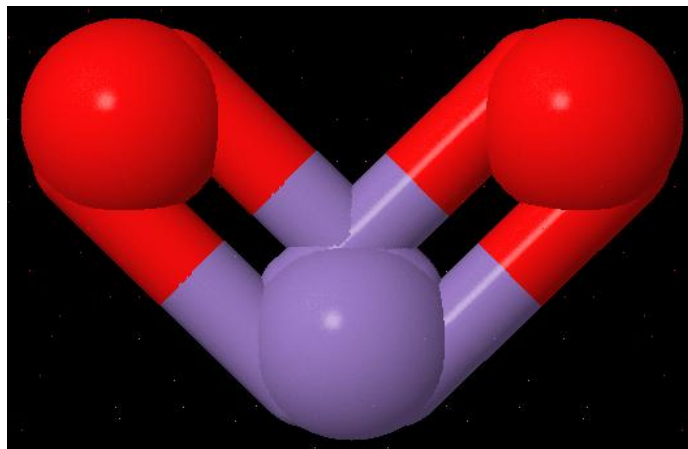Figure 2.4: Pyrolusite Mineral (Mineral, 2005)

Figure 2.5: MnO_2 molecular structure (Mineral, 2005).

2.2.1.1 Production method of Manganese (IV) Oxide

Hydrothermal method is a preferred method for the preparation of 'as-synthesized" Manganese (IV) Oxide (Yuan, 2003). This method is favorable for the preparation of low-dimensional nonstructural as it does not utilize any templates or catalysts during production. This method is superior to traditional methods since no specific and expensive equipment is required for synthesizing the nanostructured materials at lower temperatures. Various types of inorganic oxides have been synthesized with the aid of templates or catalysts to confine the growth of crystals, while catalysts may act as energetically favorable sites for the adsorption of reactant molecules.

However, the introduction of templates or catalysts to a reaction system has its draw backs. The impurities in the final product may be difficult to be removed, thereby making the overall synthesis process more complicates and costly (Pang, 2012). Some copolymer directing methods is found to be very expensive and it is tedious to remove the copolymer from the end product after synthesis. As such, MnO_2 hydrothermal treatment in water or ammonia solution at temperature 120–160 ℃ would be the most economical and simple method for the preparation of 'as-synthesized' MnO_2.

2.2.2   MWCNT - Multi walled carbon nano tubes

Iijima discovered multi walled carbon nano tubes (MWCNT) in carbon- soot made by an arc-discharge method in 1991 (Iijima, 1991). This was followed by the discovery of single walled carbon nano tubes in 1993 (Iijima, 1991). Since then, carbon nano tubes attracted much attention of many world class researchers. CNTs can be conceptualized as seamless hollow tubes rolled up from two-dimensional graphene

sheets with diameters in the nanometer range and lengths usually on the micron scale. Depending on the number of tube walls, CNTs can be classified into single-walled carbon nanotubes (SWCNTs) and MWCNTs. SWNTs are usually 1-2 nm in diameter and tens of microns in length. MWCNTs are made up of coaxial cylindrical carbon layers with an interlayer distance of 0.34 nm and a diameter typically on the order of 10-20 nm. Thus, the nano tube aspect ratio, or the length-to-diameter ratio, can be as high as 132,000,000:1, which is unequalled by any other material (Jun, 2009). They have amazing electronic and mechanical properties which lead to high strength and conductivity. Experimental and theoretical results have shown an elastic modulus of greater than 1 TPa (that of a diamond is 1.2 TPa) and have reported strengths 10-100 times higher than the strongest steel at a fraction of the weight. Also, the theoretical and experimental results show superior electrical properties of CNTs. They can produce electric current carrying capacity 1000 times higher than copper wires. Figure 2.6 shows the image of MWCNT.
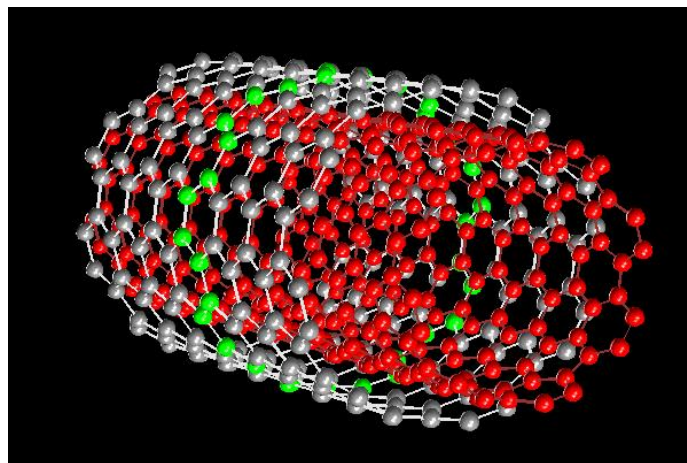

Figure 2.6: Multi walled carbon nano tubes (MWCNT) (Nano, 2012)

MWCNTs with their unique properties are leading to many promising applications. They can be used in the field of reinforcements in composites, sensors and probes, energy storage, electrochemical devices, nanometer sized electronics and so on (Ajayan, 1992). Various methods have been explored to synthesize MWCNTs. The first method for the synthesis of MWNTs was through arc growth (Iijima, 1991). Since then carbon nanotubes continue to draw much attention, several methods of producing carbon nanotubes have been reported. Among these methods, chemical vapor deposition (CVD) can achieve a controllable route for the selective production of nanotubes with defined properties (Huang, 1998). The thermal catalytic CVD is considered to be the best process for low cost and large-scale synthesis of high-quality carbon nanotubes, employing various hydrocarbons as carbon gaseous source. The growth mechanism of the CVD synthesis of carbon nanotubes involves decomposition of the carbon source, followed by dissolution of the carbon phase into metal catalytic nanoparticles and re-deposition of carbon on the catalyst surfaces. On the other hand, the laser ablation method is known to produce carbon nanotubes with the highest quality and high purity of single walls carbon nano tubes (SWCNT) (Daenen, 2003)

NANOSHEL™ is developing new methods, for rapidly testing bulk carbon nanotubes (CNTs) for chemical purity and homogeneity (Nanoshel, 2012) The different synthesis methods used to produce these materials create different mixtures of tube geometries, along with varying amounts of carbonaceous and metallic impurities. The CNTs manufactured by NANOSHEL™ are 98 percent pure because no catalyst is used while manufacturing.

2.2.2.1 Production methods of carbon nano tubes

The production of CNTs with high purity and uniformity, low cost, and at a large scale is still a major concern of the scientific community and the industry.

In 2006, the global production capacity of MWCNTs was higher than 300 tonnes (Bierdel, 2007). The Bayer Company, for instance, was operating with a nominal production capacity of 60 ton/year in 2007. In 2010, Bayer has opened the largest carbon nanotube facility in the world, increased annual capacity to 200 tonnes. The 2009 overall SWCNTs production was estimated in the hundreds of kilograms worldwide, with a production rate that could reach 50 g/h (Bierdel, 2007).

The expectation for the next 5-10 years is that the demand for CNTs will grow steadily, as long as cost/quality, purity and production yield issues are overcome. The cost of carbon nanotubes has been changing considerably in the past few years, being dependent on their purity and type as well as the supplier. The MWCNTs cost is usually between US$ 0.5-100/g, while DWCNTs can be obtained for around US$ 10/g. The cost of SWCNTs also varies a lot, usually between US$ 20-2000/g. Some of the most important methods for producing CNTs and some of the benefits and drawbacks of these processes are discussed as below (Bierdel, 2007).

a) **Arc Discharge**

Arc discharge was the method used by Iijima in 1991 to prepare MWCNTs (Iijima, 1991). In this method, DC arc plasma is generated between two carbon electrodes under an inert atmosphere, as depicted in Figure 2.7. As the anode is consumed, a soft fibrous deposit containing carbon nanotubes and other carbon particles is formed on the cathode (Journet, 1998).

To achieve SWCNTs, the electrodes are doped with a suitable catalyst, such as Ni-Co, Co-Y or Ni-Y (Saito, 1996). The tubes produced by this method are usually tangled and of varied length and diameter. However, the CNTs are of high quality, with low incidence of defects.
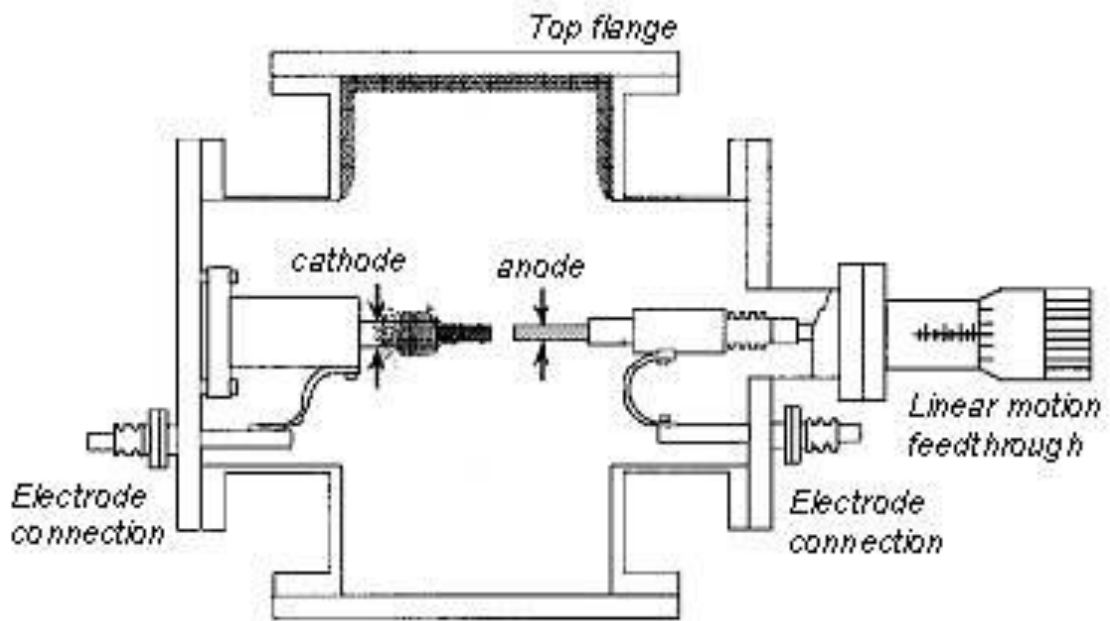

Figure 2.7: Schematic illustration of the arc-discharge method (Roch, 2007)

b) Laser Ablation / Pulsed Laser Vaporization

Laser ablation was first used for the synthesis of fullerenes (Journet, 1997). In this method, a graphite target is vaporized by laser irradiation under flowing inert atmosphere at temperatures near 1200 ^{o}C (Journet, 1997), as shown in Figure 2.8. The laser vaporization produces carbon species, which are swept by the owing gas and accumulate on a water-cooled collector (Guo, 1995). SWCNTs remarkably uniform in diameter can be produced when the graphite target is doped with a small amount of transition metals such Ni and Co.
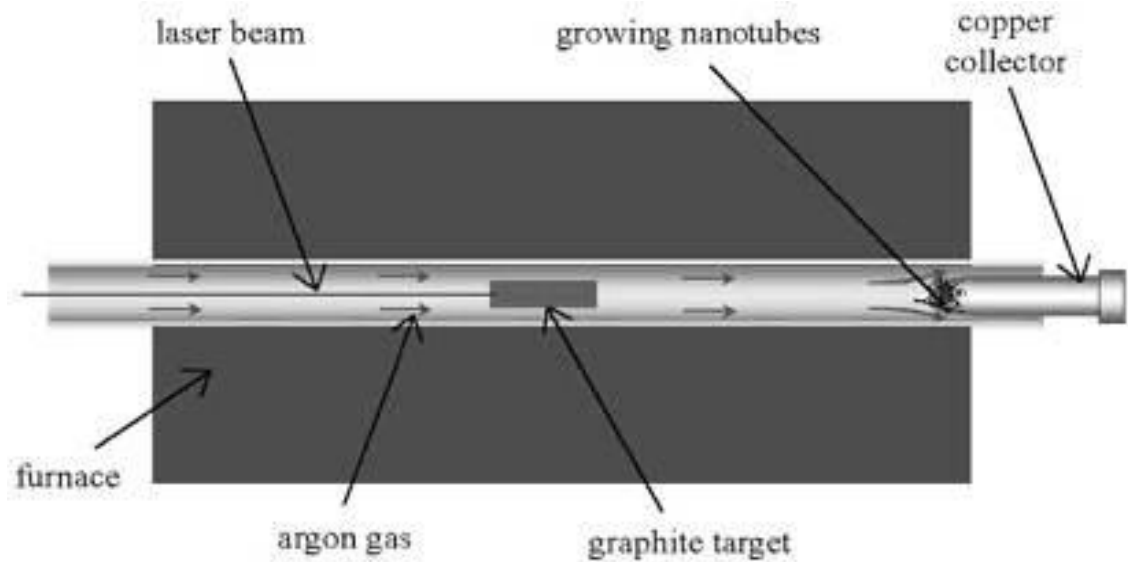
Figure 2.8: Schematics of the laser ablation method (Thostenson, 2001)

c) **Chemical Vapor Deposition (CVD)**

Chemical vapor deposition (CVD) has been used to produce carbon filaments and fibers since the 1960s (Xie, 2000). In this method, a carbon-containing gas is decomposed on a substrate in the presence of catalyst metal particles at high temperatures (600 ^{o}C or higher) (Xie, 2000), as illustrated in Figure 2.9. The lower temperatures used in this method reduce production costs. In addition, the deposition of catalysts on the substrate allows the formation of novel structures. However, CNTs made by this method generally have a very large amount of defects (Lahi, 2006).
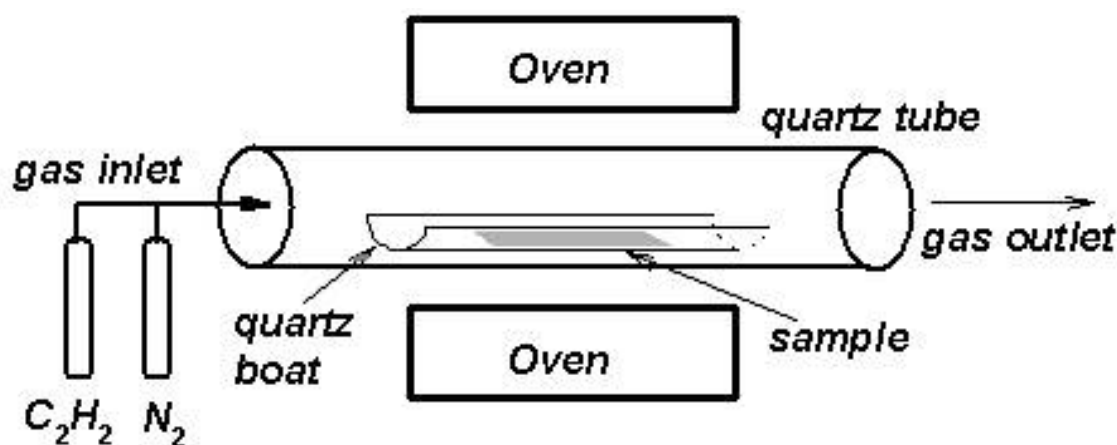
Figure 2.9: Schematics of the CVD apparatus (Xie, 2000)

d) High Pressure Conversion of Carbon Monoxide (HiPco)

The method called high pressure conversion of carbon monoxide (HiPco) is employed to produce SWCNTs by continuously flowing CO gas phase (i.e. the carbon feedstock) and Fe $(CO)_5$, the catalyst precursor (Daenen, 2003) through a heated reactor as shown in Figure 2.10. The average diameter of HiPco SWCNTs is approximately 1.1 nm and the yield reaches 70 % (Nikolaev, 1999). CNTs made by this method generally have an excellent structural integrity, although the production rates are still relatively low. The carbon nanotube production methods described above are the most often cited in the literature. Nevertheless, several adaptations of these methods and new tendencies in the production of carbon nanotubes are constantly emerging.
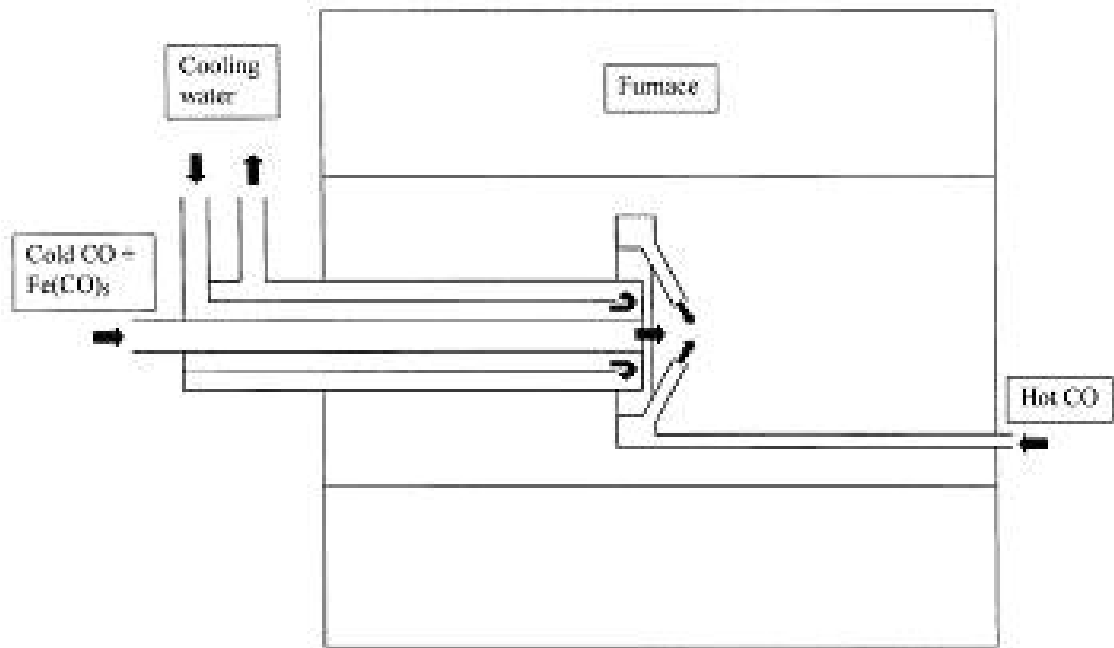
Figure 2.10: Layout of CO flow-tube reactor showing the water-cooled injector and the

`showerhead' mixer (Nikolaev, 1999)

2.3 Current researches on MnO$_2$ / MWCNT nano composites

Previous approaches to the synthesis of MnO$_2$ / carbon nano composite include various methods as physical mixing (Pinero, 2005), thermal decomposition (Fan, 2006), ball milling (Zhou, 2006), electro-deposition (Lee, 2005), sonochemical synthesis (Kawaoka, 2004), sol–gel (Hibino, 2004) and redox reaction (Wu, 2004).

2.3.1 Preparation of MnO$_2$ / MWCNT nano composites via chemical deposit process (redox reduction).

Currently, chemical route has been used widely used for the preparation of MnO$_2$ / MWCNT nano composites (Yuan, 2003). In this approach, the carbon nanotubes (CNTs) obtained either from the 3rd party supplier or thru the synthesis via CVD were purified in the solution of concentrated nitric acid to remove catalysts or templates. The purified CNTs which have been ultra-sonicated for 10 - 15 minutes in distilled water were added to the solution of KMnO$_4$ + nitric acid and placed in light-enough places for 3 h. CNTs were found to act as a reducing agent and substrate for the heterogeneous nucleation of MnO$_2$ in an aqueous KMnO4 solution. Finally, the solution was filtered and washed thoroughly with distilled water and dried at 100 - 150 ℃ in air (Xiangping, 2006). Typically, a layer of manganese dioxides (γ-MnO$_2$) was adsorbed upon carbon nanotubes (CNTs) surface by using the chemical deposit process (Xiangping, 2006). The SEM images as shown in Figure 2.11 (a) SEM images of (a) pristine CNT and MnO$_2$ / CNT nano composite prepared in the 200 ml aqueous solution of 0.1 M KMnO$_4$ containing 1.0 g CNT at 70^{0}C under (b) pH 7; (c) pH 2.5; (d) pH 1 of the initial solution (Sang, 2006).
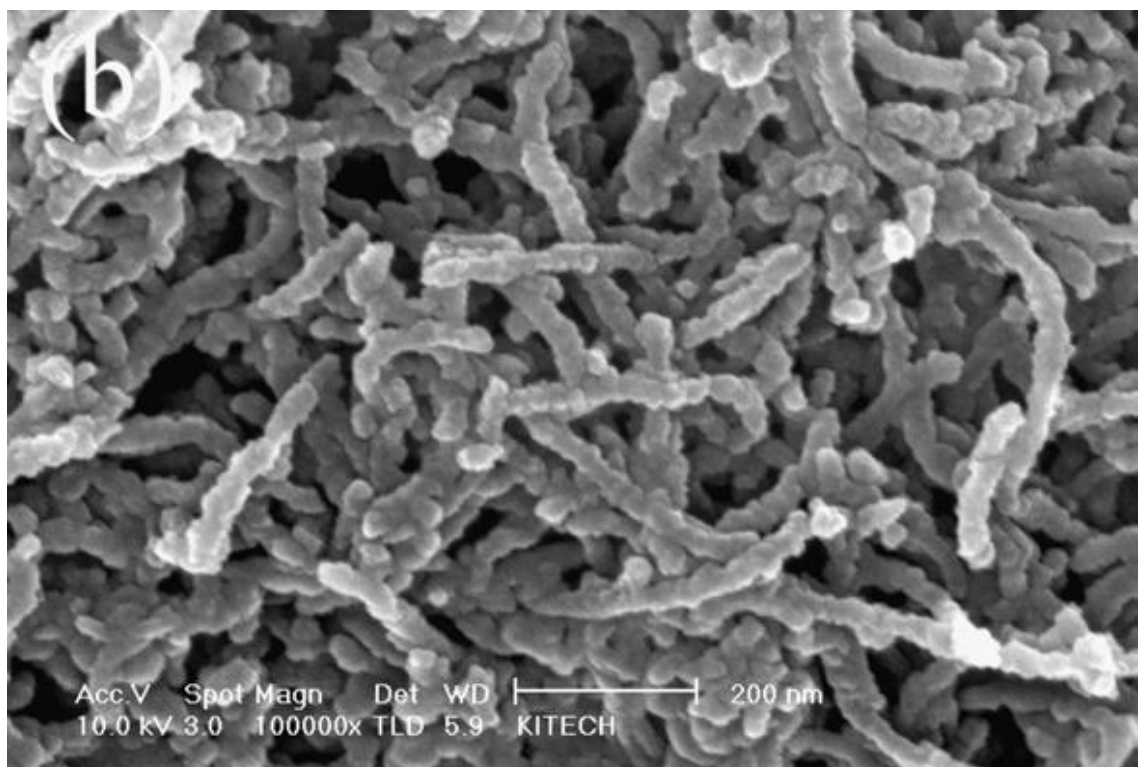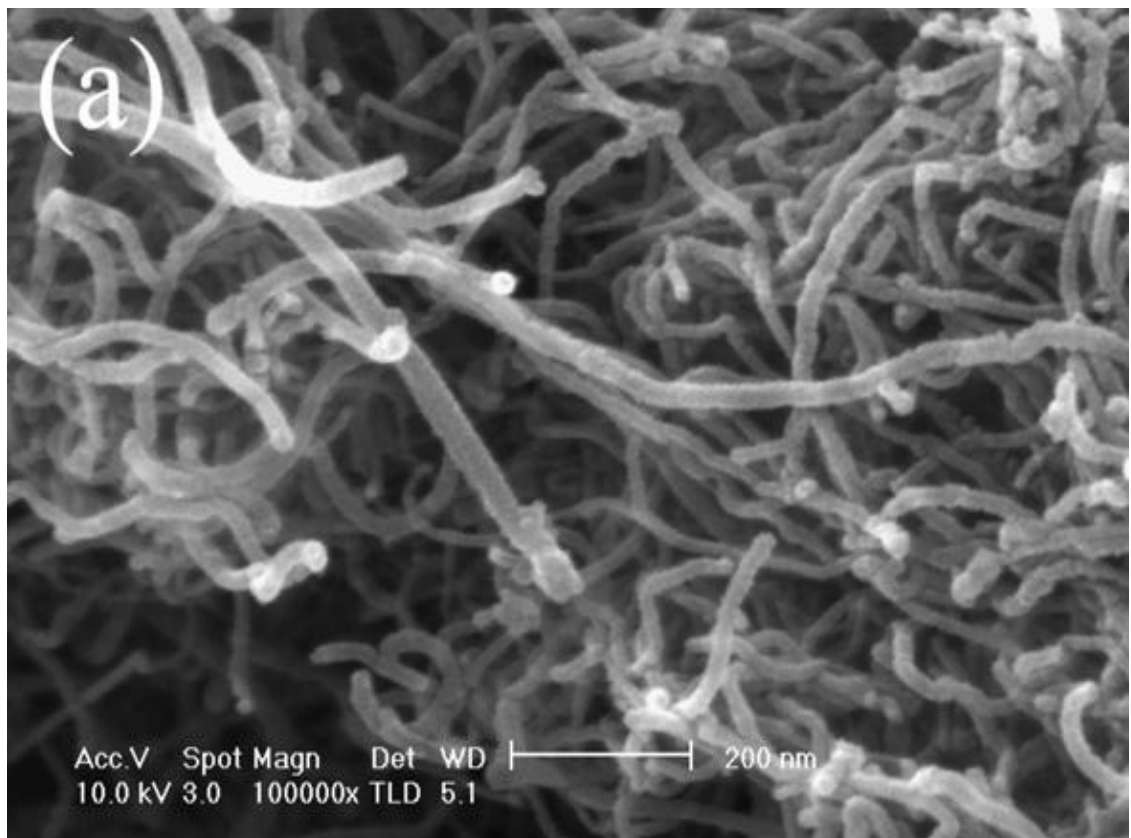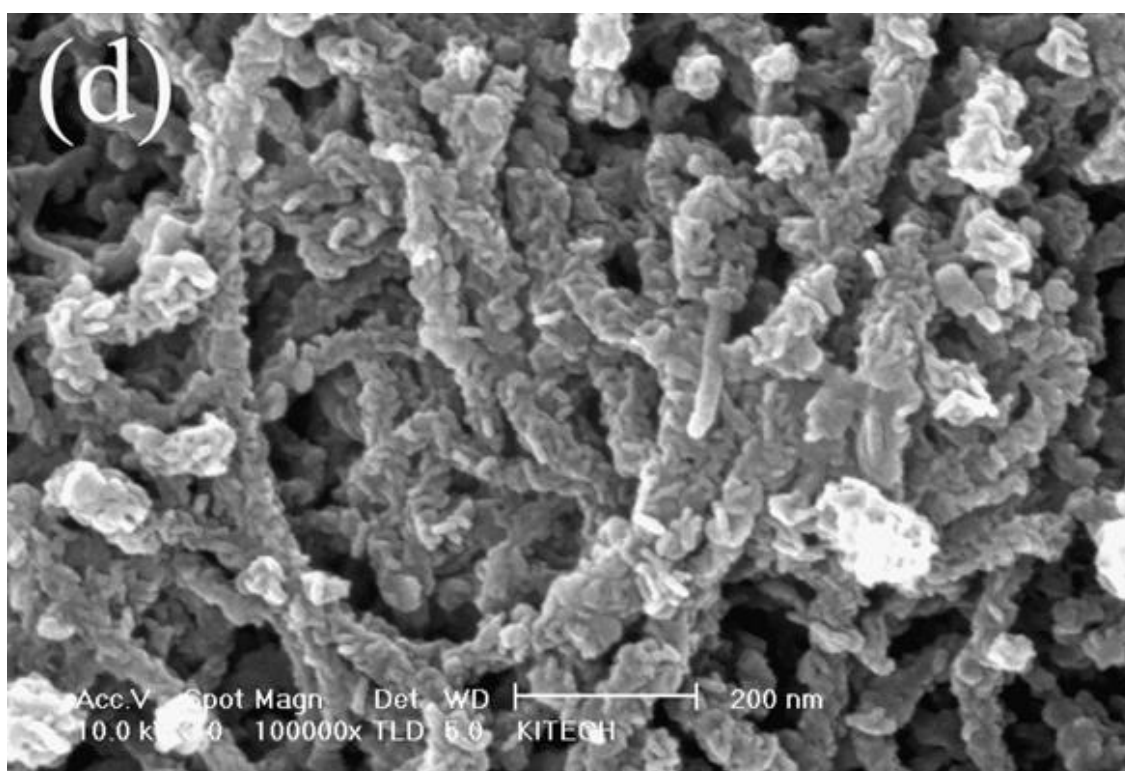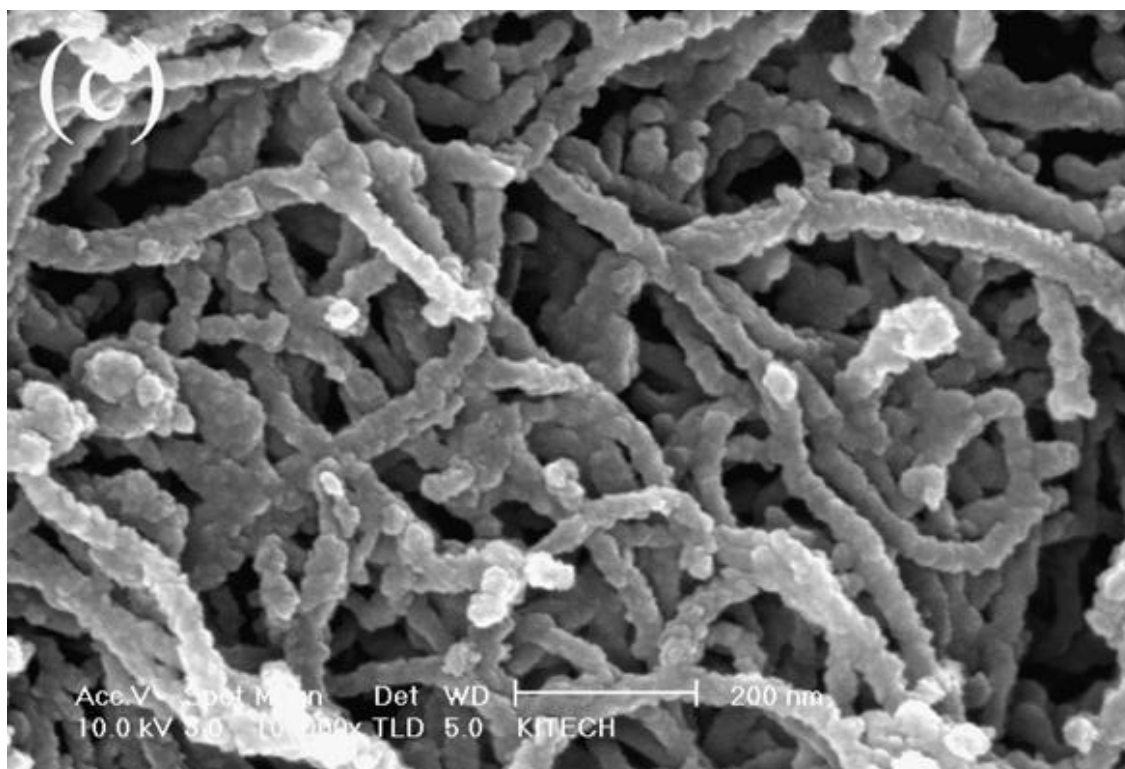
Figure 2.11: SEM images of (a) pristine CNT and MnO_2/CNT nano composite prepared

in the 200 ml aqueous solution of 0.1 M $KMnO_4$ containing 1.0 g CNT at 70^0C under

(b) pH 7; (c) pH 2.5; (d) pH 1 of the initial solution. (Sang, 2006)

Figure 2.12, shows the TEM morphologies of the coated CNTs composite with MnO_2. EDX chemical composition measurement reveals that the composite contains elements Mn and O (note: the other Cu-related peaks in the spectra came from the TEM Cu grids and the Al-related peaks from the Al sample pedestal), as shown in Figure 2.13, which implies that the nanoparticle is a kind of manganese oxide. It is expected that this γ-MnO_2 / CNTs composite will be applied to make supercapacitors (Xiangping, 2006).
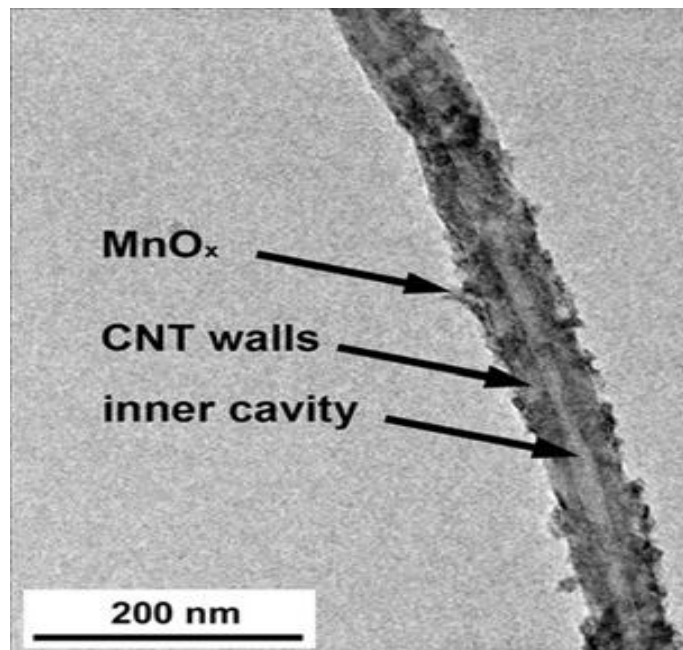
Figure 2.12: TEM image of CNT coated with MnO_2 (Minghao, 2012)
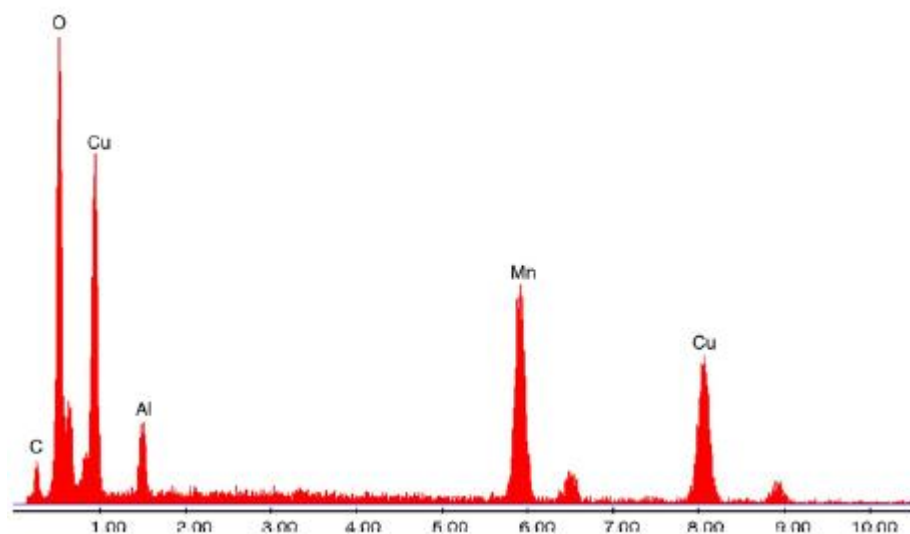
Figure 2.13: EDX image of CNT coated with MnO_2 (Sang, 2006)
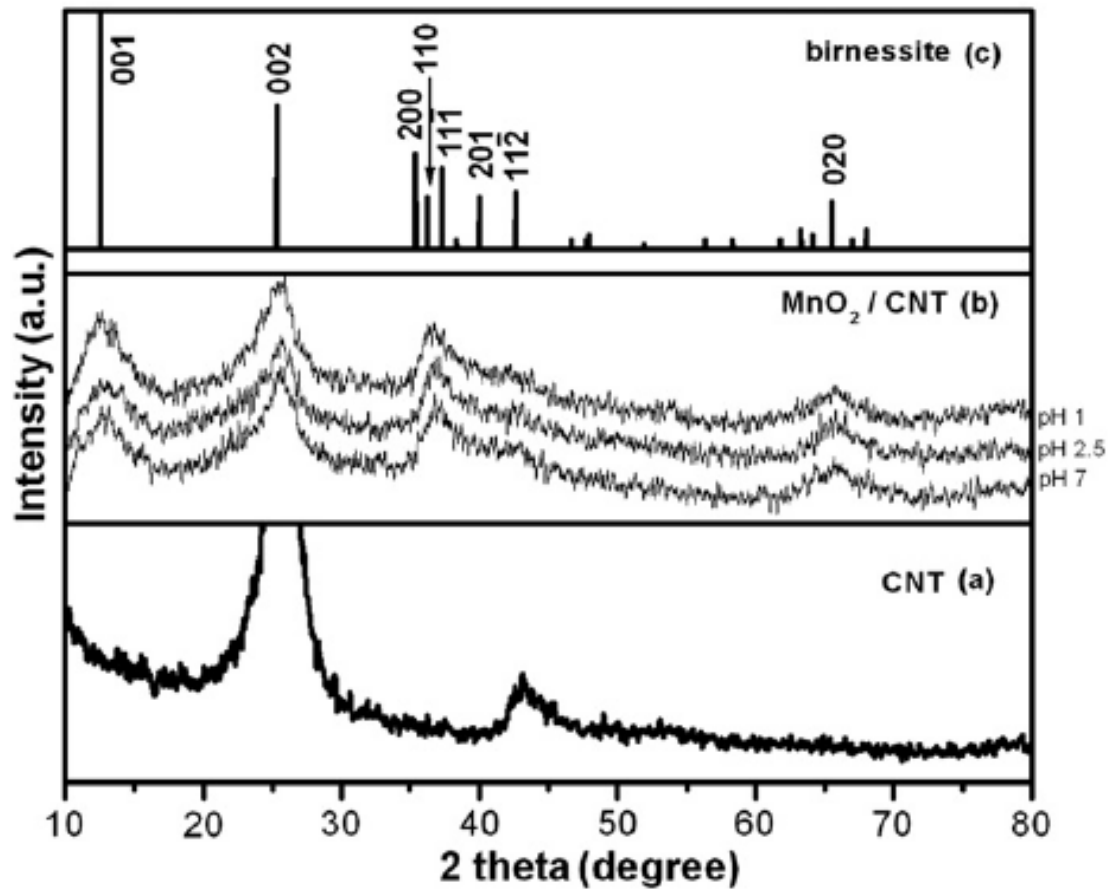
Figure 2.14: XRD image of (a) CNT (b) CNT coated with MnO_2 at different pH

(c) MnO_2 (Sang, 2006)

The XRD patterns for the (a) CNTs and for (b) MnO_2 on the CNTs and (c) MnO_2 are shown in Figure 2.14. Based on the XRD peaks of the reference oxide (JCPDS 42-1317), for birnessite-type MnO_2, there are three broad peaks at $2\theta = 28.5^o$, 37.2^o, and 56.5^o for planes (110), (101) and (211). These three peaks can be indexed to birnessite-type MnO_2 (Sang, 2006). For CNT, a sharp and a broad peak at angle of $2\theta = 25.8^o$ and 43° for planes (002) and (100), respectively (Huang, 2006).
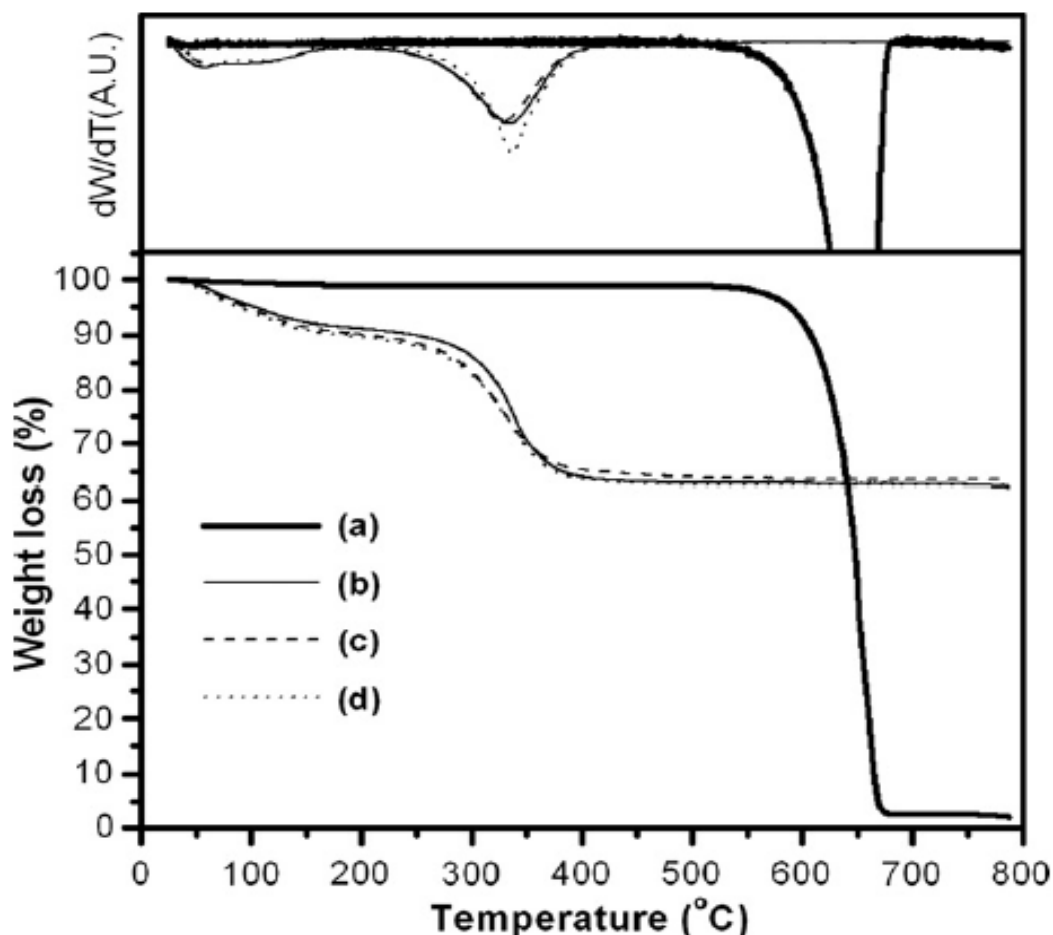
Figure 2.15: TGA / DTA image of (a) as-received CNT and MnO_2 / CNT nano composite synthesized by the reduction of MnO_4^- ions to MnO_2 in the 200 ml aqueous solution of 0.1M $KMnO_4$ containing 1.0 g CNT at 70 ^oC (b) pH 7; (c) pH 2.5; (d) pH 1 of the initial solution. (Sang, 2006)

Figure 2.15 shows the TGA and DTA results of MnO_2 / CNT nano composites. Two broad peaks were observed at temperatures near 100 and 340 ^oC. The 10% weight loss observed under 150 ^oC was mainly due to the liberation of adsorbed and interlayer water (Gaillot, 2005). This suggests that the MnO_2 spontaneously deposited on the CNTs is hydrous and that it is dehydrated when heated. The additional weight loss of 25% between 250 and 400 ^oC corresponds to the loss of oxygen atoms from the octahedral layer framework in relation to the partial reduction of Mn^{4+} to Mn^{3+} (Gaillot, 2005). CNTs are oxidized to CO_2 gas over 550 ^oC with a large amount of weight loss as

26

shown in Figure 2.15(a) (Kitiyanan, 2000). However, for MnO_2 coated CNT, weight loss of only 2% was observed over 400 ^{o}C, as shown in Figure 2.15(b)–(d). It can be inferred that a thin, uniform and continuous coating layer of MnO_2 might protect the CNTs against oxidation. A similar protection against oxygen and air oxidation by coating a thin, uniform and continuous carbide films has been reported for carbon fiber (Piquero, 1995). It is also found that the thermal stability of the CNTs, examined by thermo gravimetric analysis, was improved by the thin, uniform and continuous coating of MnO_2 over CNTs (Sang, 2006).

Both Manganese (IV) oxides and CNTs were the promising candidate electrode materials of electrochemical supercapacitors, it is therefore expected that the MnO_2 / CNTs composite can combine their excellent electricity properties for the future commercial applications. Further research is still in progress.

2.3.2 Preparation of MnO_2 / MWCNT nano composites via electro deposition with Ni Foam

Electro deposition techniques show unique principles and flexibility in the control of the structure and morphology of the film materials (Liang, 2010). Significant interests have been generated in application of electro deposition methods to fabricate MnOx / CNT composite electrodes (Zhang, 2008). To avoid the anodic oxidation and dissolution of the low-cost metallic current collectors and to offer the advantage of room-temperature processing, MnOx has been electro deposited cathodically on CNTs in $KMnO_4$ solution, through the following reaction (Dandan, 2011).

$$MnO^{-}_4 + 2H_2O + 3e^{-} = MnO_2 + 4OH^{-}$$
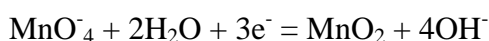
Nickel foam, a commercial material with high electronic conductivity, low weight, and 3D cross-linked grid structure providing high porosity and surface area, can be used as an ideal electrode substrate material (Li, 2008). In this work, MnOx has been potentiostatic cathodic electrodeposited onto the nickel foam–supported CNTs. Considering both the specific capacitance and the power capability, the MnOx/CNT/Ni-foam electrode with MnOx loading mass of 100 μg exhibits the excellent capacitive performance (Dandan, 2011).

2.3.3 Synthesis of MnO_2 / MWCNT nano composite via sonochemical method

Sonochemical technique was used to prepare nanostructured amorphous MnO_2 by reduction of potassium permanganate with manganese (II) acetate and adjusting the pH of the solution with ammonia hydroxide (Nam, 2010). Nanostructured MnO_2 had the flower-like shapes and nanowires by changing the pH in the aqueous solution. MnO_2 was synthesized by sonochemical methods wherein potassium permanganate and manganese (II) acetate are mixed. The preparation involves reduction of potassium permanganate with manganese acetate in a mole ratio of 2:3. The as-prepared potassium permanganate solution is then added drop-wise into the manganese acetate solution using a syringe pump and ammonium hydroxide was added in the same manner under ultrasound irradiation for 30 minutes. CNTs were added followed by ultra sonification for 30 minutes. The resulting dark precipitate was separated by decantation and washed several times with distilled water. It was subsequently dried at 40 ℃ under vacuum for 12 h. The samples shows higher specific capacitance compared to the parent composite material. This could be explained by the long chained nanowires that were thought to be providing pathways and facilitate diffusion of protons in the electrolyte, thus resulting in enhanced accessibility of ionic species to the active materials (Nam, 2010).

CHAPTER THREE

MATERIALS AND METHODOLOGY

3.1 Materials

In this study, the synthesized MnO_2 (Manganese (IV) oxide / Manganese Dioxide) was prepared by hydrothermal approach (Yuan, 2003). MnO_2 then triturated with the multi-walled carbon nano tubes (MWCNTs) at different mole ratio as shown in Table 3.3. The MWCNTs was procured from NANOSHEL® USA. The mechanical properties of MnO_2 are shown in Table 3.1 and for MWCNTs at Table 3.2.

Table 3.1: Mechanical properties of MnO_2

Type of Manganese	γ- MnO_2
Specific gravity (SG)	$5.026m/s^2$
Melting point	$1,539\ ^oC$
Density	$5.026g/cm^3$
Molecular weight	86.94g/mol
Colour	Black
Purity	80% - 85%

Table 3.2: Mechanical properties of MWCNTs

Type of MWCNT	M-SL-1, multi-walled carbon nano tubes
Purity	> 90% CNTs ; > 70% MWCNTs
Average diameter	4 – 12+ nm
Length	3 – 10 μm
Amorphous carbon	< 5% weight
Colour	Black

3.2 Apparatus used during sample preparation

List of lab apparatus used for the sample preparation are as below;

A) Beaker – 250 ml, 100 ml, 50 ml

B) Filtering funnel

C) Filtering paper – diameter 12 cm

D) Filtering flask – 100 ml

E) Volumetric Flask – 250 ml

F) Stirring rod

G) Mortar and pestle

H) Evaporating dish

I) Sample bottles – 20 ml & 100 ml

J) Spatula

K) Scalpel

3.3 List of consumables and safety equipment used for the sample preparation

A) Tissue papers

B) Aluminum foil

C) Clean cloths

D) Safety glasses (safety)

E) Lab coat (safety)

F) Rubber gloves (safety)

3.4 Sample preparation

Table 3.3 shows the calculated composite (MWCNT / MnO_2) weight using the following formula 3.1 and 3.2 as shown below:

1. The molecular weight of MnO_2 per mole is   : 86.94 g

2. The molecular weight of MWCNT per mole is   : 12.00 g

Applicable formula for weight calculation of MnO_2:

Weight (MnO_2) (g) = 86.94 (g/mole) X mole of required MnO_2 (mole) (3.1)

Example for MnO_2 calculation:

0.05 moles of MnO_2 = 0.05 moles x 86.94 g / mole = 4.35 g

Applicable formula for weight calculation of MWCNT:

Weight (MWCNT) (g) = 12.00 (g/mole) X mole of required MWCNT (mole) (3.2)

Example for MWCNT calculation:

0.45 moles of MWCNT = 0.45 moles x 12 g / mole = 5.40 g

Table 3.3: Samples with various mole ratio of MnO_2 / MWCNT

MWCNT (mol) \ MnO2 (mol)	0.05	0.1	0.15	0.2	0.25	0.3	0.35	0.4	0.45
0.05									S9
0.1								S8	
0.15							S7		
0.2						S6			
0.25					S5				
0.3				S4					
0.35			S3						
0.4		S2							
0.45	S1								

For preparation of sample S1, 0.45 moles of MWCNTs is blended with 0.05 mole of MnO_2 to prepare 0.5 moles of MWCNTs / MnO_2 composites. The calculation below shows how to determine the weight of the MnO_2 and MWCNT required in preparing 0.5 moles of composites in various MWCNTs and MnO_2 compositions.

Similar method is used to calculate the required weight for MWCNTs and MnO_2 for S2, S3, S4, S5, S6, S7, S8, S9, S10 and S11. Table 3.4 summarized the results.

Table 3.4: Samples weight as calculated.

Sample	S1	S2	S3	S4	S5	S6	S7	S8	S9	Total Weight (g)
Weight of MnO_2	4.35	8.69	13.04	17.39	21.74	26.08	30.43	34.78	39.12	195.62
Weight of MWCNT	5.40	4.80	4.20	3.60	3.00	2.40	1.80	1.20	0.60	27.00

For the MnO_2 sample preparation in large quantity (250 grams) as required for this study, γ- MnO_2 samples were divided into 50 grams in 5 x 250 ml beakers (B1, B2, B3, B4 and B5) and diluted with 50 ml of distilled water. The samples were stirred with magnetic stirrer for 15 – 20 minutes. Upon completion, the magnetic stirring rods were removed carefully and slightly rinsed with distilled water to remove the balance MnO_2 residue. The stirred MnO_2 samples are hydrothermally treated in the convection oven (OF-12) at 150°C for 24 hours. After 24 hours, the samples are carefully removed from the convection oven and cooled at room temperature, prior to wash with distilled water again. These samples are filtered into the 250 ml filtering flask. The samples are dried in the convection oven for 2 hours at 120°C. The samples are then collected in a clean dry bottle for further analysis.

Prior to testing, MWCNTs and MnO_2 need to be grinded together with mortar and pestle (solid state method) to form the composite. Each sample S1 – S9 are individually triturated for 15 – 20 minutes. The electronic balance is used to measure the required portions of MWCNTs and MnO_2 according to Table 3.4. Figure 3.1 shows the arrays of prepared samples.
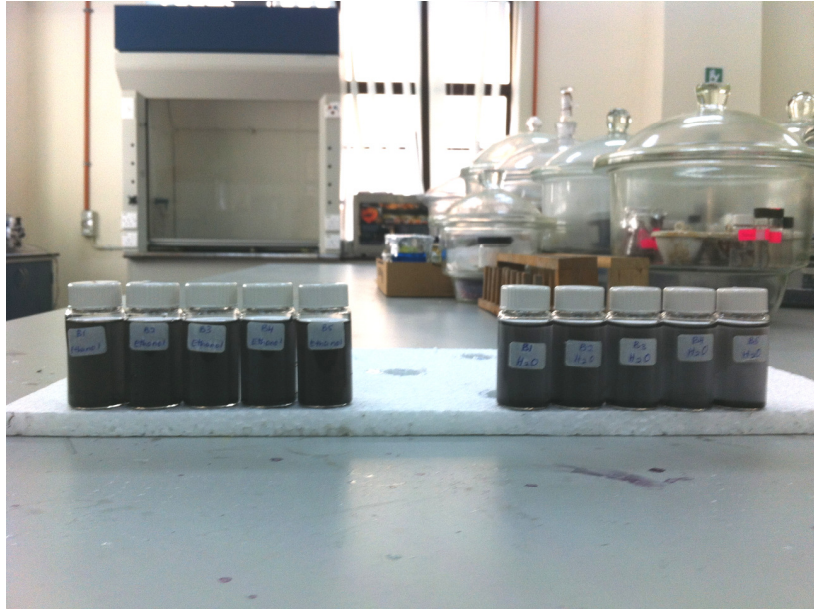
Figure 3.1: Prepared samples for testing

Sample S10 is used as a control for MnO_2 whereby, 0.2 mole or 17.39 grams of MnO_2 was used and stored in 100 ml sampling bottles. Similarly, S11 is the control sample for MWCNTs, whereby 1 mole or 12 grams of MWCNTs was used and stored in a 100 ml sampling bottle.

3.4 Characterization techniques

3.4.1 Surface analysis

3.4.1.1 Field Emission Scanning Electron Microscope (FESEM)

Prepared samples S1 – S11 are tested in FESEM Laboratory at the Engineering Faculty, UM. The detail of the FESEM is shown in Table 3.5. For the test preparation, the samples, less than 1 gram each, were placed on a metal base / pallet with carbon tape without any conducting coating. Each sample is visualized at the magnification of 5,000 X, 10,000 X, 20,000X and 40,000 X. The surface structure of each composite sample is studied to find the structural property of the composite formed via different mole fractions of MnO_2 and MWCNTs.

Table 3.5: Field Emission Scanning Electron Microscope (FESEM) / Energy Dispersive X-ray Spectroscopy (EDX)

Equipment	Model	Function	Pictures
FESEM / EDAX Location: FESEM Lab, Faculty of Engineering, UM	ZEISS AURIGA	To study surface structure and to identify element composition	

3.4.2 Energy Dispersive X-ray Spectroscopy (EDX)

3.4.2.1 Compositional analysis

EDX is used for elemental analysis of the nano composites. The detail of the equipment is shown in Table 3.5. Each sample from S1 – S11 is tested in two methods, which is via the area view, with the magnification from 5,000X to 10,000X and secondly via spot view with the magnification around 20,000X to 100,000X. The traced element recorded either from spot view or area view is recorded via the software EDAX TSL Microanalysis Solution for further discussion.

3.4.3 Transmission Electron Microscopy (TEM)

3.4.3.1 Size & surface analysis

Samples S1 – S11 were prepared with dispersion of the composites, 0.5 mg with ethanol 15 ml, followed by the sonication for 2 hours until all the samples are fully dispersed into the alcohol solution. The sonication was performed with the ultrasound bath sonication, Chromtech. The detail of the ultrasound sonication bath equipment is shown in Table 3.7. Immediately upon completion of the sonication, a drop of each sample was placed on carbon coated copper grids and allowed to dry for 3 days before the observation. The observation was done with 120kV with the emission current of 2µA. The filament current is 3.365A with the illumination angle of 160µ rad. The magnification was set at 10,000 X. The details of TEM machine is shown in Table 3.6.

Table 3.6: Transmission Electron Microscopy (TEM)

Equipment	Model	Function	Pictures
TEM Location: TEM Lab, Faculty of Medicine, UM	LEO LIBRA 120kV	To examine crystal size and diffraction	

Table 3.7: Ultrasound sonication bath

Equipment	Model	Function	Pictures
Ultra Sound Bath Sonicator Location: Advanced Material's Lab, Faculty of Engineering, UM	Chromtech	Sample sonification for complete dispersion	

3.3.5 Structural Analysis

3.3.5.1 X-ray Diffraction (XRD) analysis

The crystallographic structures of the MnO_2 / MWCNT composite were determined by a power X-Ray diffraction system, PaNalytical EMPYREAN, details as per Table 3.8, using Cu Kα radiation ($\lambda = 0.15406$ nm) for samples S1 – S11.

To analyze the crystalline sizes across the sample, Scherrer Equation (3.1) is used based on the highest peaks corresponding to the required element, which in this case, the composite MnO_2 / MWCNT. The sizes of the crystalline are determined.

$$t = 0.9\,\lambda\,/\,(\beta \cos\theta) \hspace{3cm} (3.3)$$

Where;

t = crystallite size (nm);

λ = wavelength of the radiation (nm);

β = full width half maximum (FWHM) (rad) from Bragg's peak = $(2B_2 - 2B_1)/2$

θ = degree (is half of 2 θ);

Table 3.8: Details of X-ray Diffraction (XRD)

Equipment	Model	Function	Pictures
XRD Location: XRD Lab, Faculty of Science (Geology), UM	PaNalytical EMPYRE AN	To study crystallograph ic structure	

3.3.6 Thermal analysis

3.3.6.1 Thermogravimetry (TGA) analysis

TGA is used to determine the weight changes as a function of temperature and time to investigate the possible chemical reactions that occur between materials with atmosphere. In this process one of the components decomposes into a gas, which dissociates into the air. It is a process that utilizes heat and stoichiometry ratios to determine the percent by mass ratio of a solute. Analysis is carried out by raising the

temperature of the sample gradually and plotting weight (mg) against temperature (degree C). This is accomplished by heating up the powder to 1000ºC at a heating rate of 10ºC/min. For these studies, sample S1-S11 were tested with Mettler Toledo TGA/SDTA 851^e analysis unit at the engineering lab in UM as shown in Table 3.9.

Table 3.9: Details of Thermogravimetry (TGA)

Equipment	Model	Function	Pictures
TGA Location: TGA Lab, Faculty of Engineering, UM	Mettler Toledo TGA/SDTA 851^e	To study thermal stability	

CHAPTER FOUR

RESULTS AND DISCUSSION

4.1 Structural studies of MnO₂ / MWCNT composites

Figures 4.1(a) – (k) show the X-ray diffraction (XRD) patterns of the MnO₂ / MWCNT composite samples. The XRD pattern of the γ- MnO₂ / MWCNT composite exhibits many well-defined peaks as shown in Figures 4.1(a) to 4.1(i). The presence of γ-MnO₂ (JCPDS 42-1317) is confirmed with the four broad peaks observed at angle of $2\theta = 28.5^o$, 37.2^o, 56.5^o and 59.7^o for planes (110), (101), (211) and (220) respectively (Yan, 2009). The presence of MWCNT is confirmed with a sharp and a broad peak at angle of $2\theta = 25.8^o$ and 43° for planes (002) and (100), respectively (Huang, 2006). The XRD patterns from Figures 4.1 (a), (b) and 4.1(c) in comparison with the native elements of γ-MnO₂ in Figure 4.1 (d) and MWCNT in Figure 4.1 (e), confirmed that the presence of γ-MnO₂ / MWCNT composites. This is in line with the FESEM / EDX results in Figures 4.2 (c), 4.3(c), 4.4(c), 4.5(c), 4.6(c), 4.7(c), 4.8(c), 4.9(c) and 4.10(c). From the XRD pattern of the MnO₂ / MWCNT nano composite S1 – S9, diffraction peaks from the MnO₂ phase can be observed while the diffraction peaks from the MWCNT are not obvious due to the coating of the MnO₂ layer on the surface of MWCNT.

The peaks are becoming sharper at angle of $2\theta = 28.5^o$ for γ-MnO₂. This proves that the crystallite size of the composites increases as more γ-MnO₂ is added. However, the crystallite size of γ-MnO₂ for sample S9 (0.45 mole γ-MnO₂ and 0.05 mole MWCNT), is closer to the control sample S10 of MnO₂ at 91.07 nm. This reveals that the addition of γ-MnO₂ has increased the crystallite size of the γ-MnO₂ / MWCNT composites from 60.71 to 90.71 nm as shown in Table 4.1.

Table 4.1: Crystallite size of γ-MnO_2 in the composite with the highest peak at the angle of $2\theta = 28.50°$

Samples	S1	S2	S3	S4	S5	S6	S7	S8	S9	S10
(thickness) (nm)	60.71	63.05	58.55	54.64	81.96	78.06	65.57	78.06	91.07	91.07

Peaks at the angle of $2\theta = 25.8°$ and $43°$ are corresponding to the MWCNT component in the composite. Initially, peak width was imminent for sample S1 and become weaker at sample S9. The crystallite size increased until sample S4, to 15.98 nm, but reduced to the average size of 11.24 nm thereafter. This could be caused by the anomalies in the crystallite sizes of MWCNT as purchased which was also observed under TEM. In general, the crystallite sizes of MWCNT do not vary, as observed for γ-MnO_2. Results are shown in **Table 4.2.**

Table 4.2: Crystallite size of MWCNT in the composites with the highest peak at angle of $2\theta = 25.8°$.

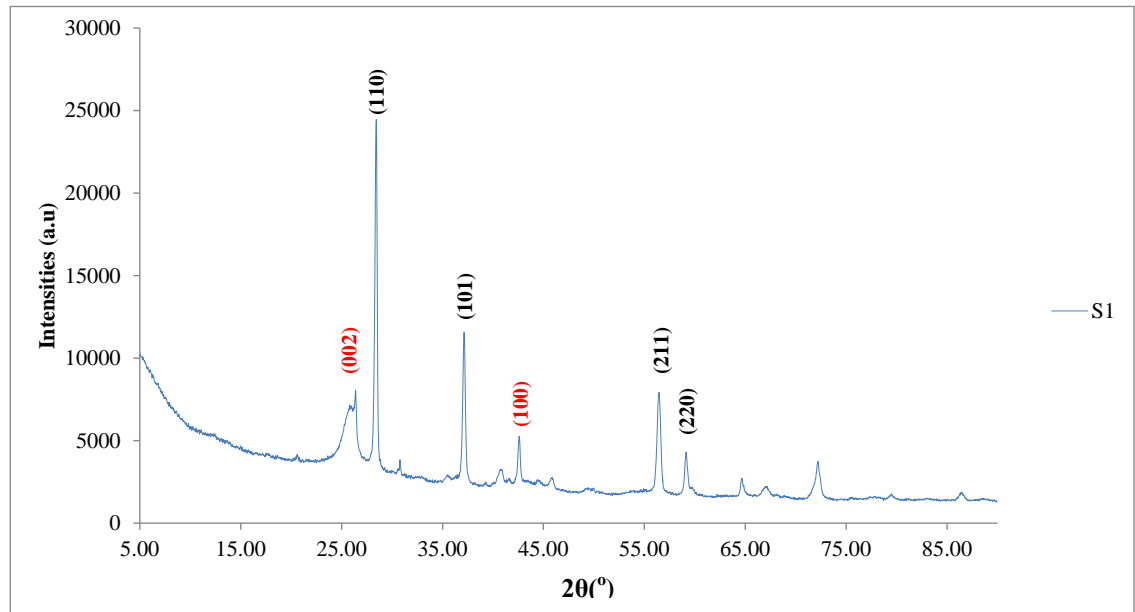| Samples	S1	S2	S3	S4	S5	S6	S7	S8	S9	S10
(thickness) (nm)	9.59	11.48	11.64	15.98	11.56	7.84	9.16	11.81	11.24	11.64

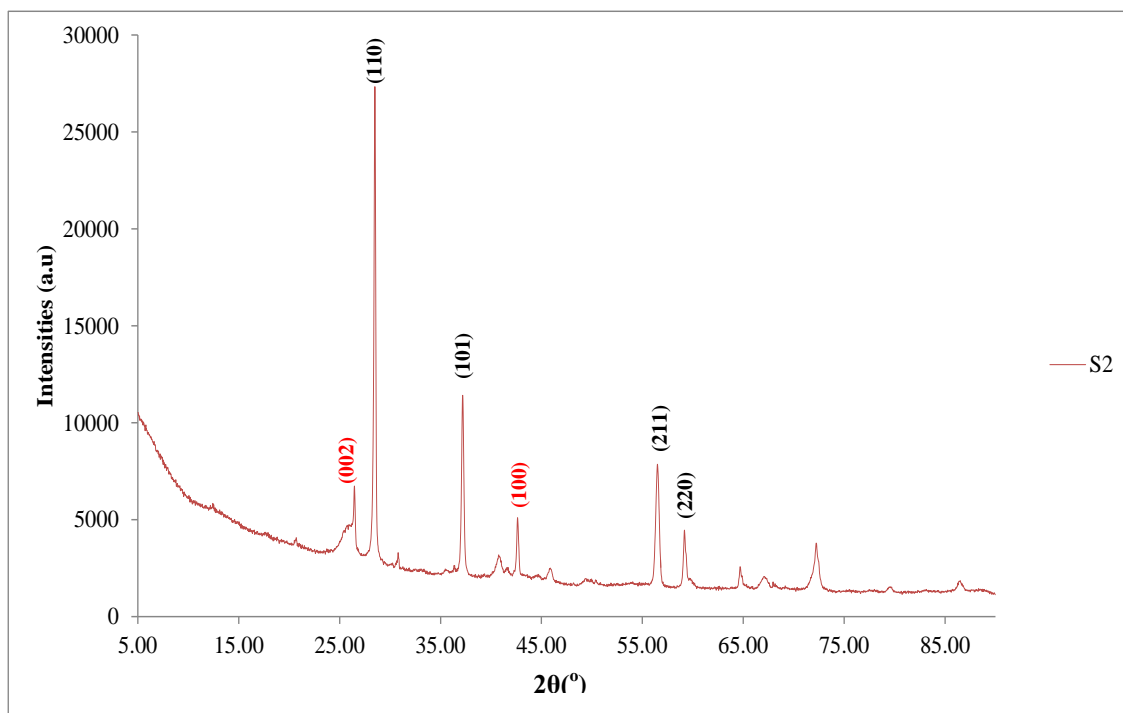Figure 4.1 (a) XRD pattern of sample S1

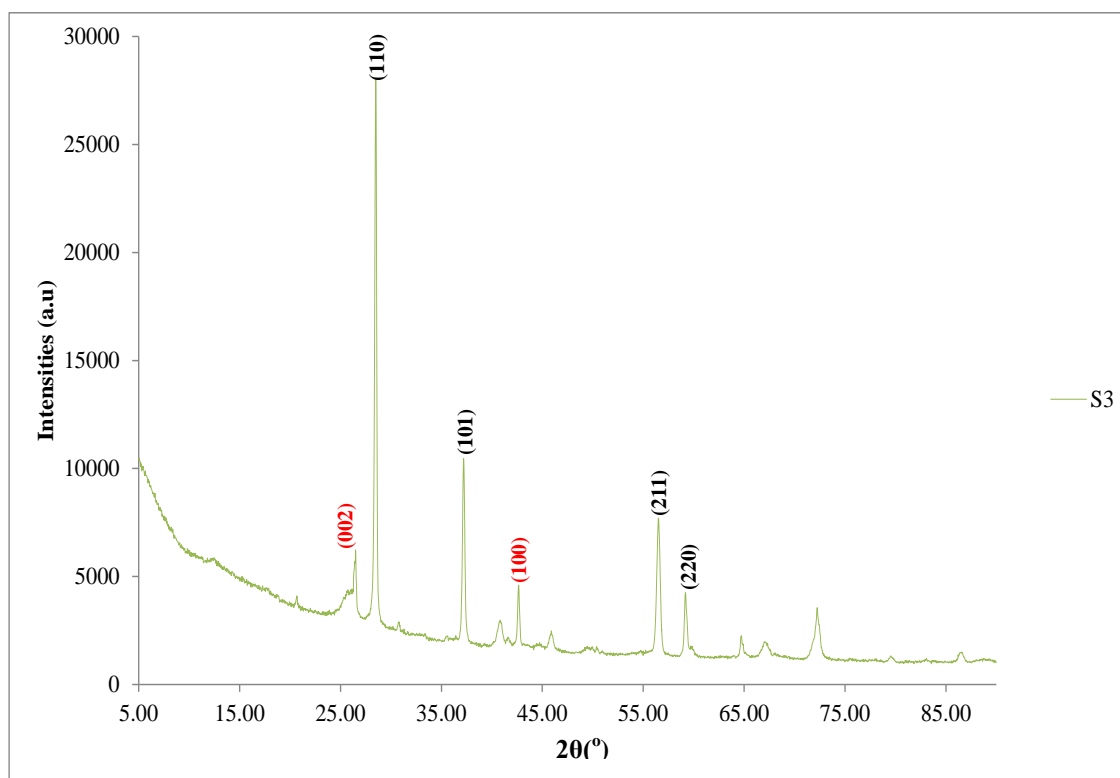Figure 4.1 (b) XRD pattern of sample S2
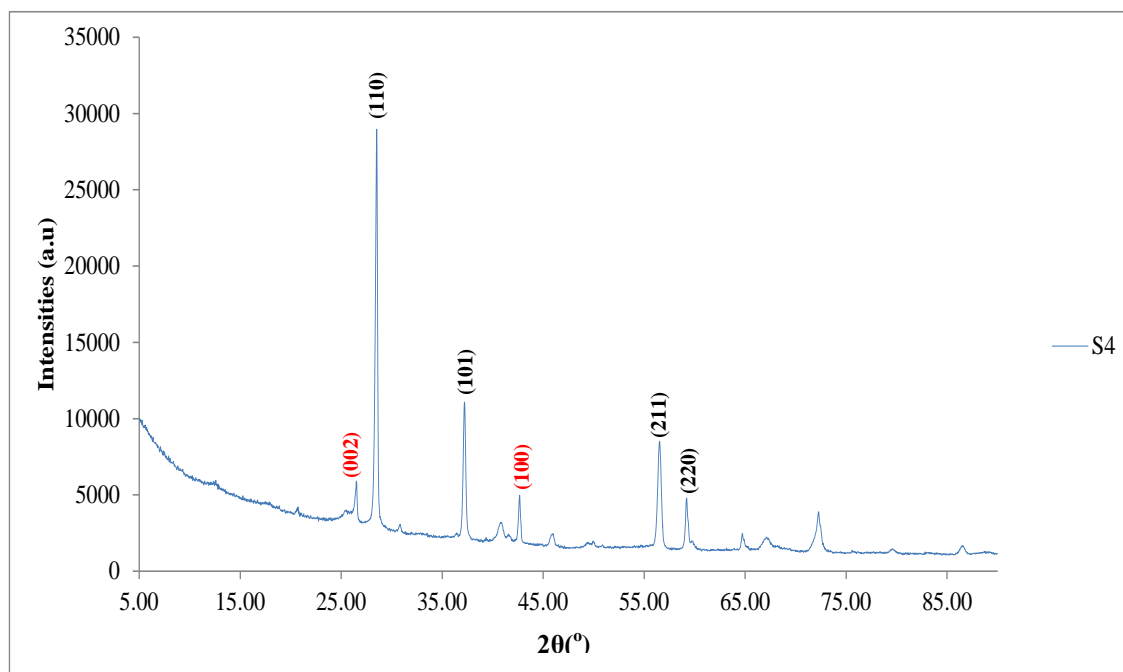

Figure 4.1 (c) XRD pattern of sample S3

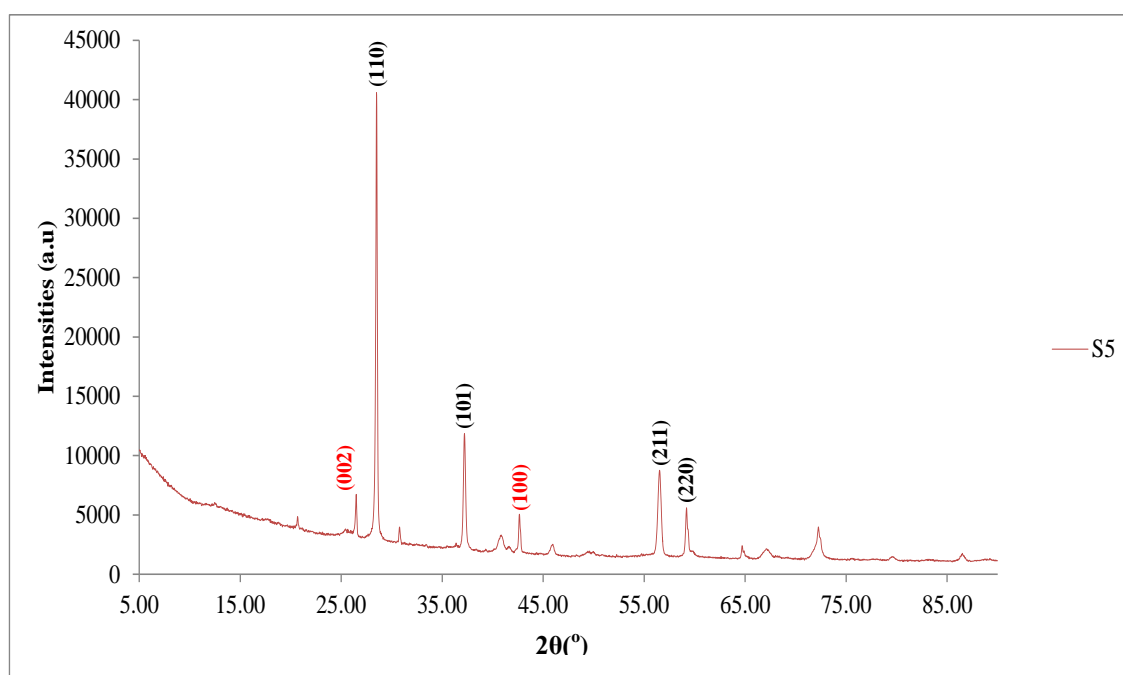Figure 4.1 (d) XRD pattern of sample S4
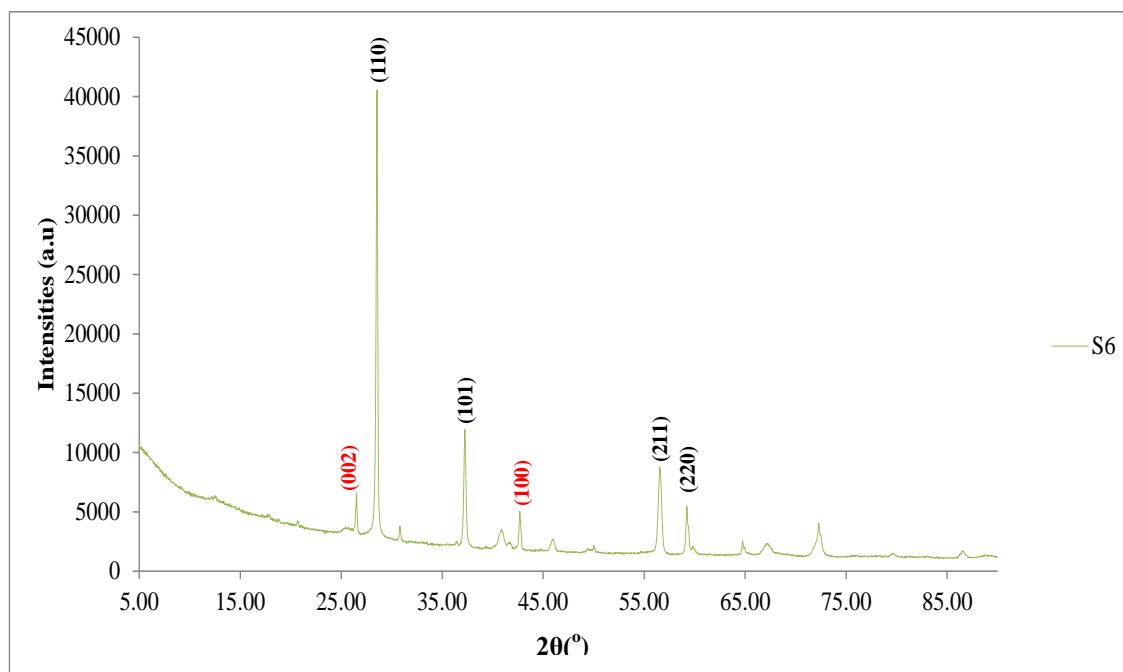

Figure 4.1 (e) XRD pattern of sample S5

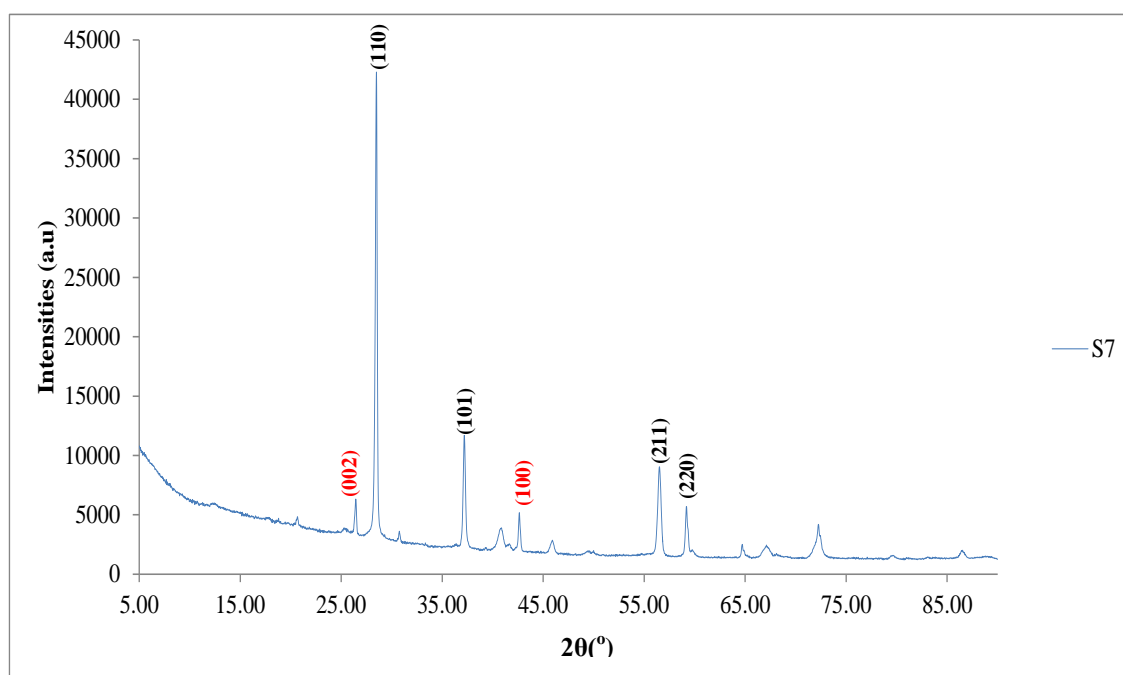Figure 4.1 (f) XRD pattern of sample S6

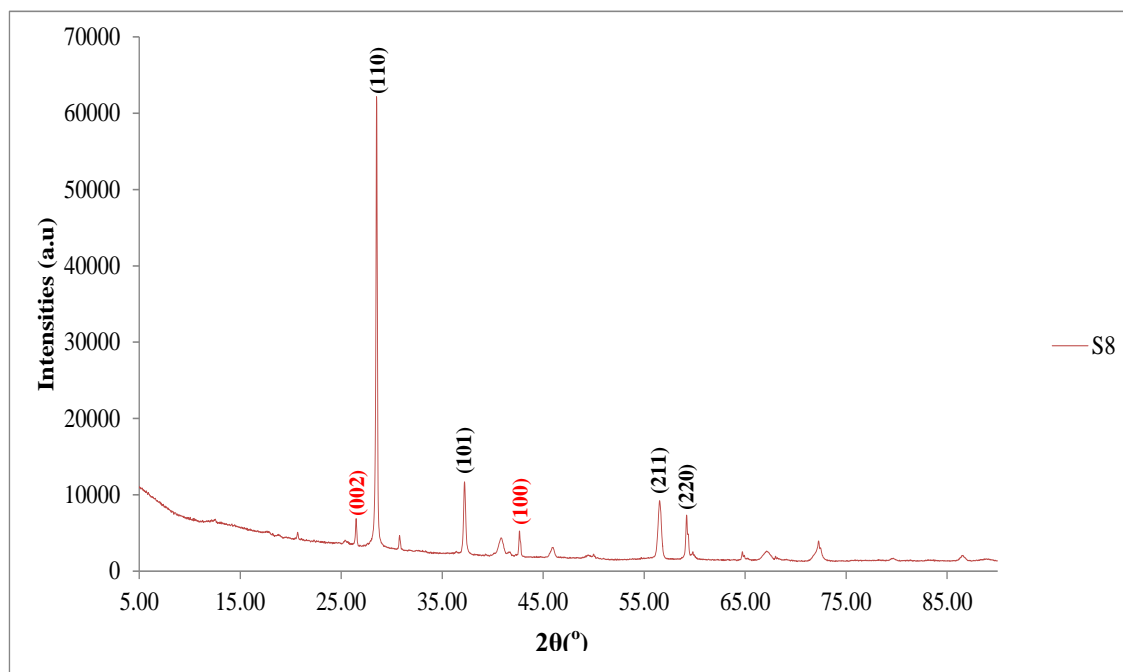Figure 4.1 (g) XRD pattern of sample S7
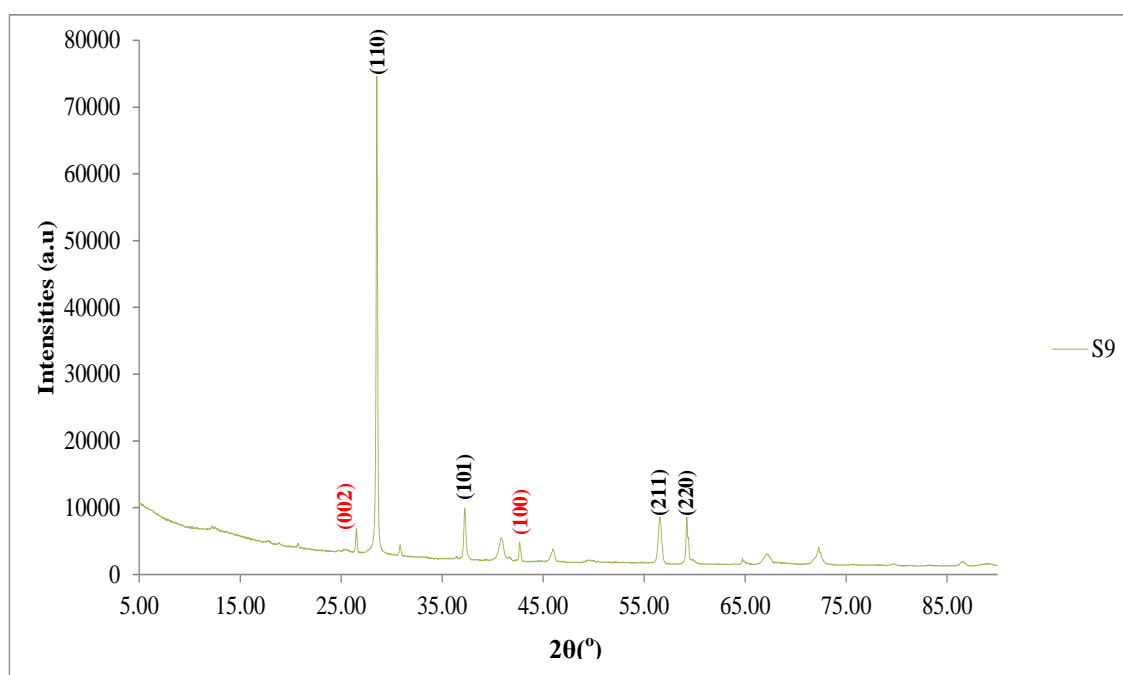
Figure 4.1 (h) XRD pattern of sample S8

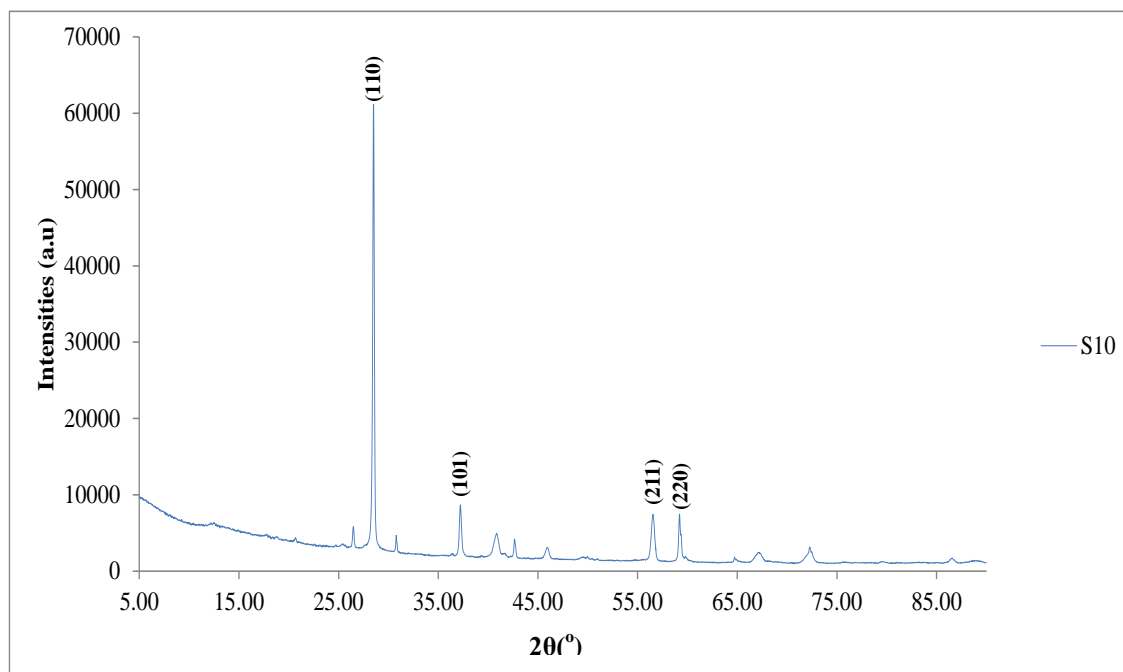Figure 4.1 (i) XRD pattern of sample S9
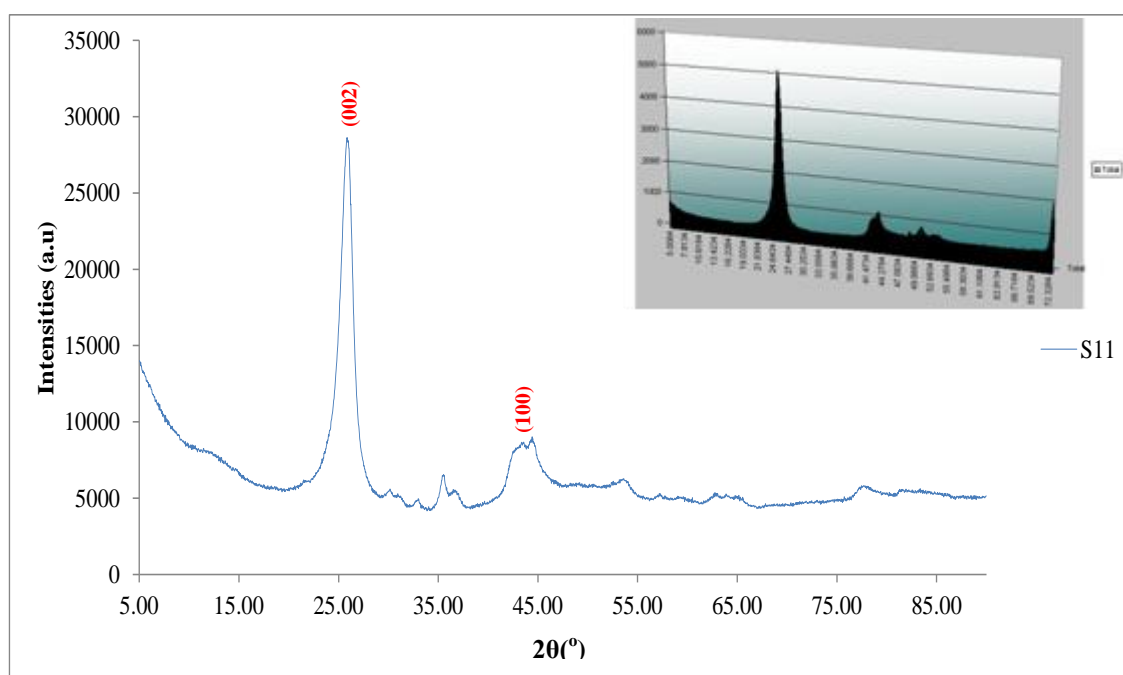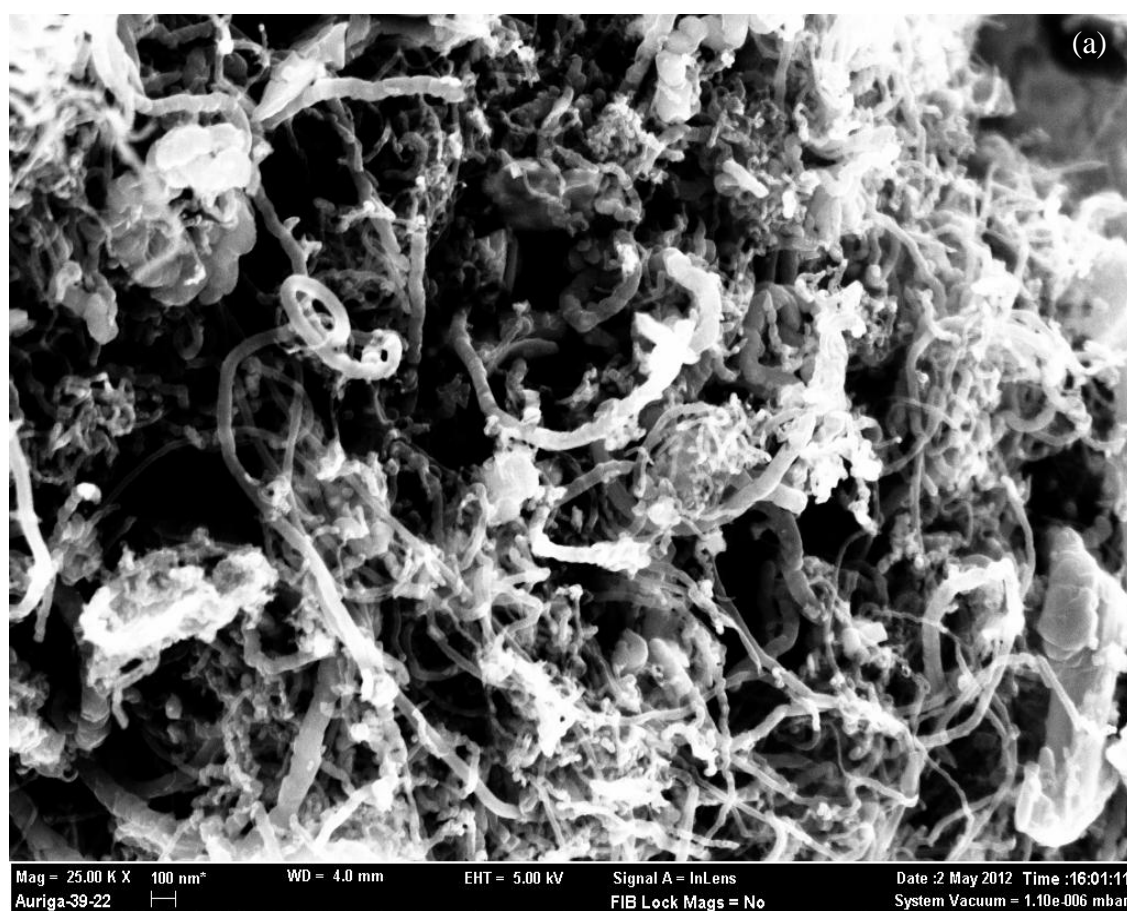
Figure 4.1 (j) XRD pattern of sample S10

Figure 4.1 (k) XRD pattern of sample S11; (inset picture shows the XRD pattern done

by NANOSHEL® USA)

4.2 Surface studies of MnO$_2$ / MWCNT composites

4.2.1 Sample S1

The surface properties of Samples of S1-S11 were characterized with the Field Emission Scanning Electron Microscopy (FESEM), Elemental Diffraction X- Ray (EDX) and Transmission Electron Microscopy (TEM). Figure 4.2 shows the FESEM / EDX / TEM results of the composites S1 (0.05 mole MnO$_2$ + 0.45 mole MWCNT). Each sample was accompanied by the EDX analysis targeted on an area or spot of the samples.

(b)

Pa 1 = 25.26 nm

Pa R1

Pa 1

Mag = 100.00 K X   100 nm*   WD = 4.0 mm   EHT = 5.00 kV   Signal A = InLens   Date :2 May 2012   Time :16:07:29
Auriga-39-22   FIB Lock Mags = No   System Vacuum = 1.08e-006 mbar

c:\edax32\genesis\genmaps.spc   31-May-2012 16:17:33
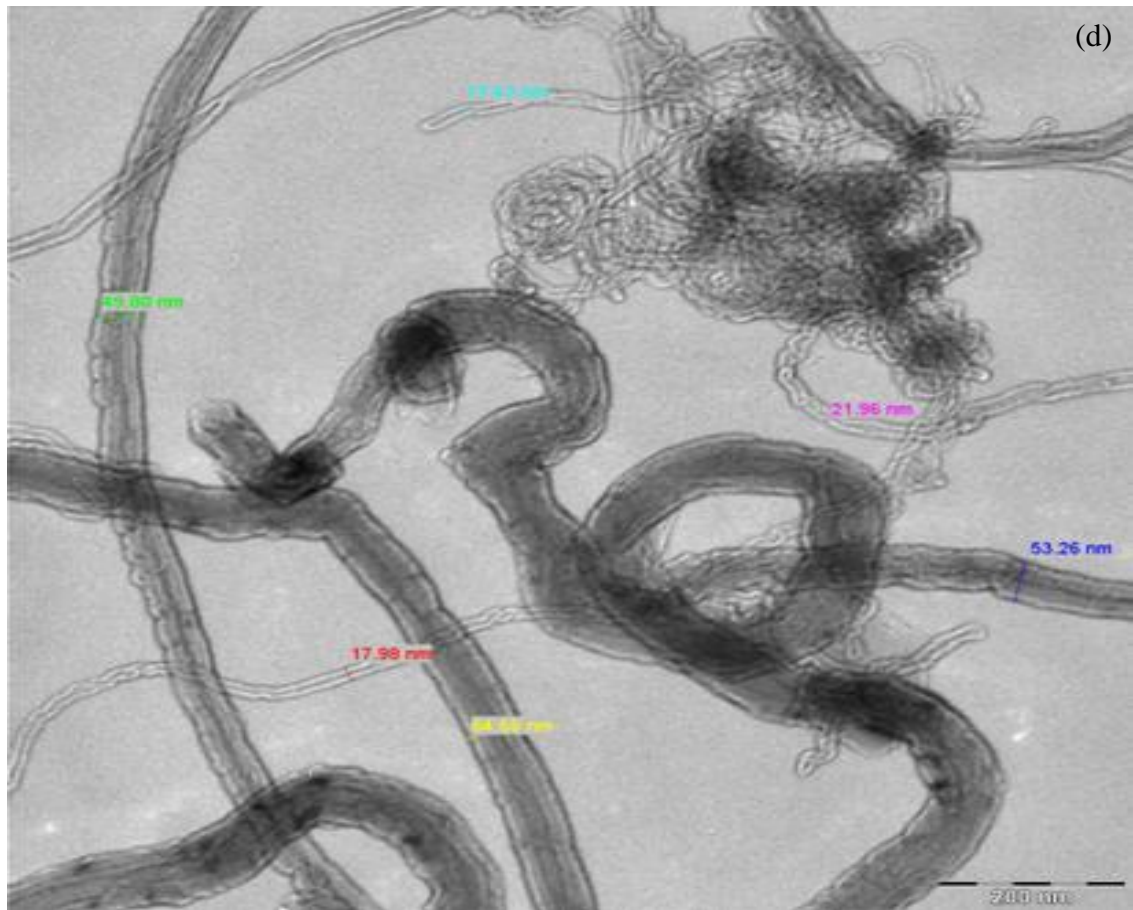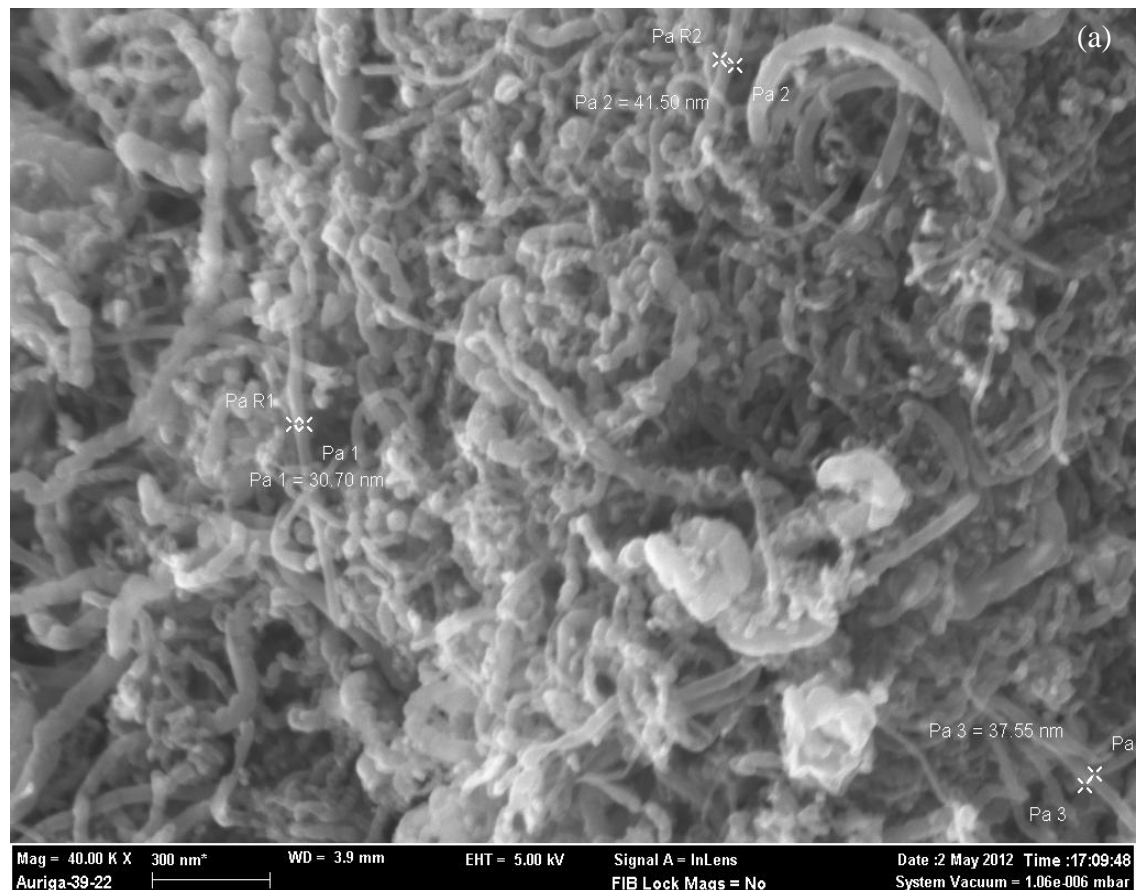LSecs : 17

(c)
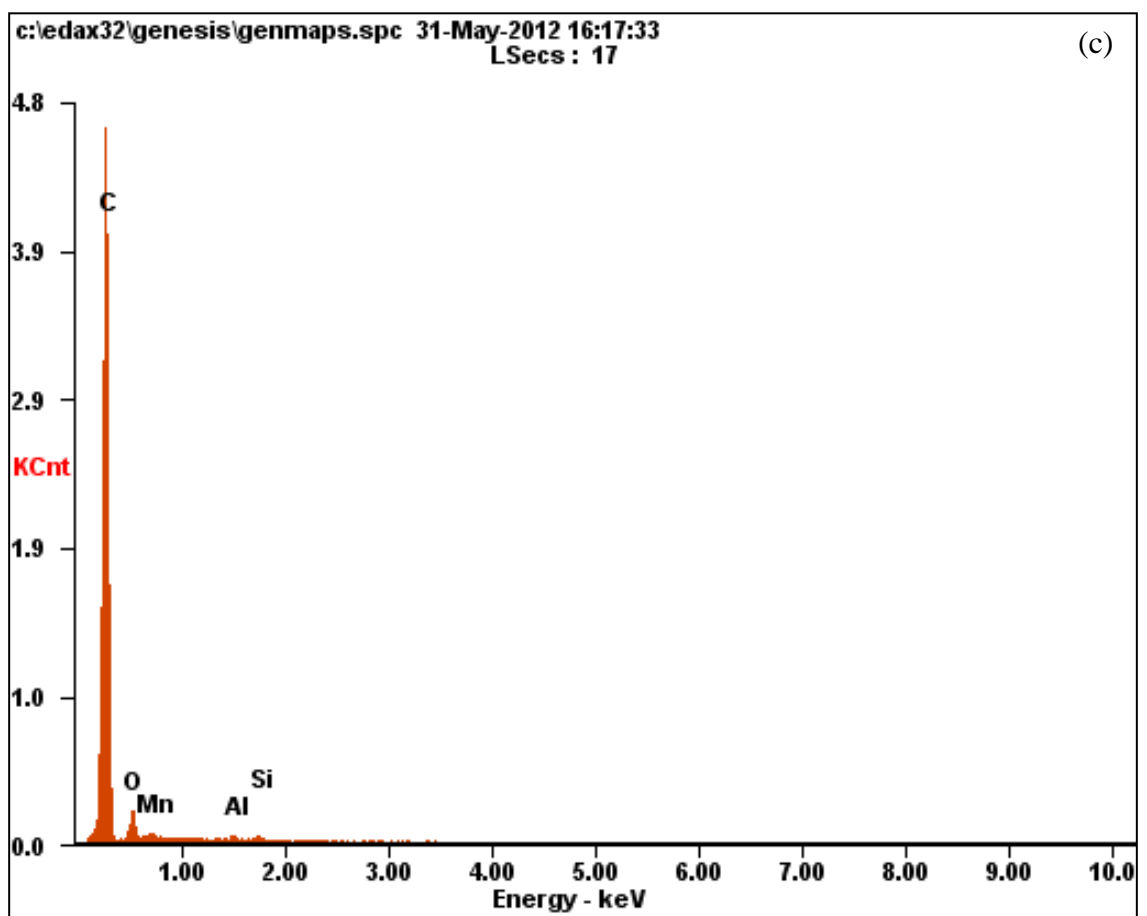
Figure 4.2: Results of sample S1 (a) FESEM image at 25k X (b) FESEM image at 100k
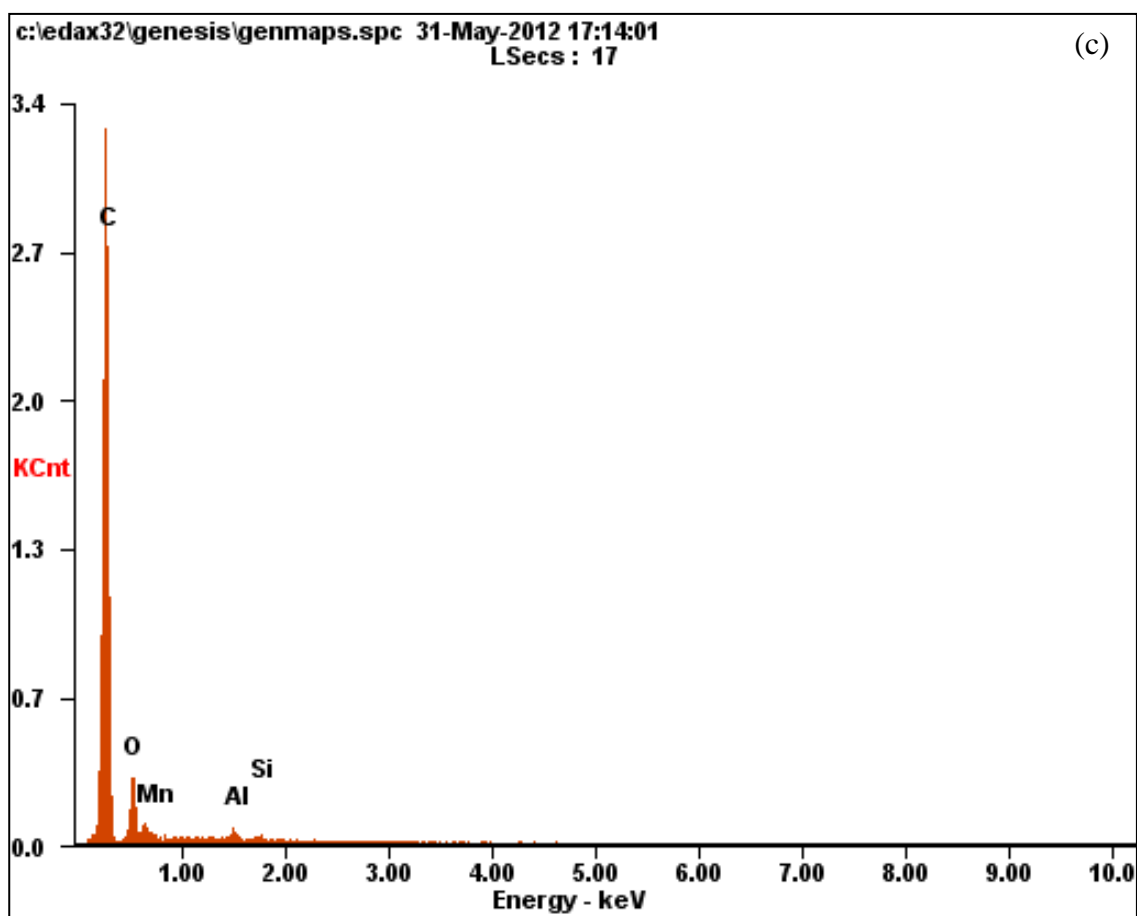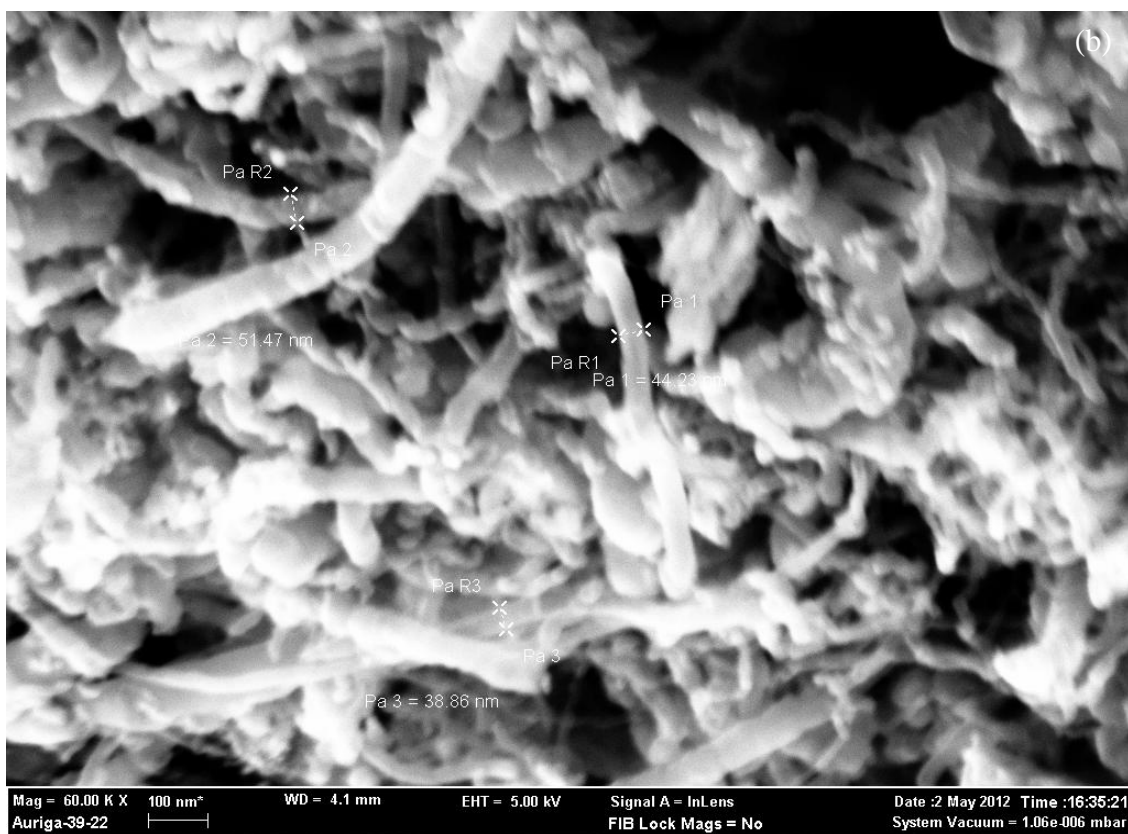
X (c) EDX spectrum (d) TEM image

Figure 4.2 (a) and (b) show the carbon nano tubes exhibit regular morphology for both multi walled (MWCNT). Based on the observation, the surface of the thinner multi walled carbon nano tubes (< 17 nm) represents a smooth walls compared to the thicker multi walled tubes (> 17 nm) with a slightly rough surface. Generally, multi walled nano tubes are prone to oxidization and more reactive with other metals groups such as MnO_2 due to the larger surface area. It is also observed that MnO_2 are attracted to the MWCNT surfaces as clearly seen via TEM image, Figure 4.2 (d). The diameter of the MWCNT increased up to 65 nm due to the formation of MnO_2 layer. This can be clearly seen from the TEM results 4.2(b), where the MWCNT can be seen in the middle of the composite with the diameter of approximately 20 nm, coated by MnO_2, with the thickness of 45 nm. The EDX spectrum, Figure 4.2 (c), reveals the presence of Mn, O,

and C in the composition, with higher weight percentage of MWCNT compared to MnO$_2$, which conforms to sample preparation at Table 3.1. Some Si and Al impurities (< 1.8% wt) were found from the MnO$_2$ sample. These impurities are observed as the original MnO$_2$ sample as received from the manufacturer confirms the presence of Al and Si in low quantities. These components normally come together with MnO$_2$ as a part of the composition as impurities.

4.2.2 Sample S2

Figure 4.3 shows the FESEM / EDX / TEM results of the composites S2 (0.10 mole MnO$_2$ + 0.40 mole MWCNT). The rest of the measurement parameters are in accordance to S1. Based on Figure 4.3 (a) and (b), the mole increase of MnO$_2$ shows more MWCNT coated with MnO$_2$ compared to S1. The diameter of composites S2 varies from 11 − 60 nm via TEM as shown in Figure 4.3 (d). EDX performed on S2 as shown at Figure 4.3 (c), shows more weight presence of MnO$_2$ (> 8% wt), compared to S1 (< 3% wt).

(b)

Pa R2
Pa 2
Pa 2 = 51.47 nm

Pa 1
Pa R1
Pa 1 = 44.23 nm

Pa R3
Pa 3
Pa 3 = 38.86 nm

Mag = 60.00 K X   100 nm*   WD = 4.1 mm   EHT = 5.00 kV   Signal A = InLens   Date :2 May 2012 Time :16:35:21
Auriga-39-22   FIB Lock Mags = No   System Vacuum = 1.06e-006 mbar

c:\edax32\genesis\genmaps.spc 31-May-2012 17:14:01
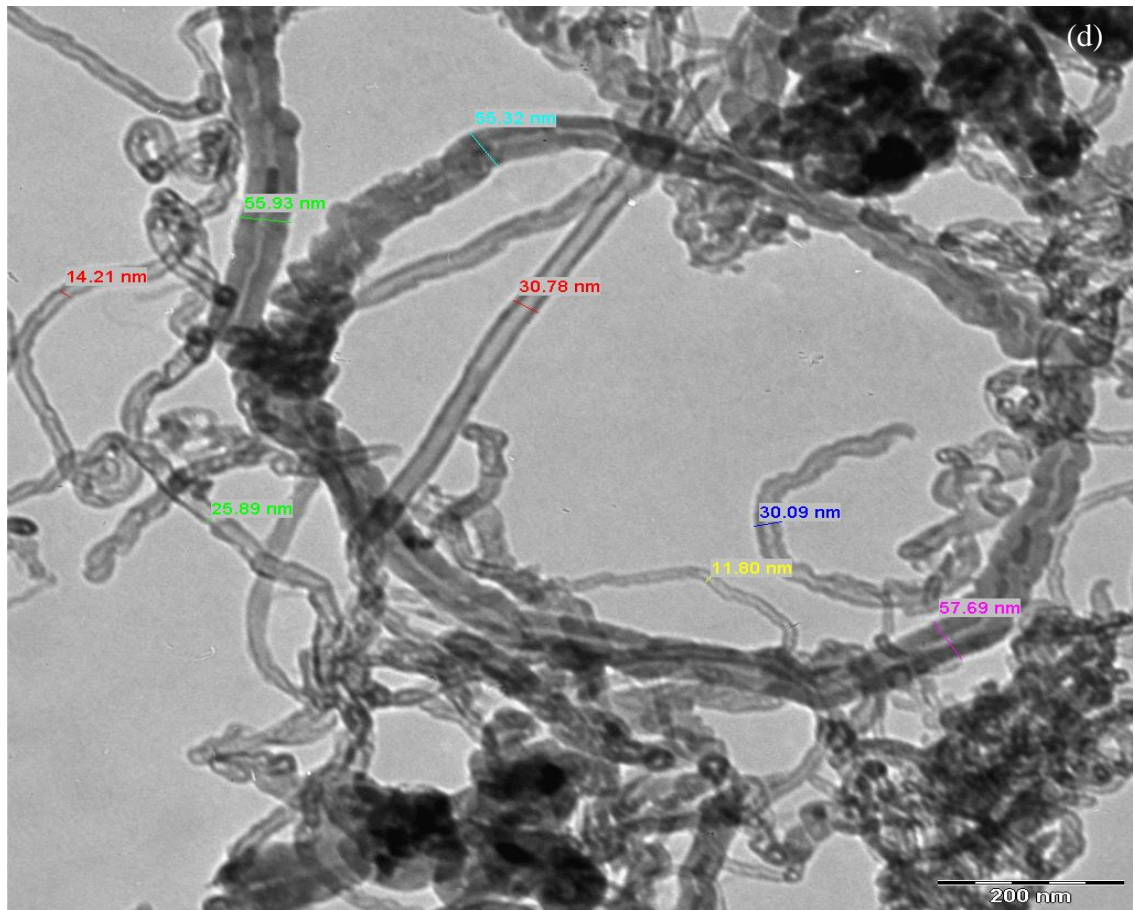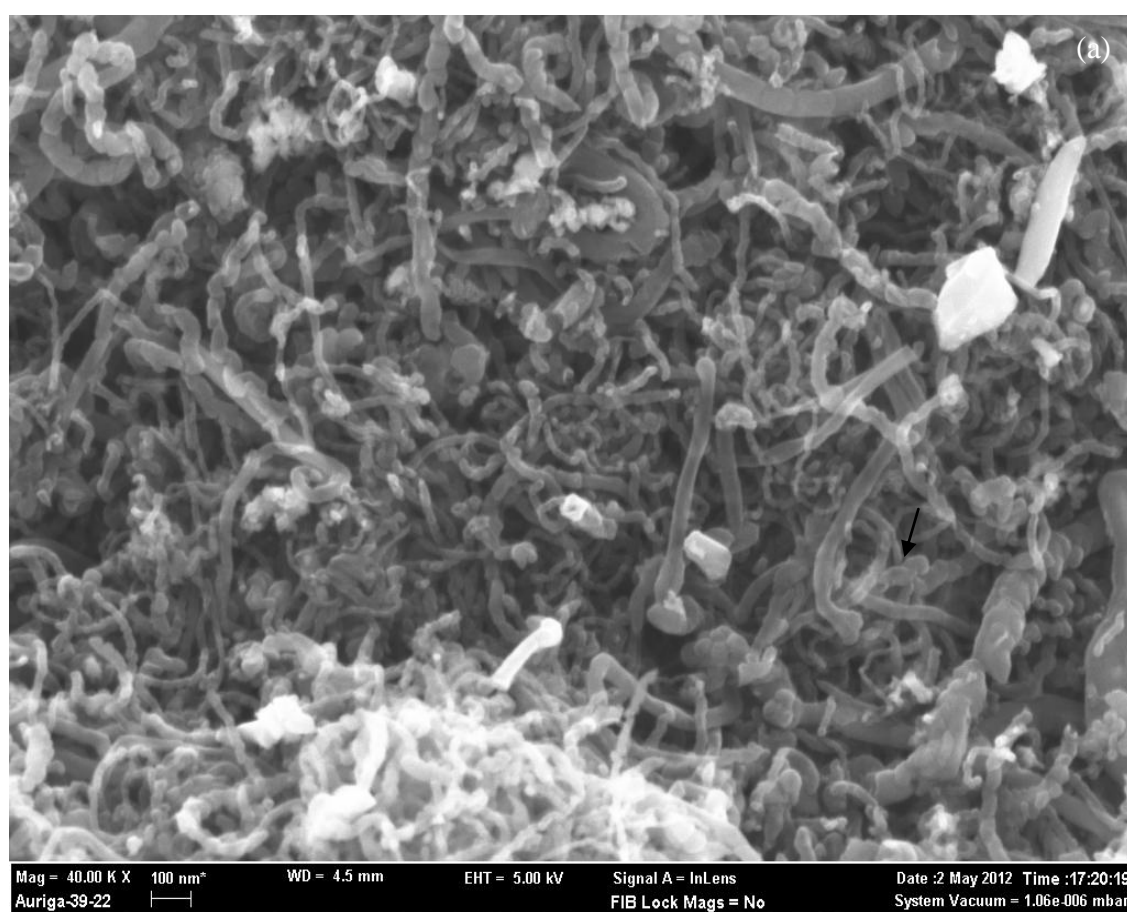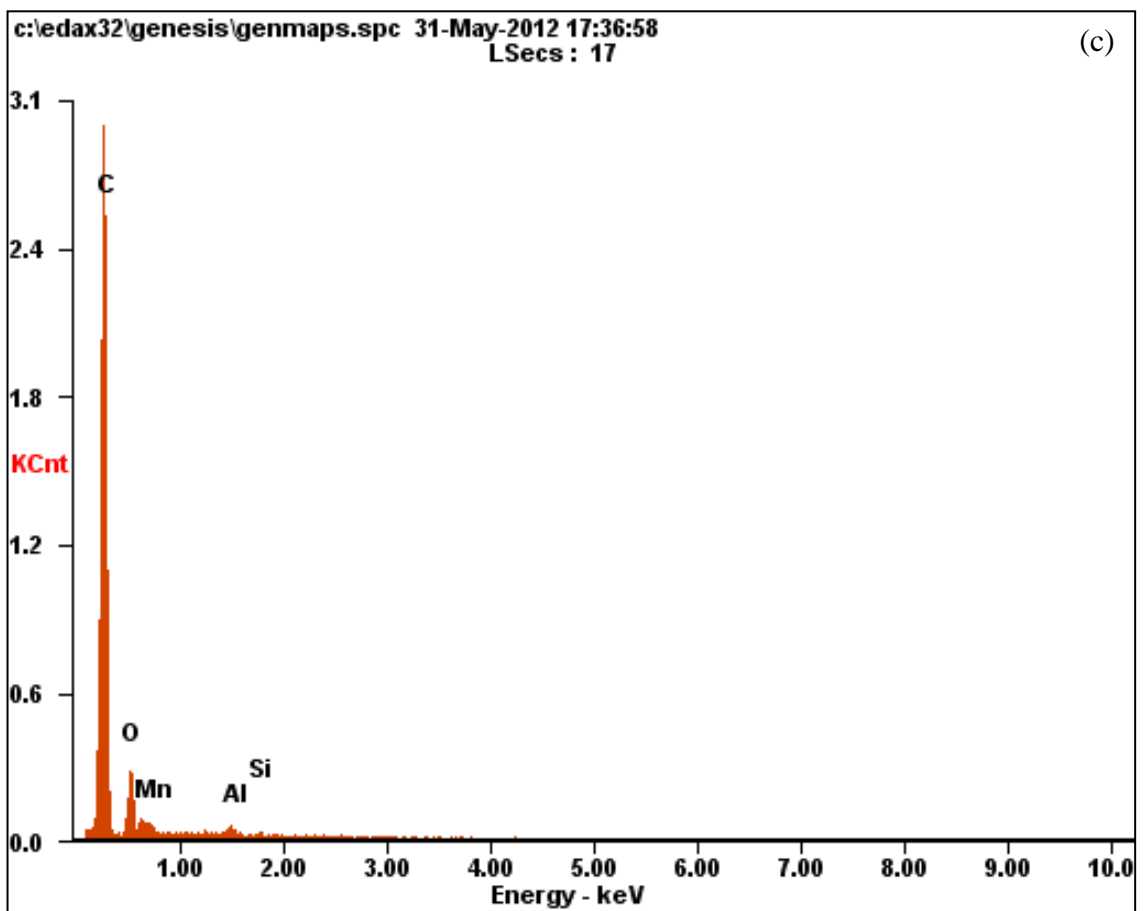LSecs : 17

(c)

50

Figure 4.3: Results of Sample S2 (a) FESEM image at 40kX (b) FESEM image at 60kX

(c) EDX spectrum (d) TEM image

4.2.3 Sample S3

Figure 4.4 shows the FESEM / EDX / TEM results of the composites S3 (0.15 mole MnO_2 + 0.35 mole MWCNT). The rest of the measurement parameters are in accordance to S1. Based on Figure 4.4 (a) and (b), the presence of higher mole of MnO_2 shows more MWCNT coated with MnO_2 compared to S1 and S2. The diameter of composites S3 varies from 13 − 120 nm via TEM as shown in Figure 4.4 (d). EDX performed on S3 as shown at Figure 4.4 (c), shows more weight presence of MnO_2 (> 14% wt), compared to S2 (> 8% wt).

(b)

Mag = 100.00 K X   100 nm*   WD = 4.5 mm   EHT = 5.00 kV   Signal A = InLens   Date :2 May 2012 Time :17:24:13
Auriga-39-22   FIB Lock Mags = No   System Vacuum = 1.06e-006 mbar

c:\edax32\genesis\genmaps.spc 31-May-2012 17:36:58
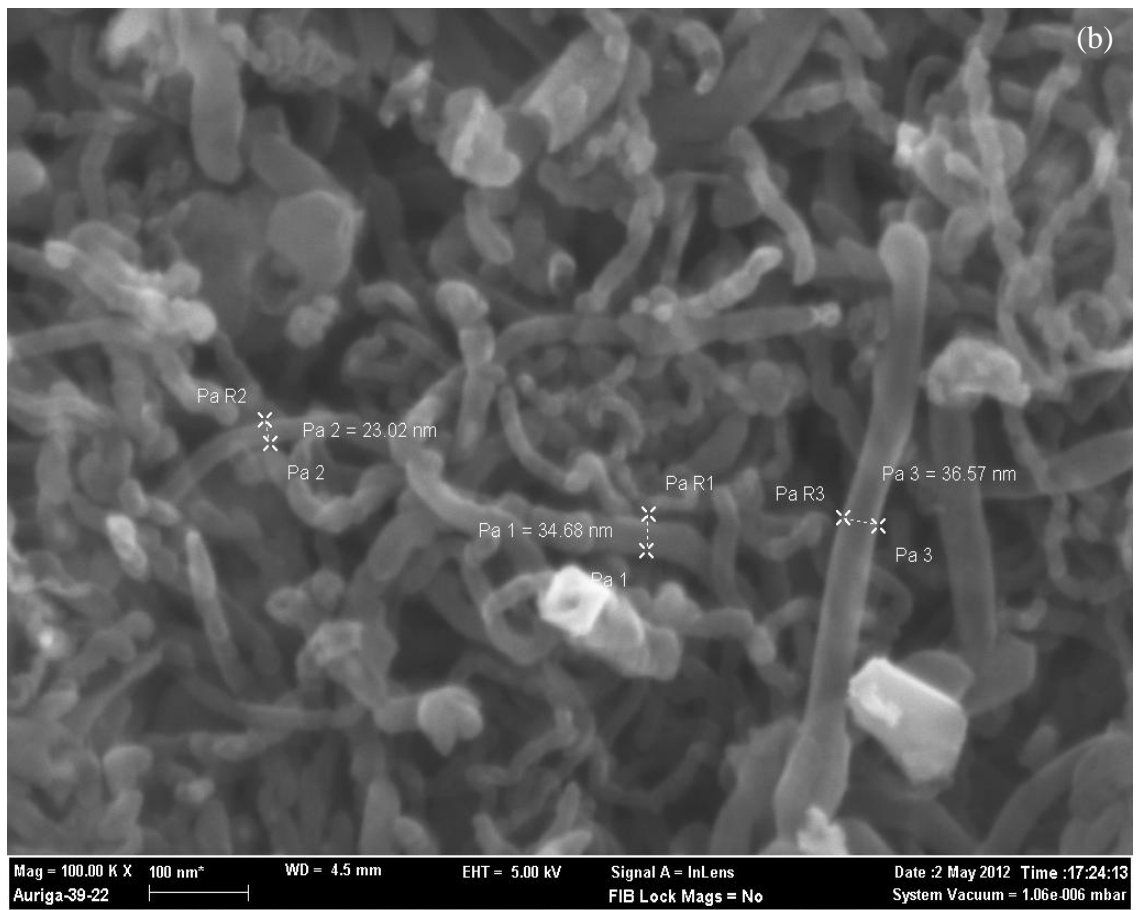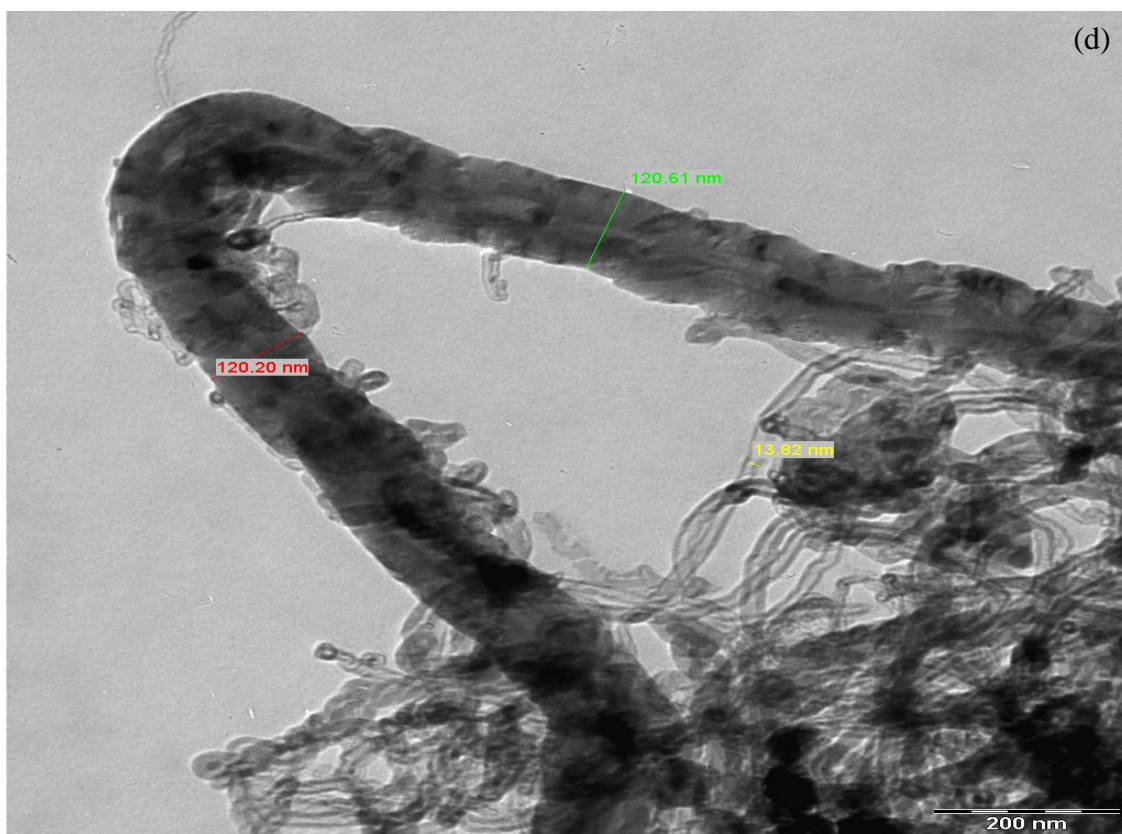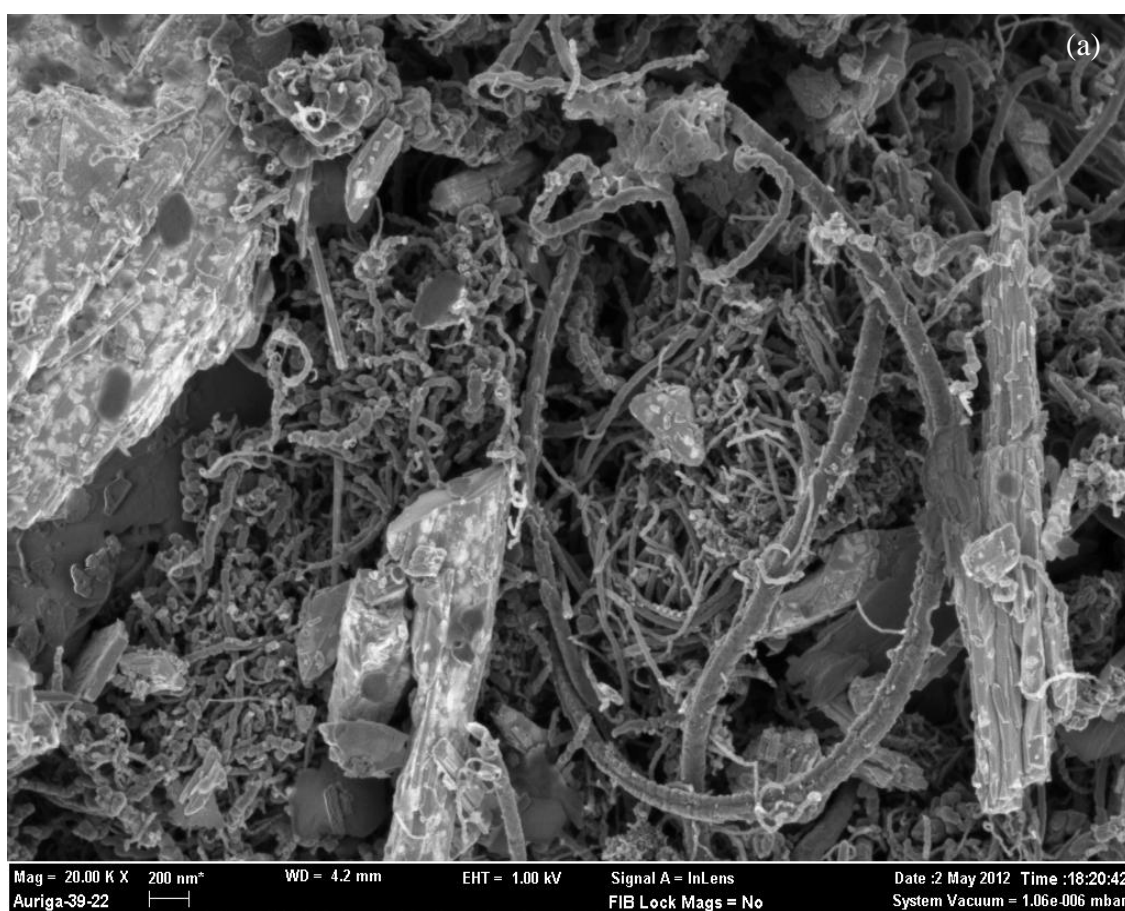LSecs : 17

(c)

53

Figure 4.4: Results of Sample S3 (a) FESEM image at 40kX (b) FESEM image at

100kX (c) EDX spectrum (d) TEM image

4.2.4 Sample S4

Figure 4.5 shows the FESEM / EDX / TEM results of the composites S4 (0.20 mole MnO_2 + 0.30 mole MWCNT). Based on Figure 4.5 (a) and (b), more MWCNT coated with MnO_2 were observed compared to S2 and S3 with rougher surfaces. The diameter of composites S4 varies from 50 − 55 nm as shown at Figure 4.5(d). EDX performed on S4, Figure 4.5(c), shows more weight presence of MnO_2 (> 38% wt), compared to S3 (> 14% wt).

(b)

Mag = 40.00 K X   200 nm*   WD = 4.8 mm   EHT = 1.00 kV   Signal A = InLens   Date :3 May 2012 Time :15:57:11
Auriga-39-22   FIB Lock Mags = No   System Vacuum = 2.51e-006 mbar

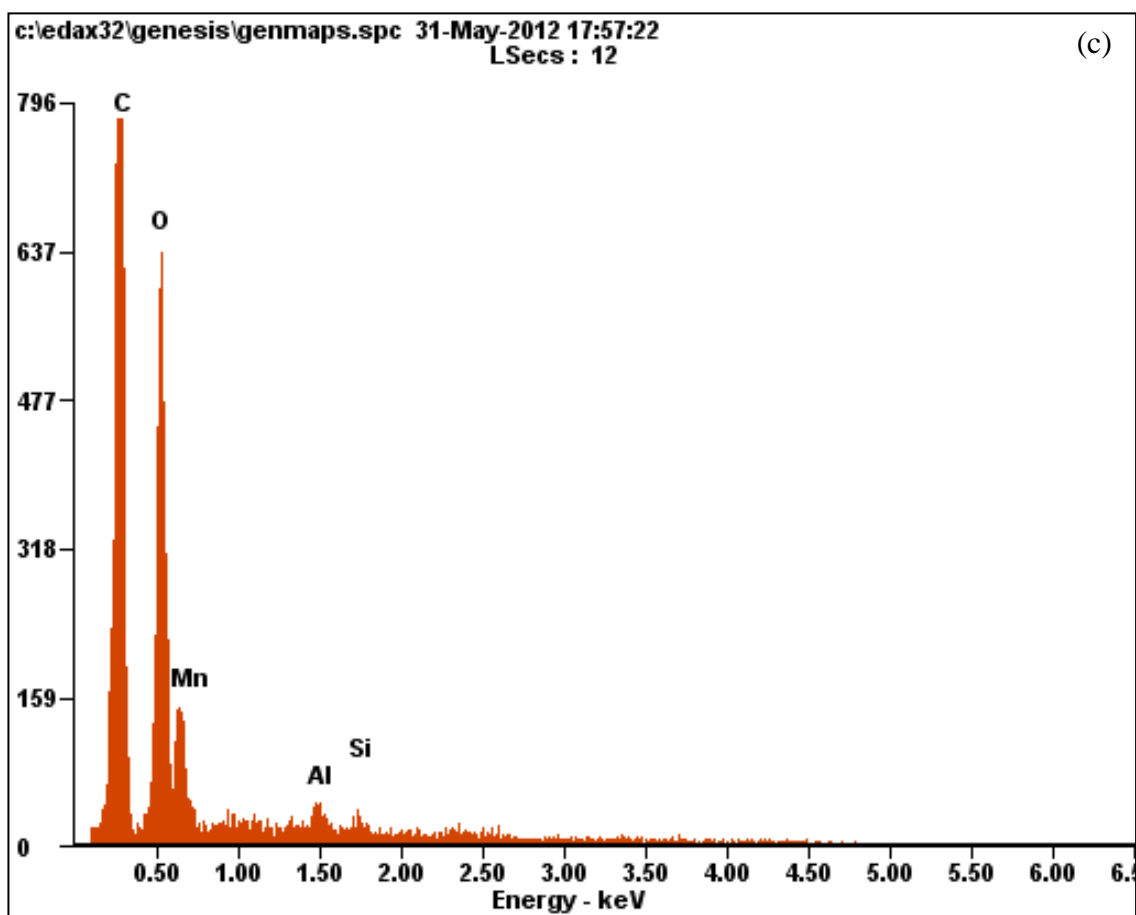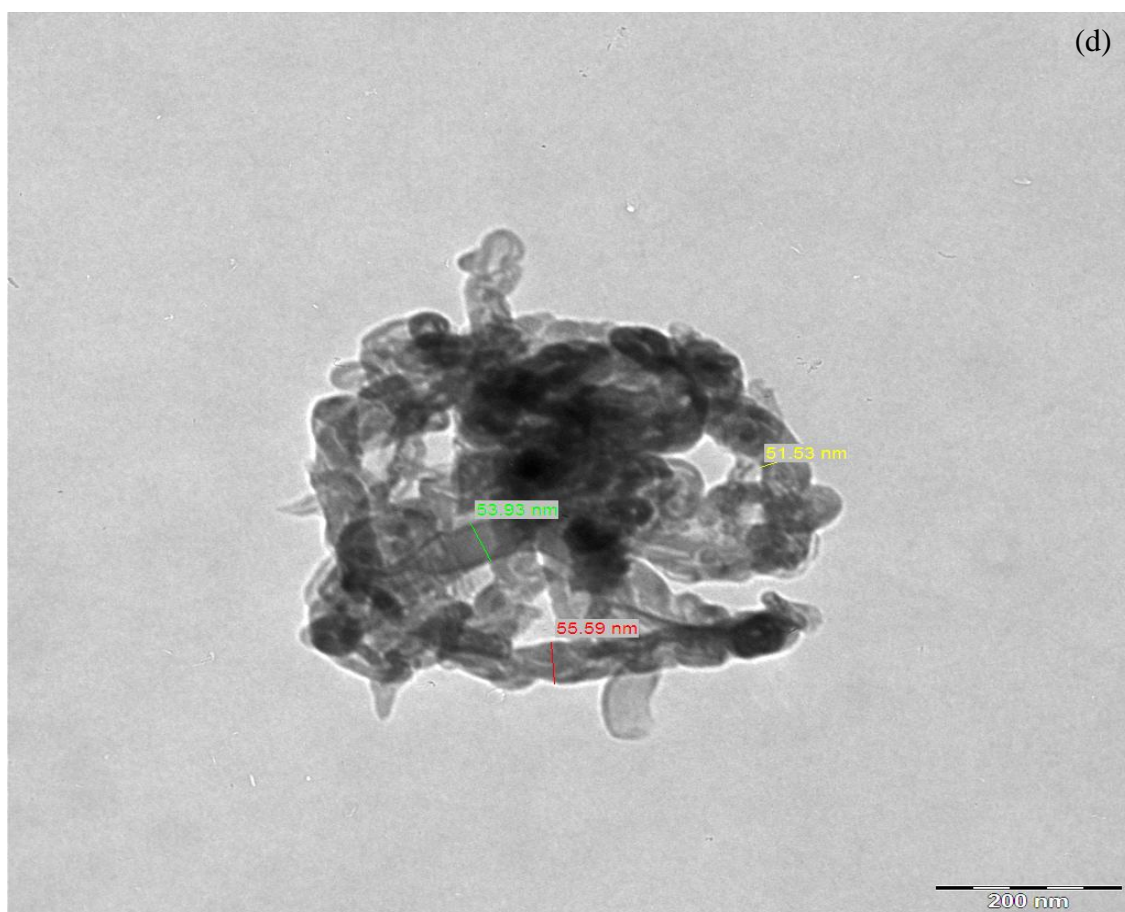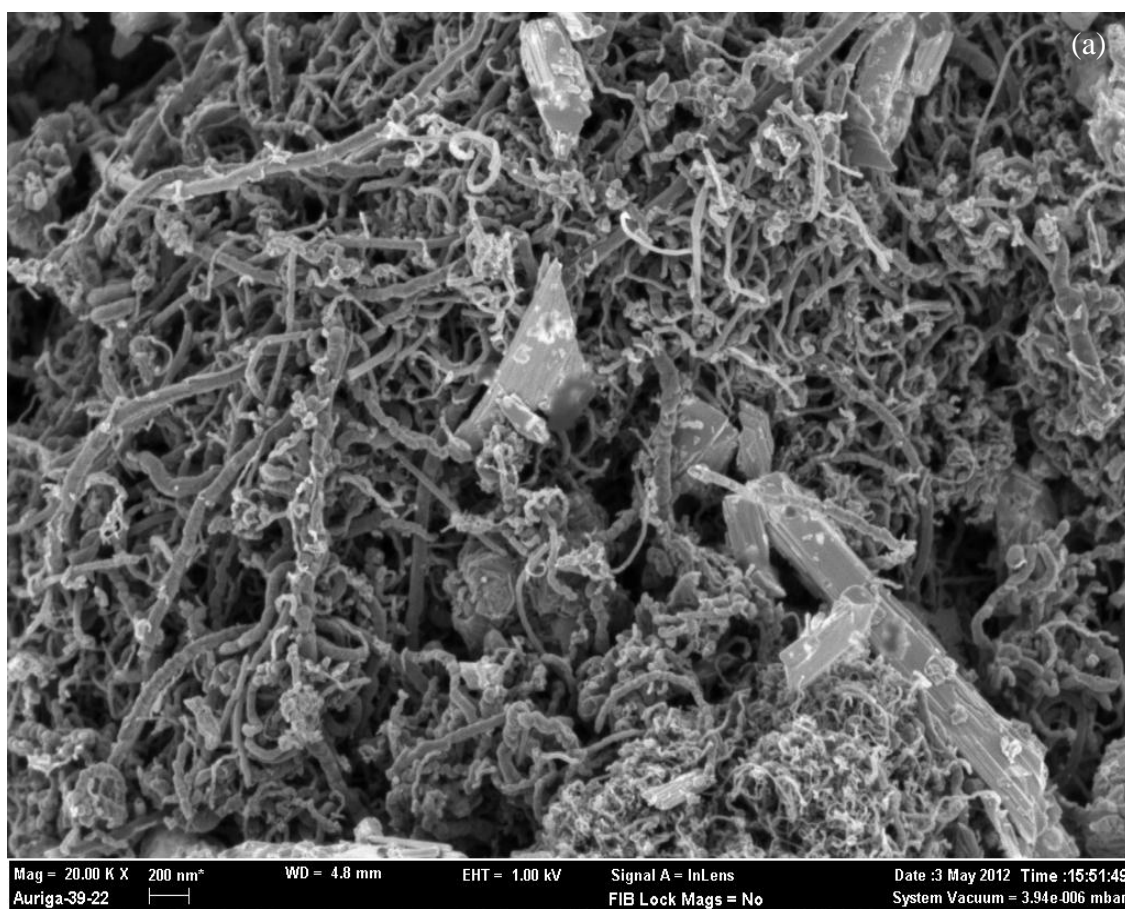c:\edax32\genesis\genmaps.spc 31-May-2012 17:57:22
LSecs : 12

(c)

Figure 4.5 Results of Sample S4 (a) FESEM image at 20kX (b) FESEM image at 40kX

(c) EDX spectrum (d) TEM image

4.2.5 Sample S5

Figure 4.6 shows the FESEM / EDX / TEM results of the composites S5 (0.25 mole MnO_2 + 0.25 mole MWCNT). Based on Figure 4.6 (a) and (b), the mole increase of MnO_2 shows more MWCNT coated with MnO_2. The diameter of composites S5 via TEM varies from 5 – 35 nm. Figure 4.6 (c) shows EDX spectrum on S5 with higher weight presence of MnO_2 (> 57% wt), compared to S4 (> 38% wt).

| Mag = 20.00 K X | 200 nm* | WD = 4.8 mm | EHT = 1.00 kV | Signal A = InLens | Date :3 May 2012 Time :15:51:49 |
| Auriga-39-22 | ⊢——⊣ | | | FIB Lock Mags = No | System Vacuum = 3.94e-006 mbar |

(b)

Mag = 40.00 K X   200 nm*   WD = 4.8 mm   EHT = 1.00 kV   Signal A = InLens   Date :3 May 2012 Time :15:52:31
Auriga-39-22   FIB Lock Mags = No   System Vacuum = 3.66e-006 mbar

c:\edax32\genesis\genmaps.spc 01-Jun-2012 18:08:26
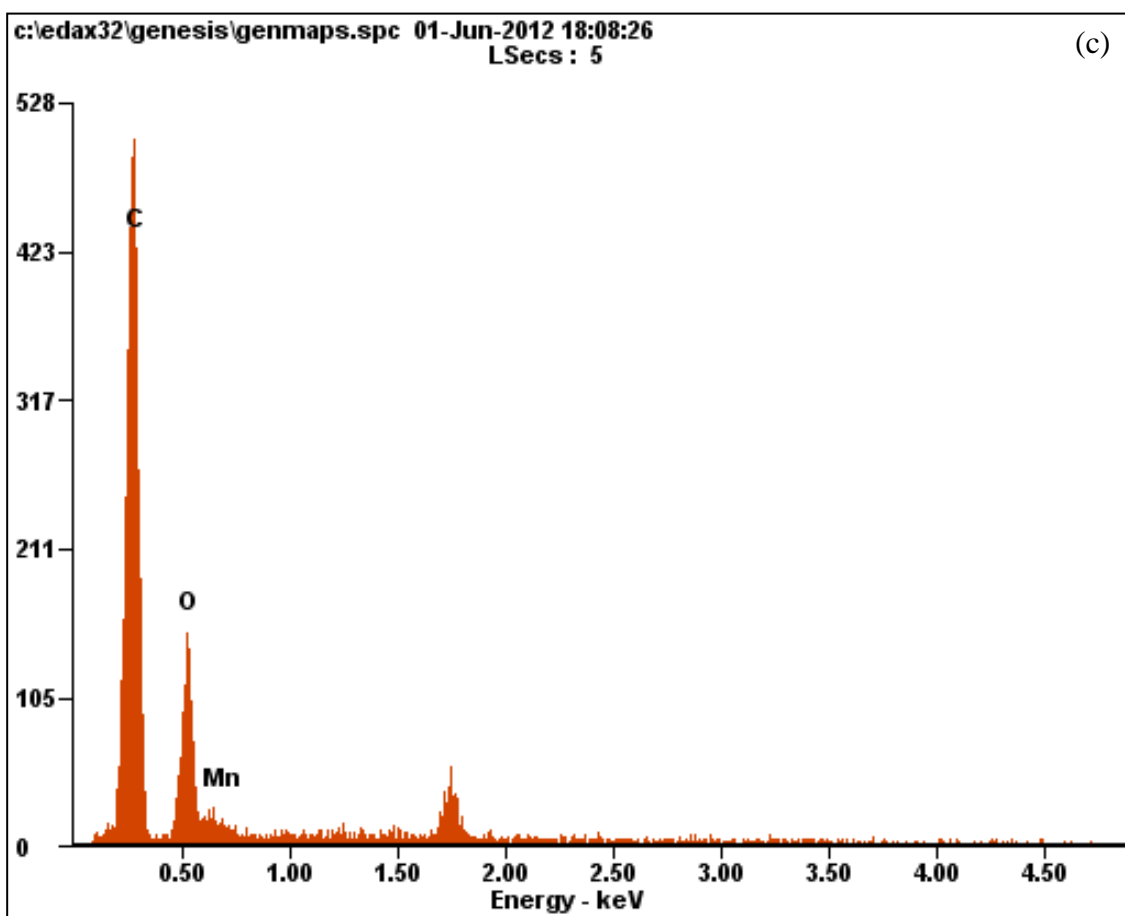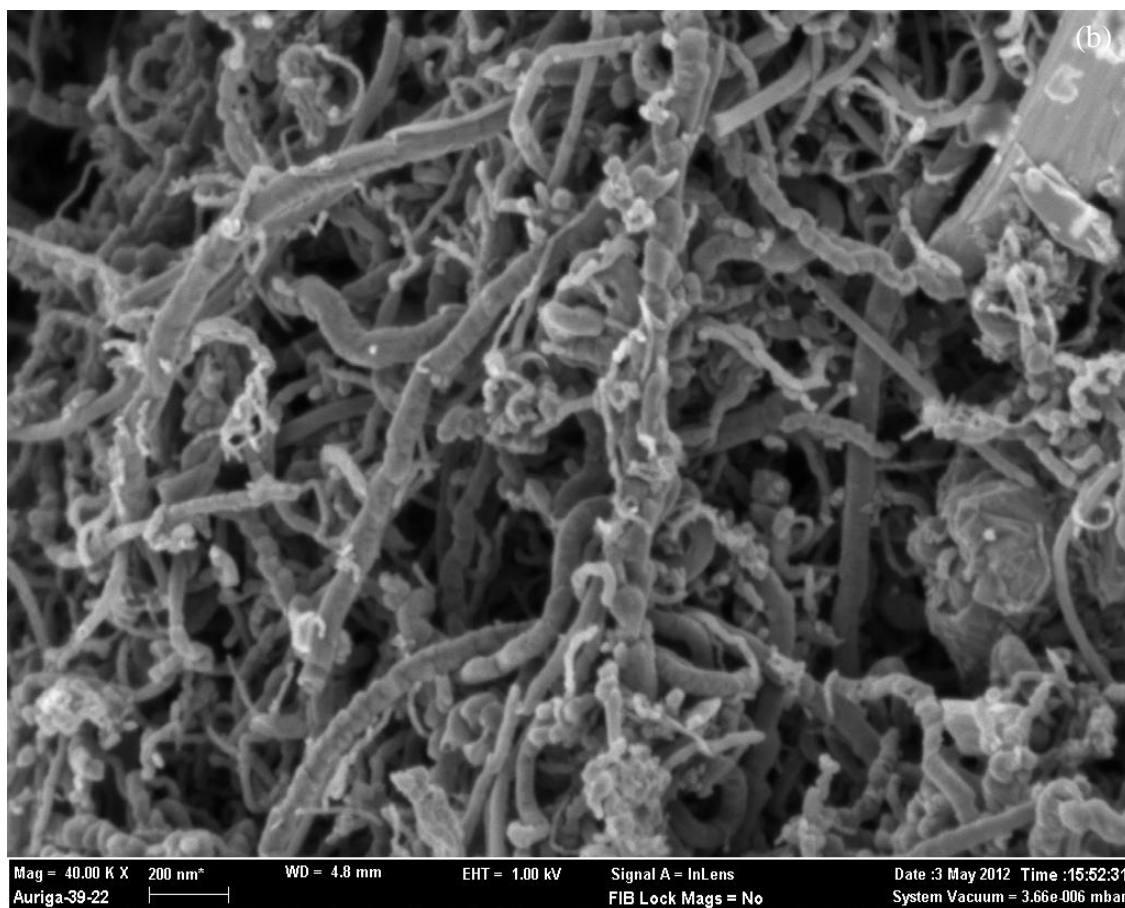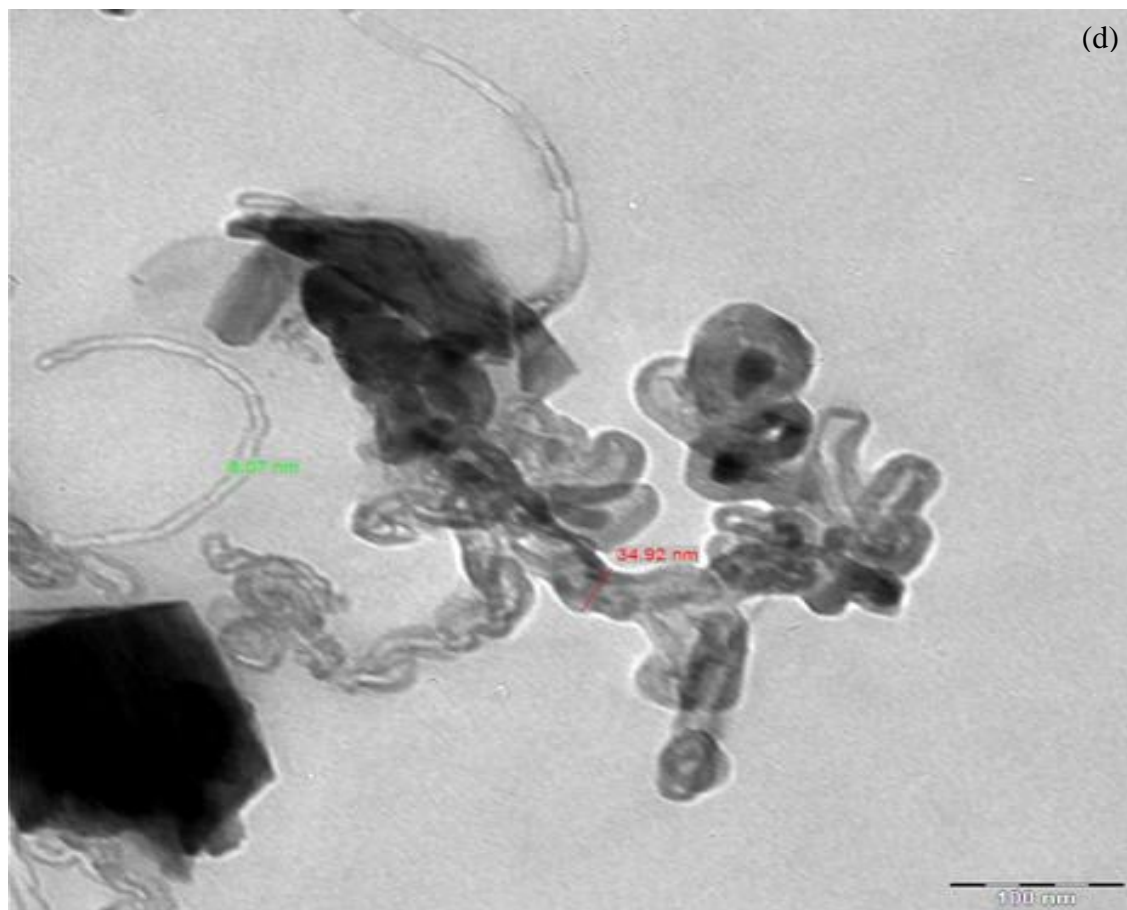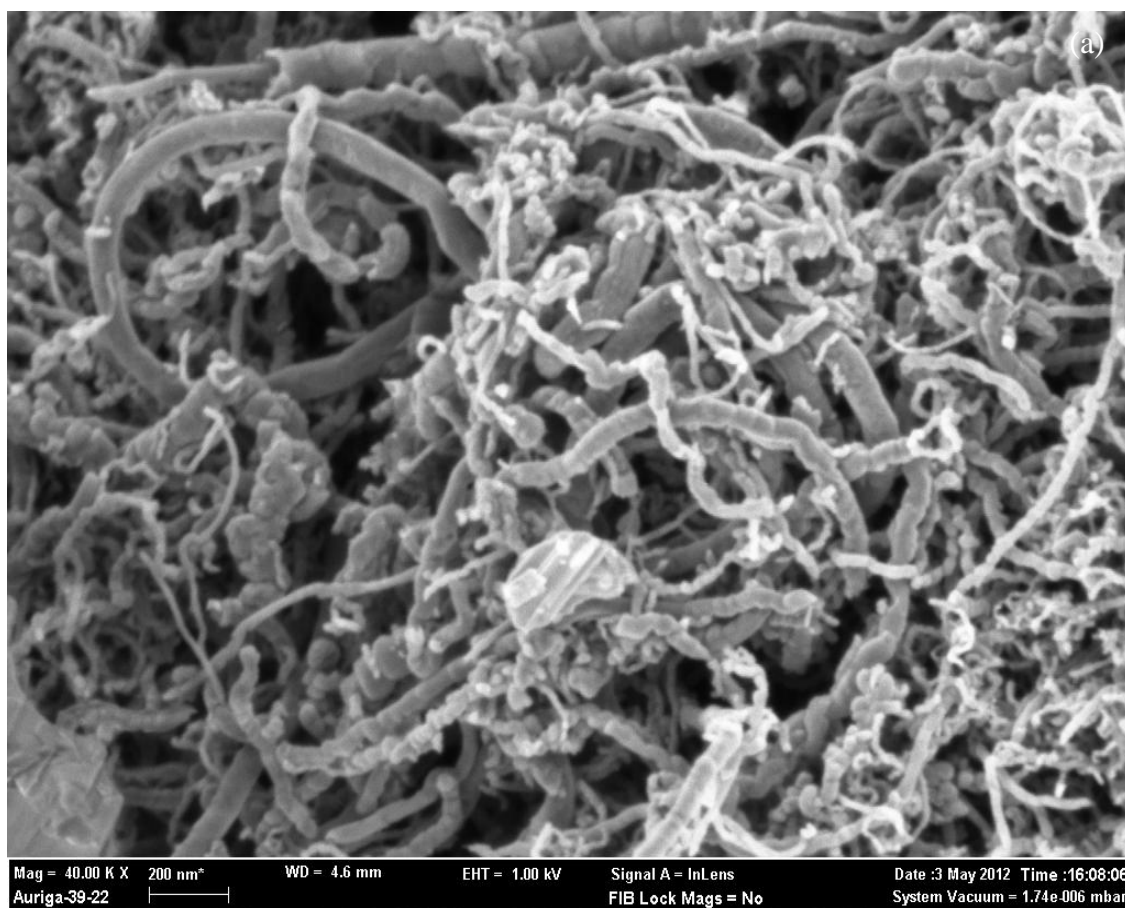LSecs : 5

(c)

(d)

Figure 4.6: Results of Sample S5 (a) FESEM image at 20kX (b) FESEM image at 40kX

(c) EDX spectrum (d) TEM image

4.2.6 Sample S6

Figure 4.7 shows the FESEM / EDX / TEM images of the composites S6 (0.30 mole MnO_2 + 0.20 mole MWCNT). Based on Figure 4.7 (a) and (b), the mole increase of MnO_2 shows more MWCNT coated with MnO_2. The spread of the composite are even throughout the sample, with more composite with similar composition and diameter can be found. The observation under TEM shows the diameter of the composite is around 63 nm, as shown in Figure 4.7 (d). Figure 4.7 (c) shows EDX spectrum on S6 with higher weight presence of MnO_2 (> 64% wt), compared to S5 (> 57% wt).
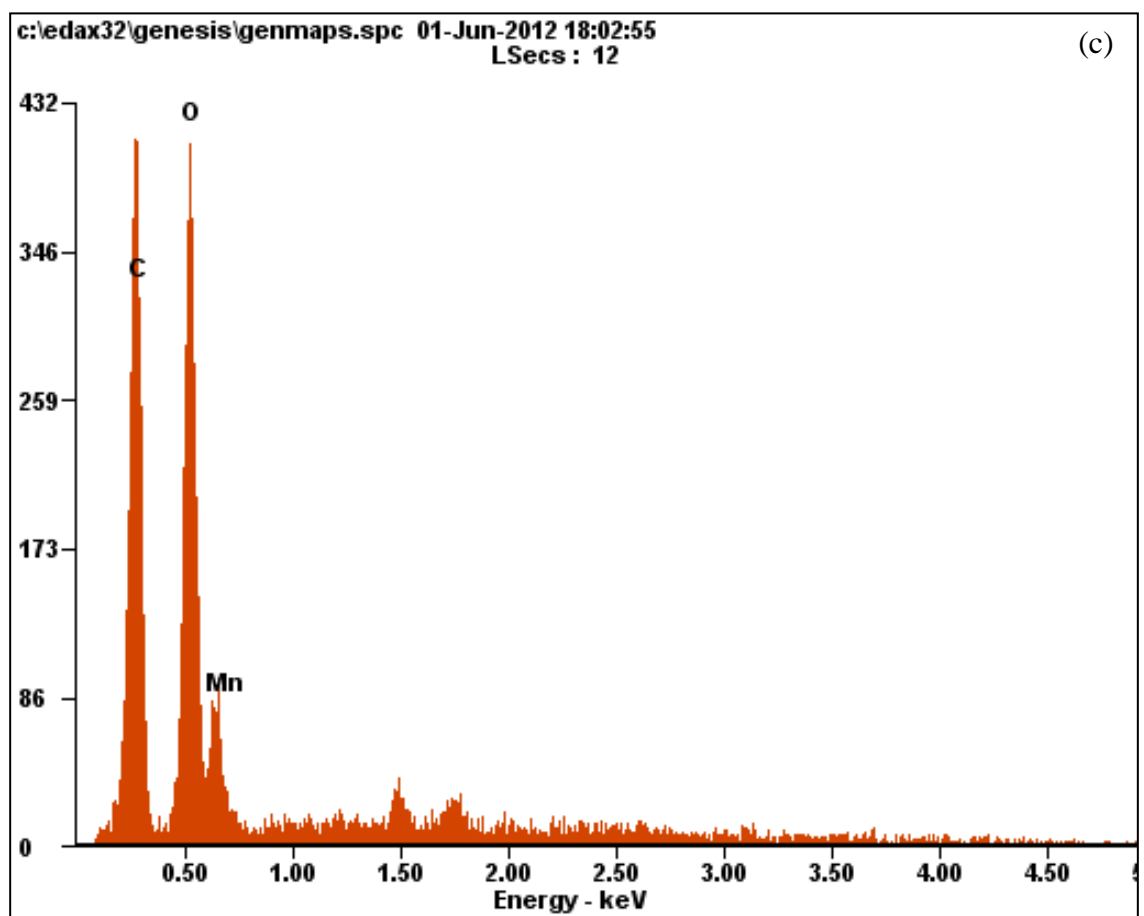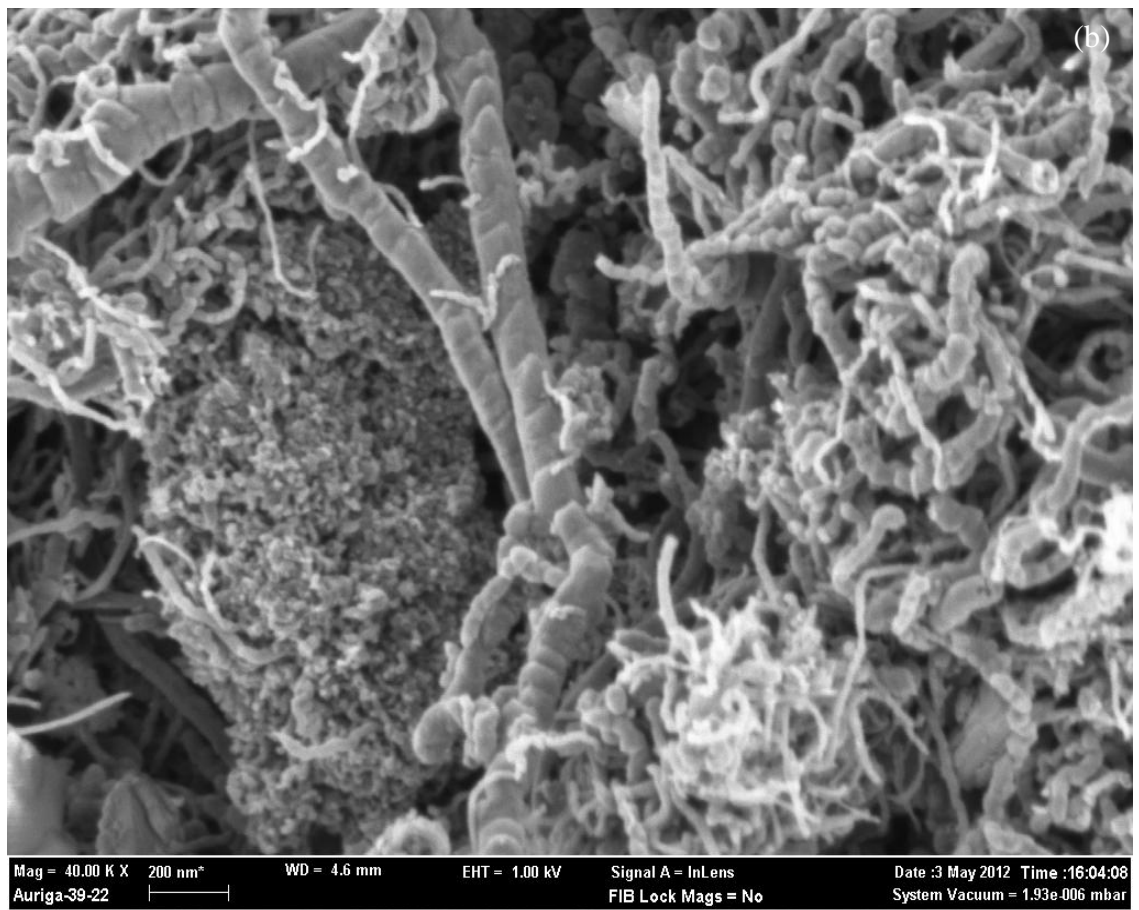
62

Figure 4.7: Results of Sample S6 (a) FESEM image at 40kX (b) FESEM image at 40kX

(c) EDX spectrum analysis (d) TEM image analysis

4.2.7 Sample S7

Figure 4.8 shows the FESEM / EDX / TEM images of the composites S7 (0.35 mole MnO_2 + 0.15 mole MWCNT). Based on Figure 4.8 (a) and (b), the mole increase of MnO_2 shows more MWCNT coated with MnO_2. The spread of the composite are even throughout the sample, with more composite with similar composition and diameter are observed. The diameter of composites S7 is around 52 nm, as shown Figure 4.8 (d) observed via TEM. Figure 4.8 (c) shows the EDX spectrum on S7 with more weight presence of MnO_2 (> 70% wt), compared to S6 (> 64% wt).

Mag = 40.00 K X   300 nm*   WD = 5.2 mm   EHT = 1.00 kV   Signal A = InLens   Date :3 May 2012   Time :16:42:36
Auriga-39-22   FIB Lock Mags = No   System Vacuum = 1.28e-006 mbar

(b)

Pa 2
Pa R2
Pa 2 = 51.47 nm
Pa 3 = 41.87 nm
Pa 3
Pa R3
Pa 1
Pa R1
Pa 1 = 58.08 nm

Mag = 40.00 K X   200 nm*   WD = 5.1 mm   EHT = 1.00 kV   Signal A = InLens   Date :3 May 2012 Time :16:16:47
Auriga-39-22   FIB Lock Mags = No   System Vacuum = 1.54e-006 mbar

c:\edax32\genesis\genmaps.spc 01-Jun-2012 17:34:10
LSecs : 5

(c)

65
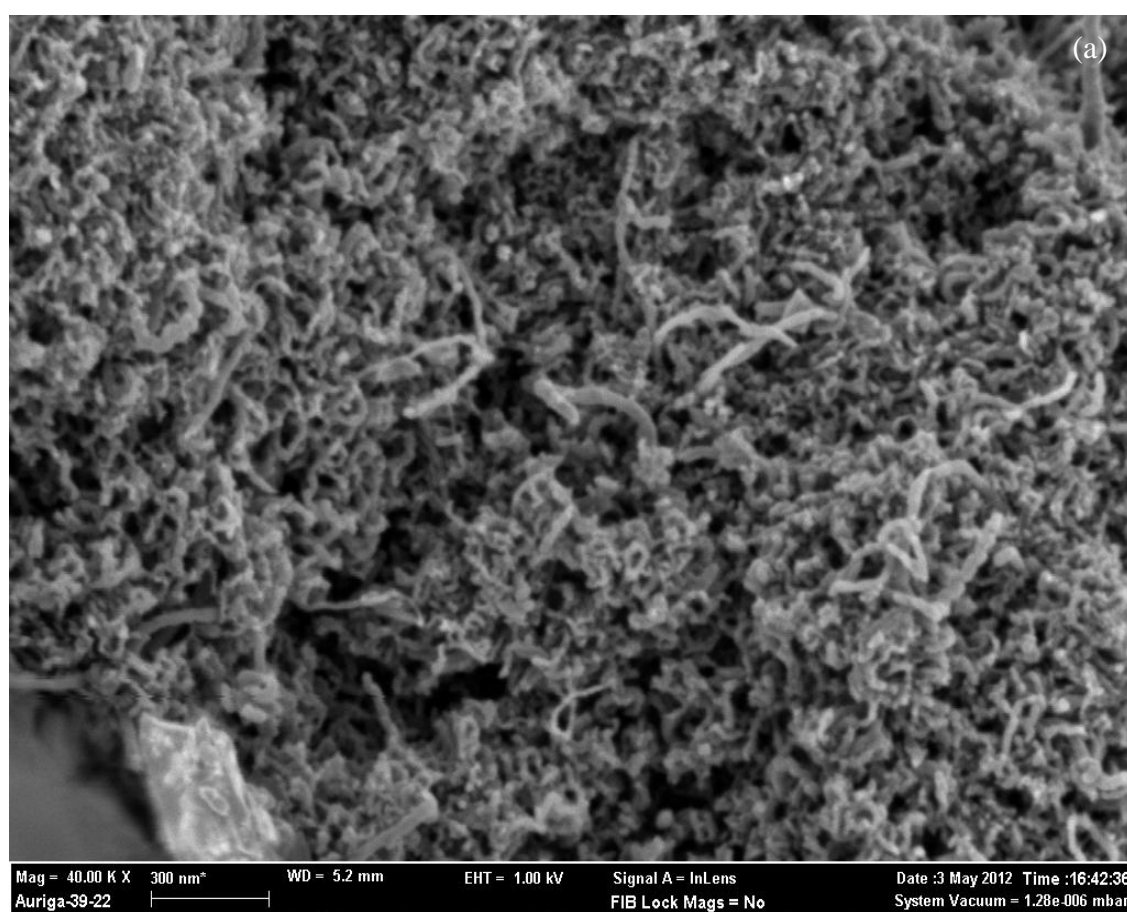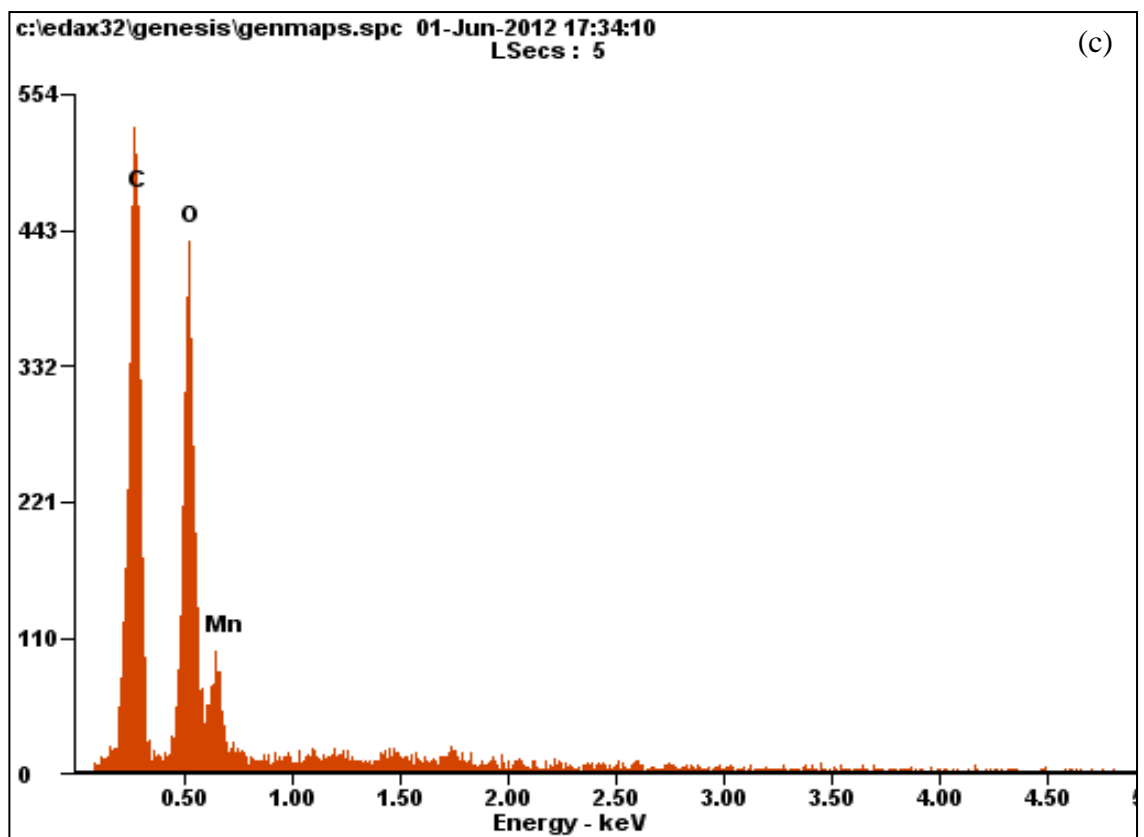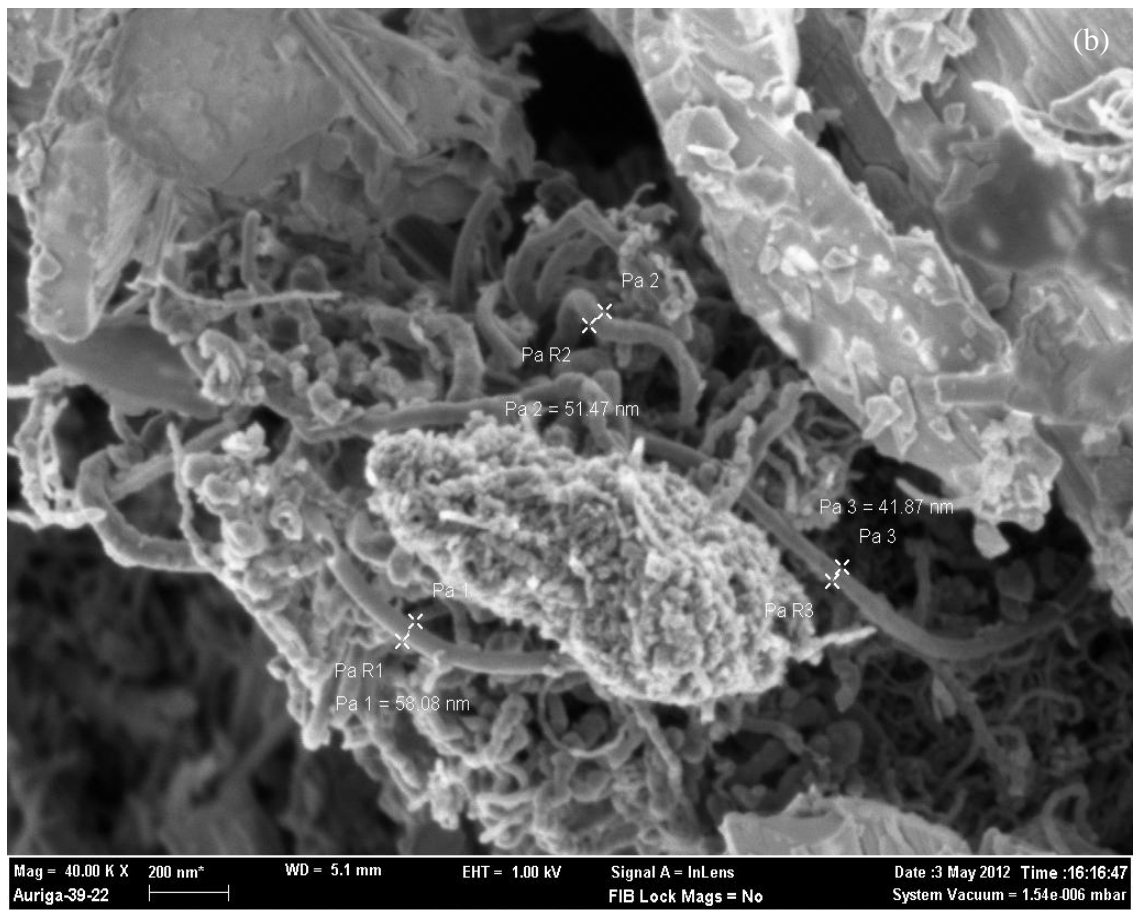
Figure 4.8: Results of sample S7 (a) FESEM image at 40kX (b) FESEM image at 40kX

(c) EDX spectrum (d) TEM image

4.2.8 Sample S8

Figure 4.9 shows the FESEM / EDX / TEM results of the composites S8 (0.40 mole MnO_2 + 0.10 mole MWCNT). Based on Figure 4.9 (a) and (b), more MnO_2 can be observed in solid form as well as coated on MWCNT. However, the spread of the composite are homogeneous throughout the sample. The diameter of composites S8, as shown in Figure 4.9 (d), shows the diameter around 57 nm. Figure 4.9 (c) shows the EDX spectrum on S8. The weight presence of MnO_2 (> 70% wt) is higher compared to S7 (> 64% wt).

(b)

Mag = 40.00 K X   300 nm*   WD = 5.2 mm   EHT = 1.00 kV   Signal A = InLens   Date :3 May 2012 Time :16:28:47
Auriga-39-22   FIB Lock Mags = No   System Vacuum = 1.38e-006 mbar

c:\edax32\genesis\genmaps.spc 01-Jun-2012 17:22:38
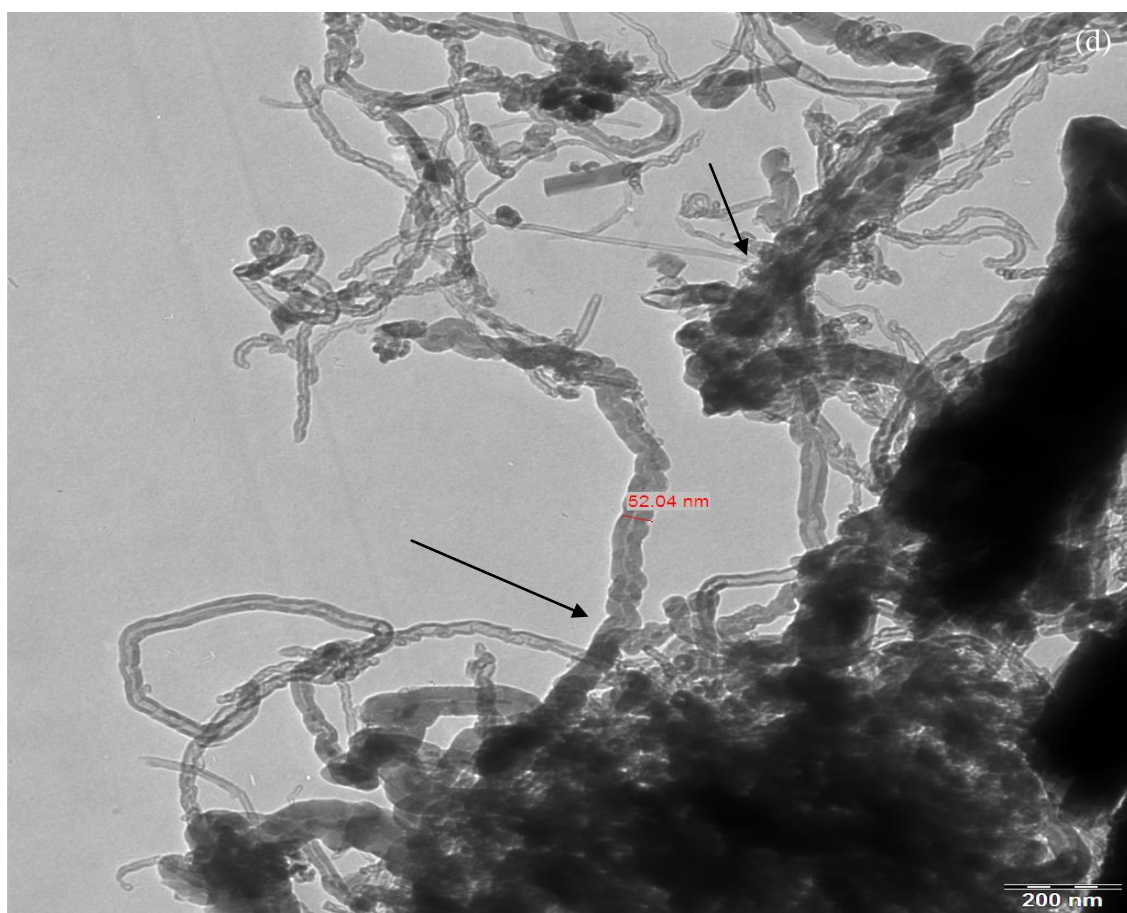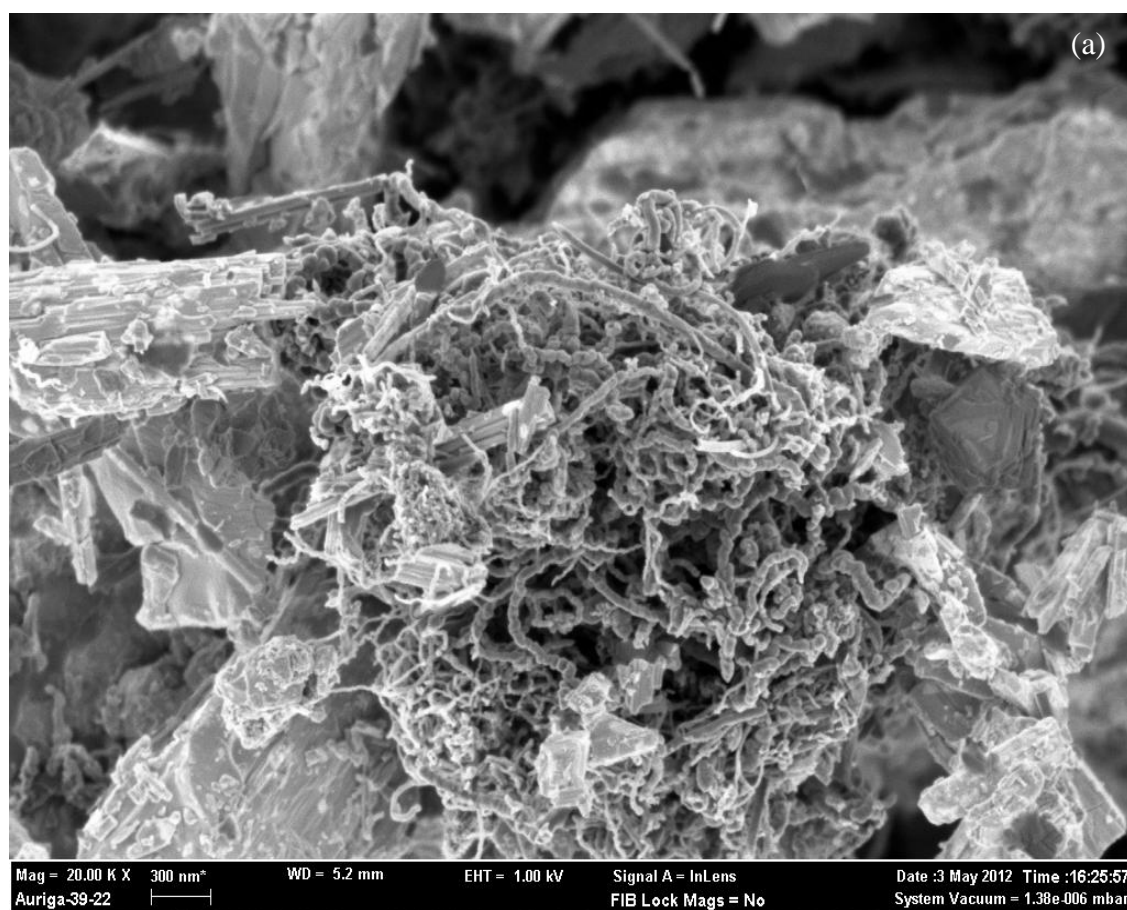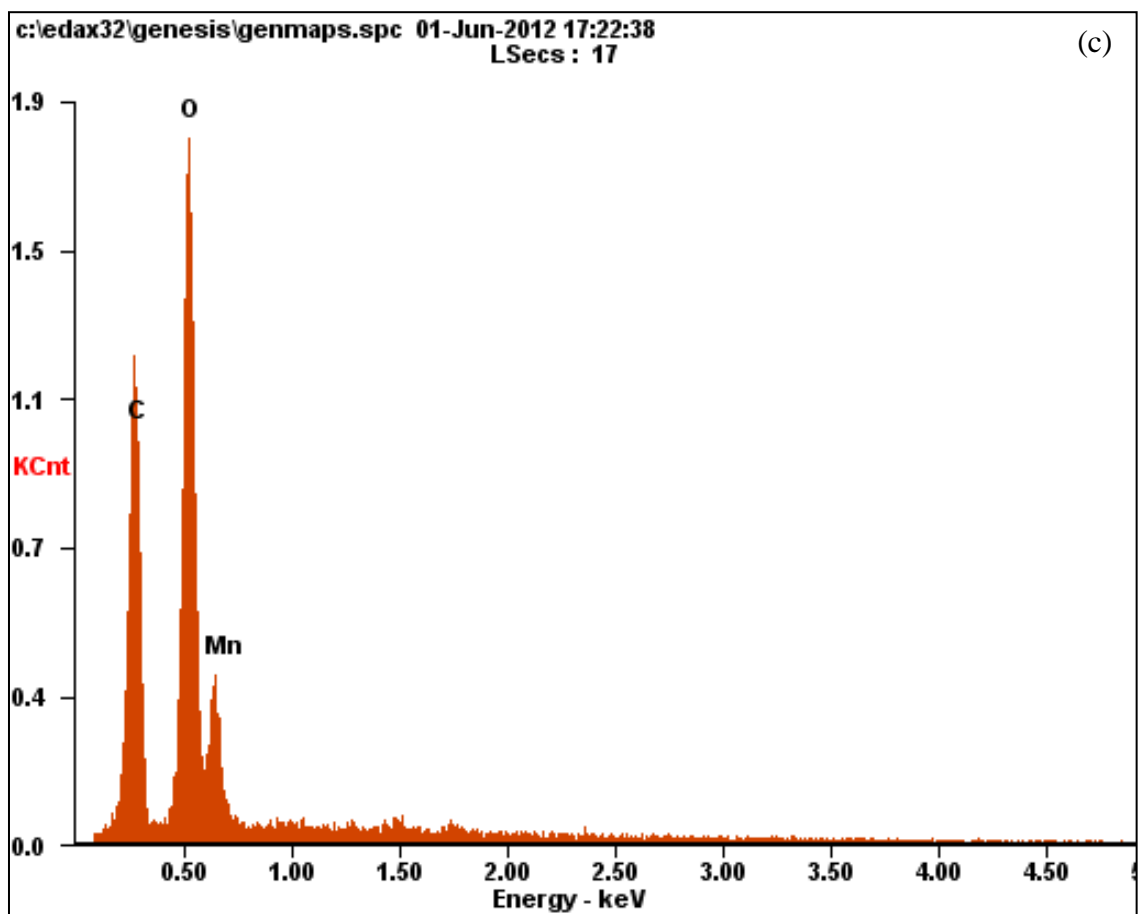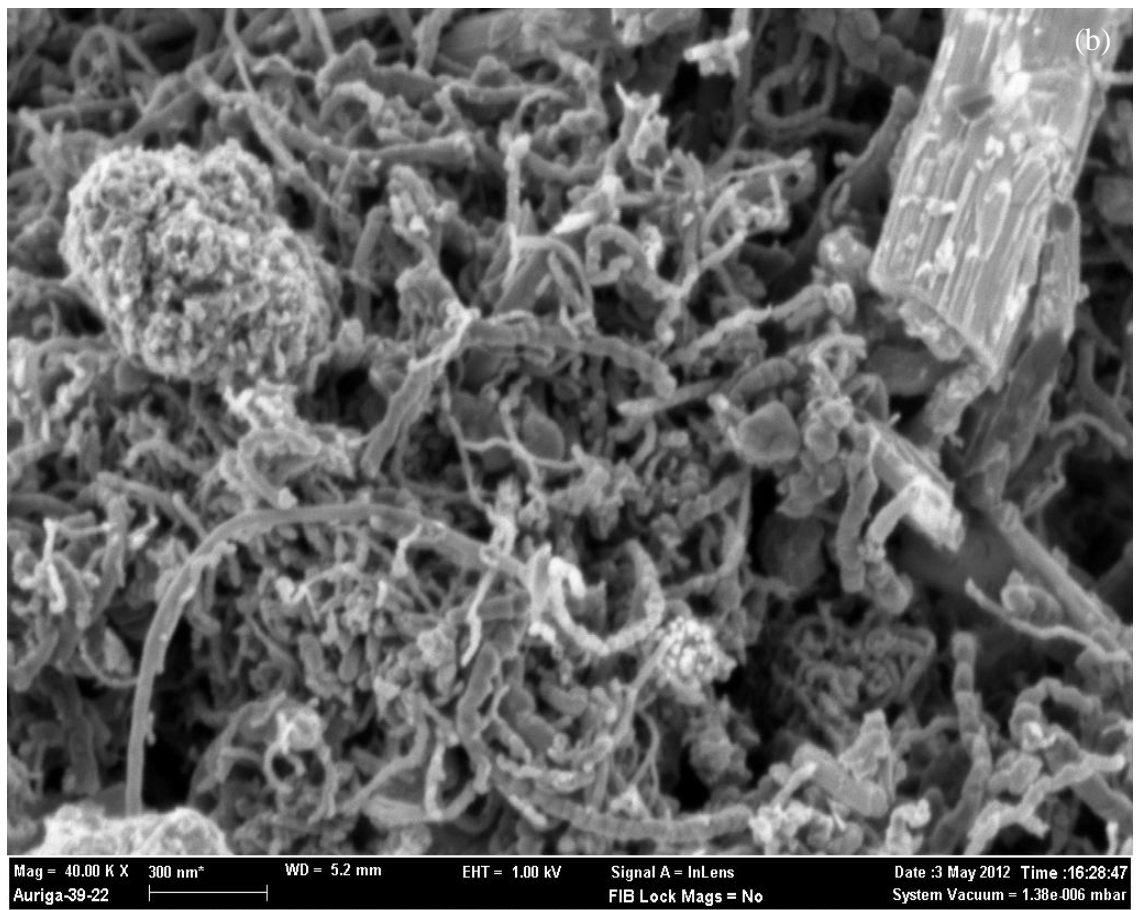LSecs : 17

(c)

Figure 4.9: Results of sample S8 (a) FESEM image at 20kX (b) FESEM image at 40kX

(c) EDX spectrum (d) TEM image

4.2.9 Sample S9

Figure 4.10 shows the FESEM / EDX / TEM results of the composites S9 (0.45 mole MnO_2 + 0.05 mole MWCNT). Based on Figure 4.10 (a) and (b), homogeneous composites in sizes can be observed. TEM images as shown in Figure 4.10 (d) shows the diameter of composites S9 around 71 nm. Figure 4.10 (d) shows the EDX spectrum on S9, which shows slightly more weight presence of MnO_2 (> 72% wt), compared to S8 (> 70% wt).
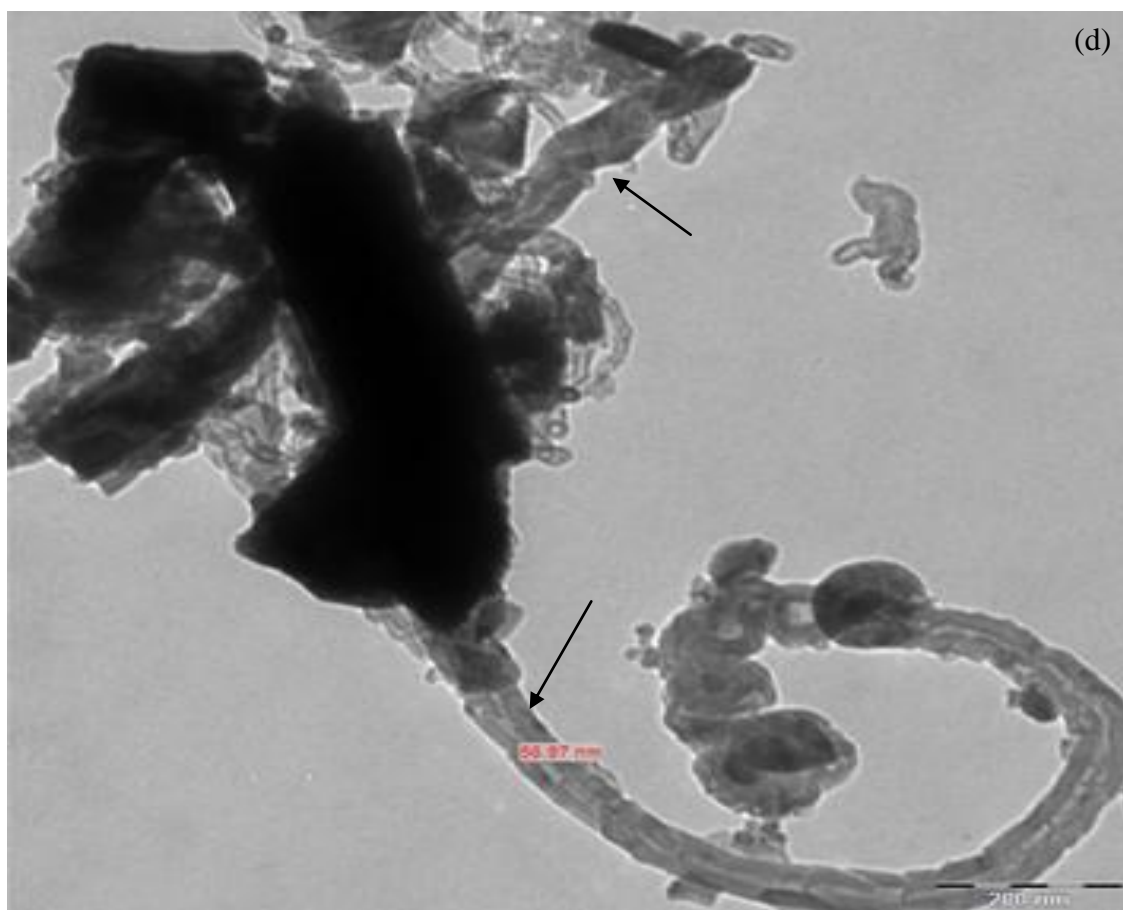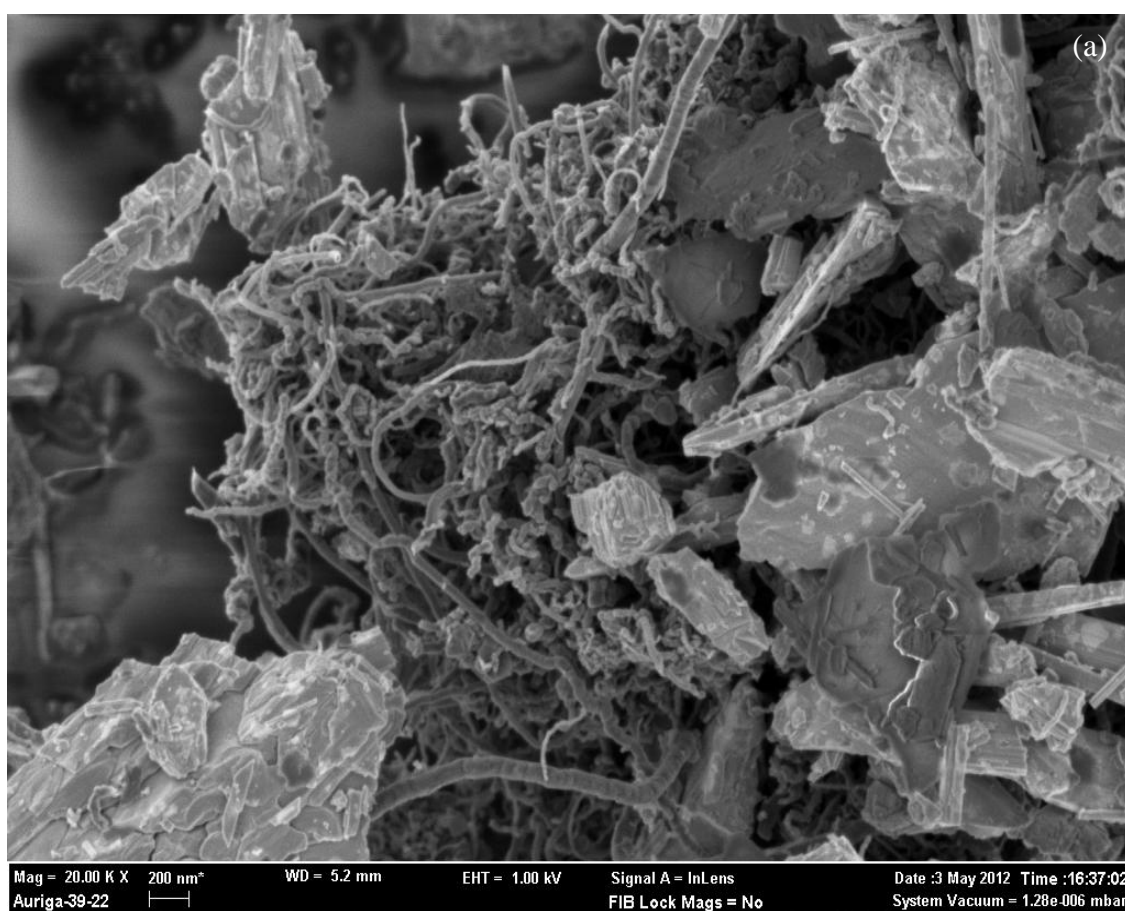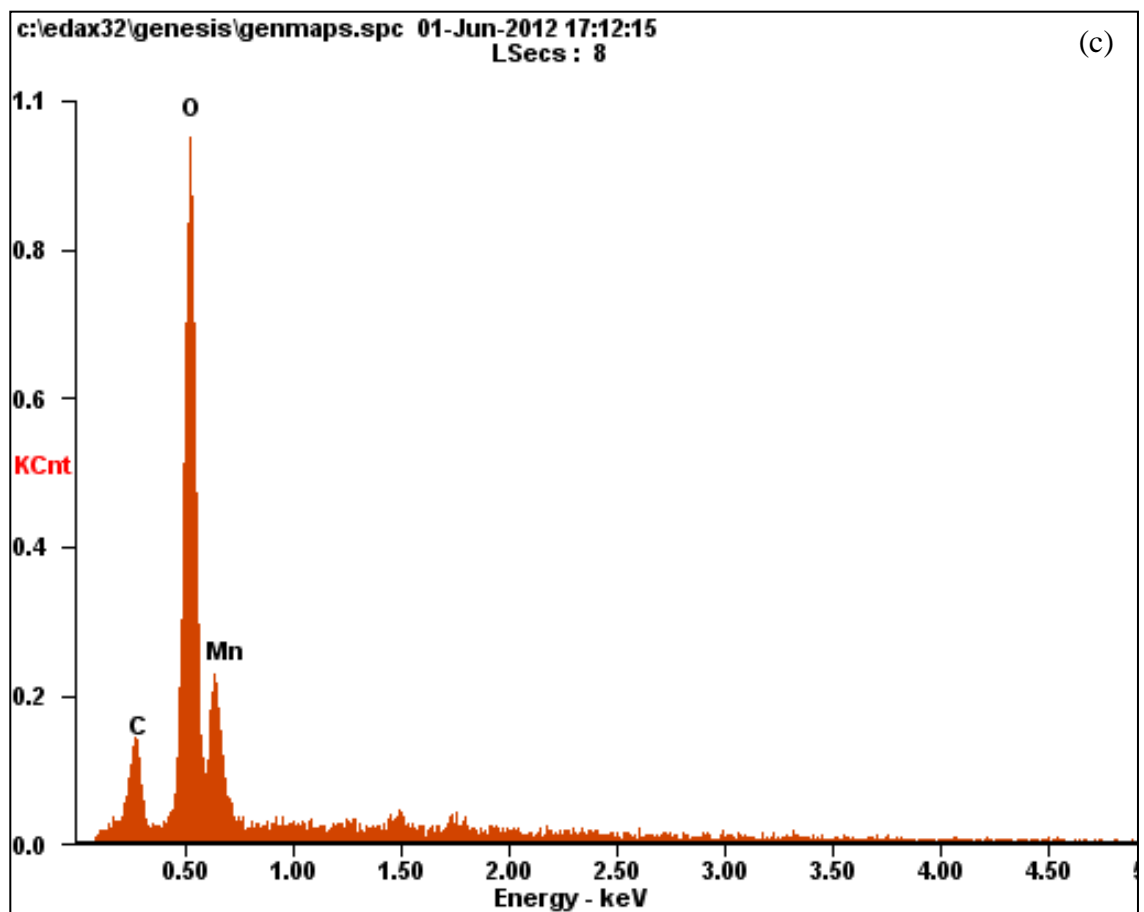
Figure 4.10: Results of Sample S9 (a) FESEM image at 20kX (b) FESEM image at

40kX (c) EDX spectrum (d) TEM image

4.2.10 Sample S10 (Control for MnO2)

Figure 4.11 shows the FESEM / EDX / TEM results of the control sample S10 (0.2 mole MnO_2 - 17.39g). Based on Figure 4.11 (a) and (b), the diameter of MnO_2 is around 77 nm as shown in Figure 4.11(d). Figure 4.11 (c) shows the EDX spectrum on S10 with higher presence of MnO_2 (> 79% wt), compared to S9 (> 72% wt). This confirms with the original sample procured with the supplier at 80% purity.

(b)

Pa R2
Pa 2
Pa 2 = 27.63 nm
Pa 3
Pa 1
Pa R3
Pa R1
Pa 3 = 27.53 nm
Pa 1 = 29.14 nm

Mag = 80.00 K X   100 nm*   WD = 3.2 mm   EHT = 1.00 kV   Signal A = InLens   Date :2 May 2012 Time :11:59:01
Auriga-39-22   FIB Lock Mags = No   System Vacuum = 1.23e-006 mbar

c:\edax32\genesis\genmaps.spc 31-May-2012 12:49:28
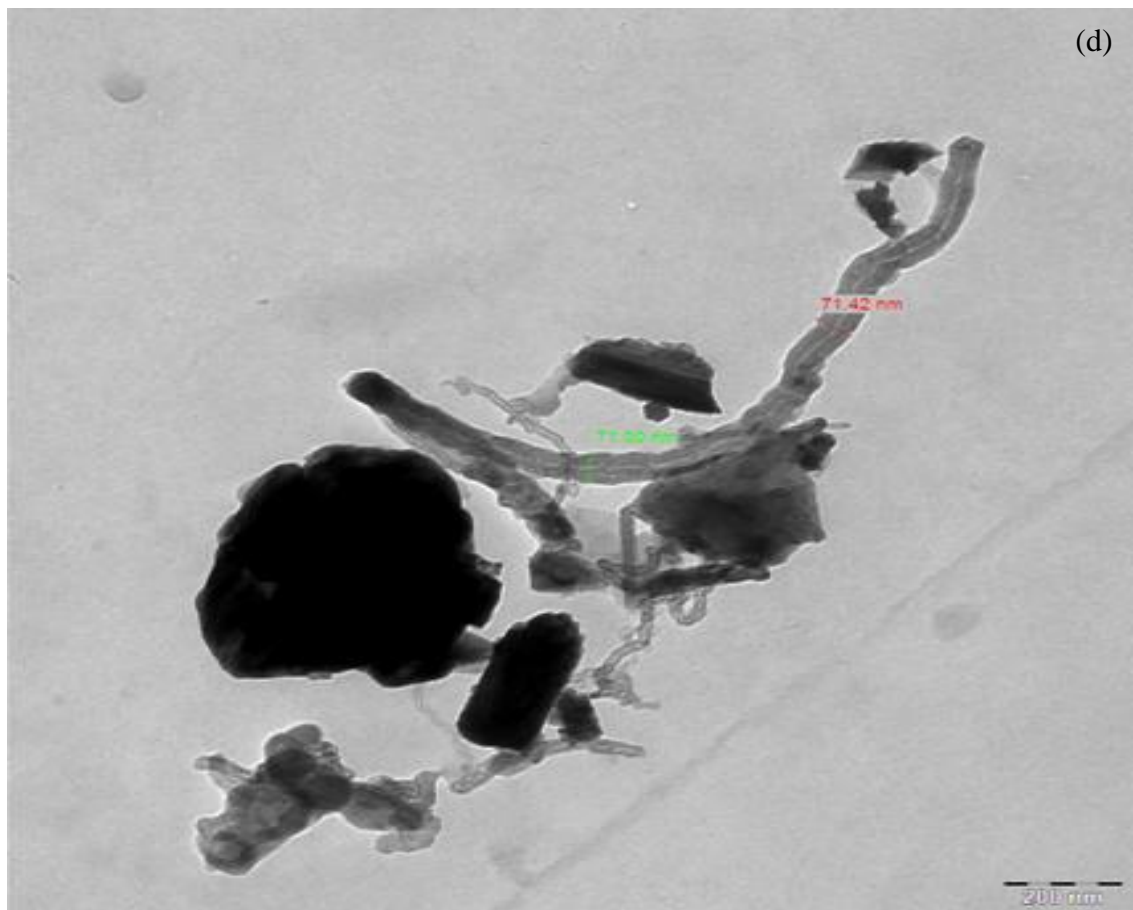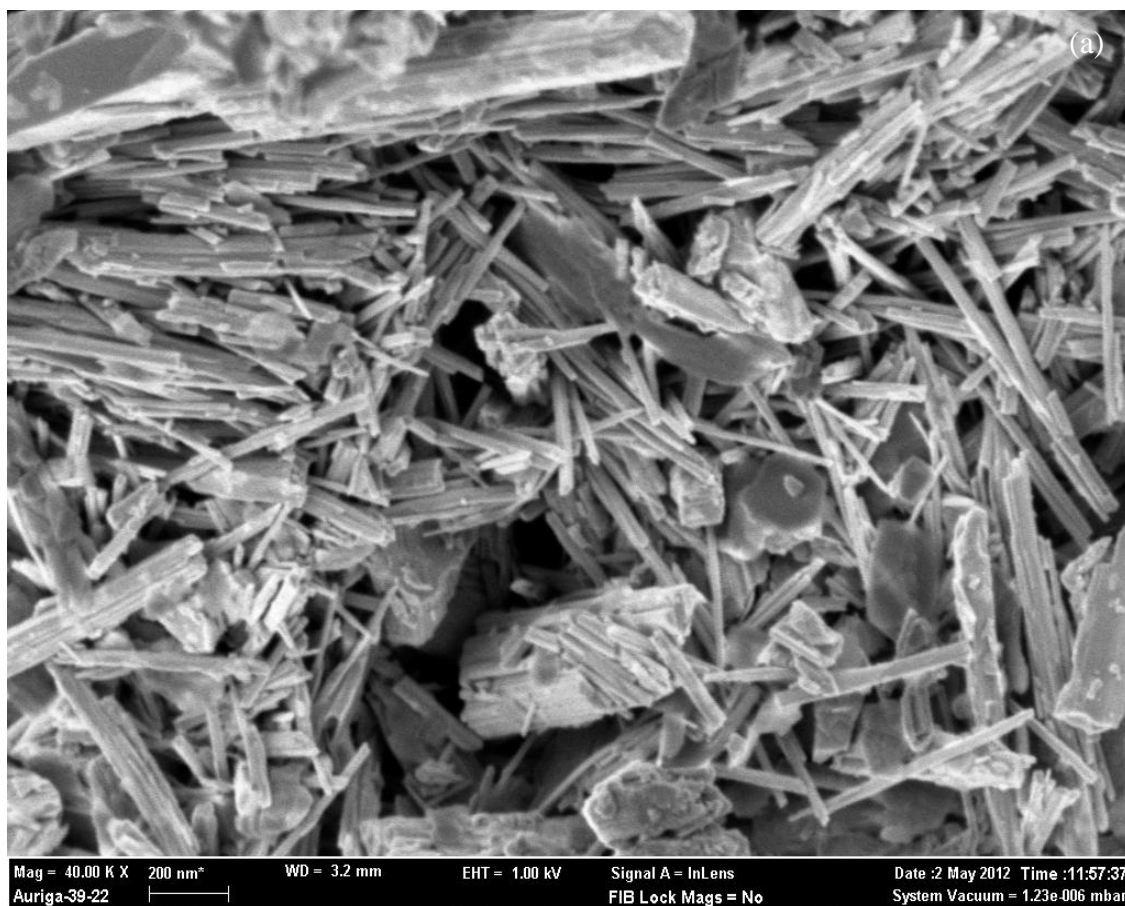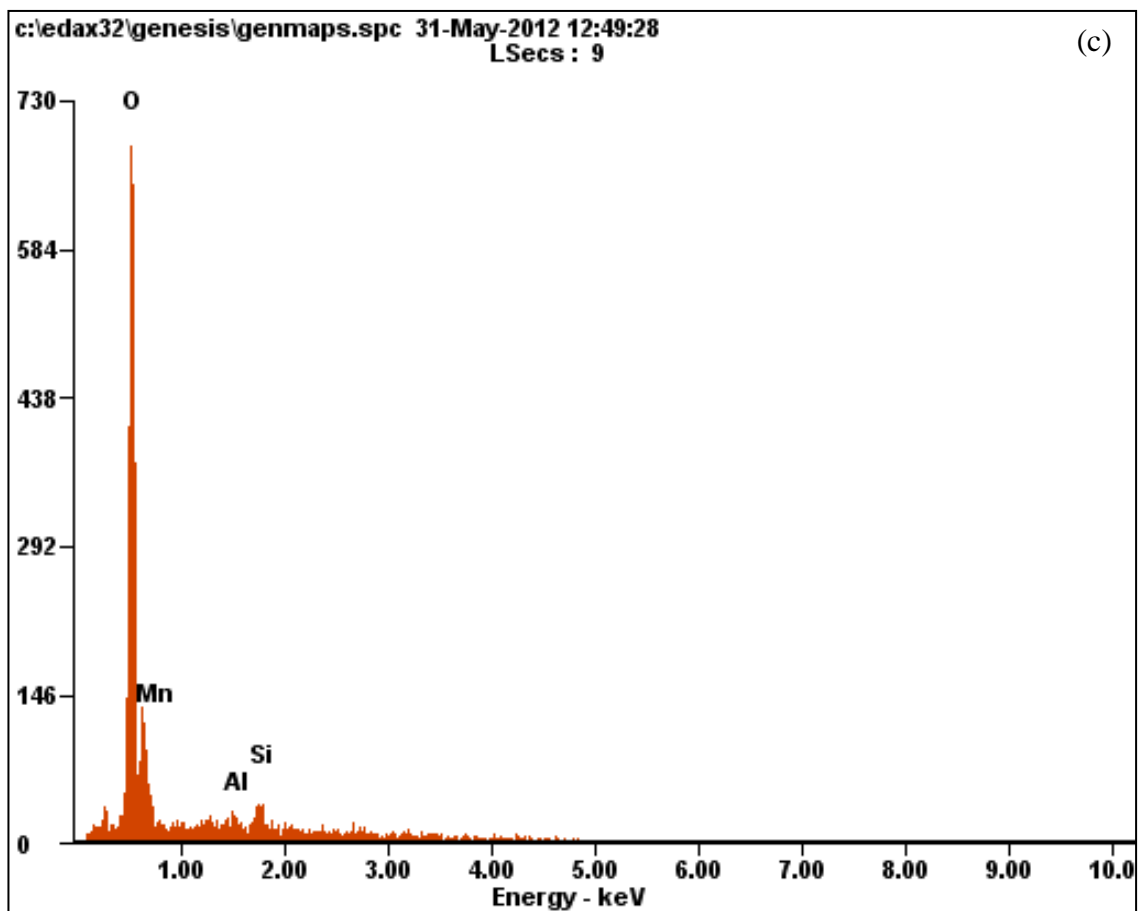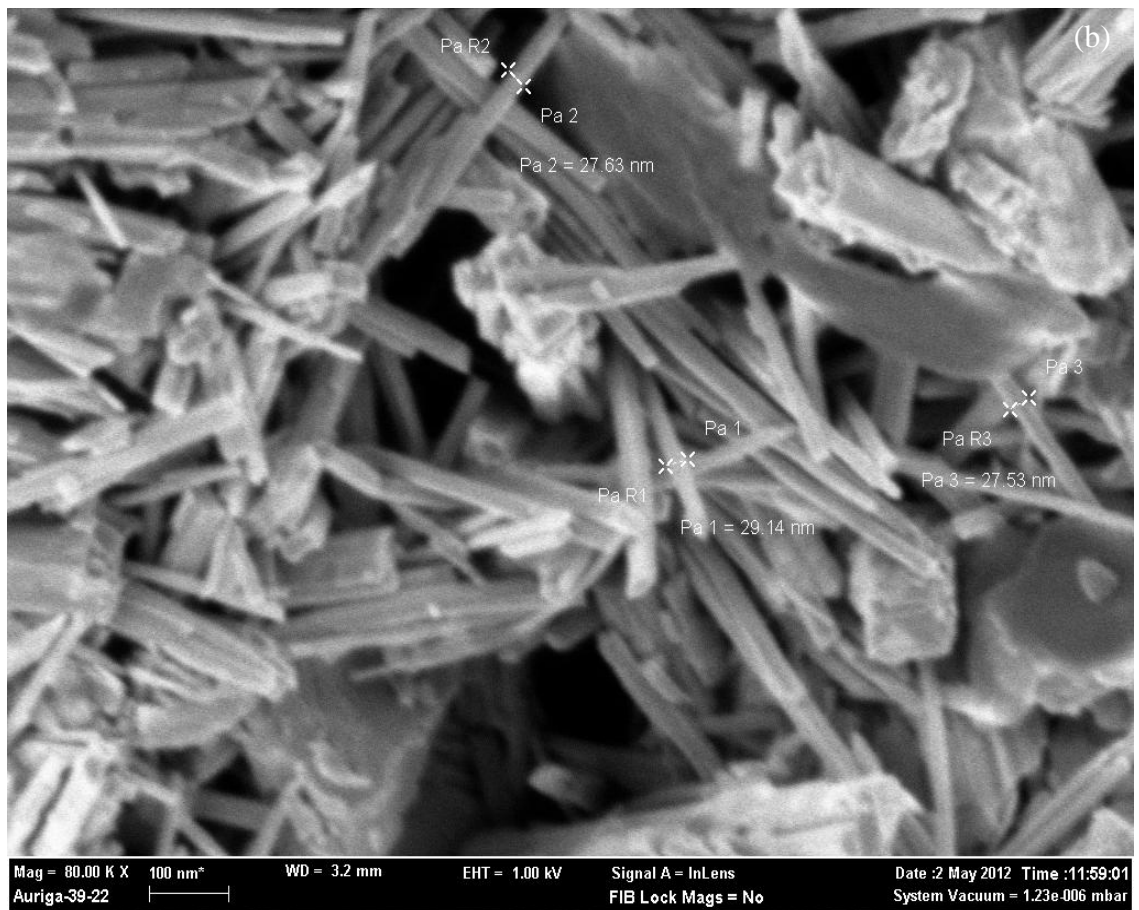LSecs : 9

(c)

74

Figure 4.11: Results of Sample S10 (a) FESEM image at 40kX (b) FESEM image at

80kX (c) EDX spectrum (d) TEM image

4.2.11 Sample S11 (Control for MWCNT)

Figure 4.12 shows the FESEM / EDX / TEM results of the composites S11 (1 mole MWCNT - 12g). Based on Figure 4.12 (a) and (b), the diameter of MWCNT as shown in Figure 4.12 (d) is less than 20 nm. Figure 4.12 (c) shows the EDX spectrum on S11 with weight presence of Carbon (> 90% wt).

| Mag = 10.00 K X 1 μm* | WD = 4.6 mm | EHT = 1.00 kV | Signal A = InLens | Date :3 May 2012 Time :16:45:30 |
| Auriga-39-22 | | | FIB Lock Mags = No | System Vacuum = 1.23e-006 mbar |

(b)

Mag = 40.00 K X 200 nm* WD = 4.6 mm EHT = 1.00 kV Signal A = InLens Date :3 May 2012 Time :16:46:29
Auriga-39-22 FIB Lock Mags = No System Vacuum = 1.23e-006 mbar

c:\edax32\genesis\genmaps.spc 01-Jun-2012 16:51:48
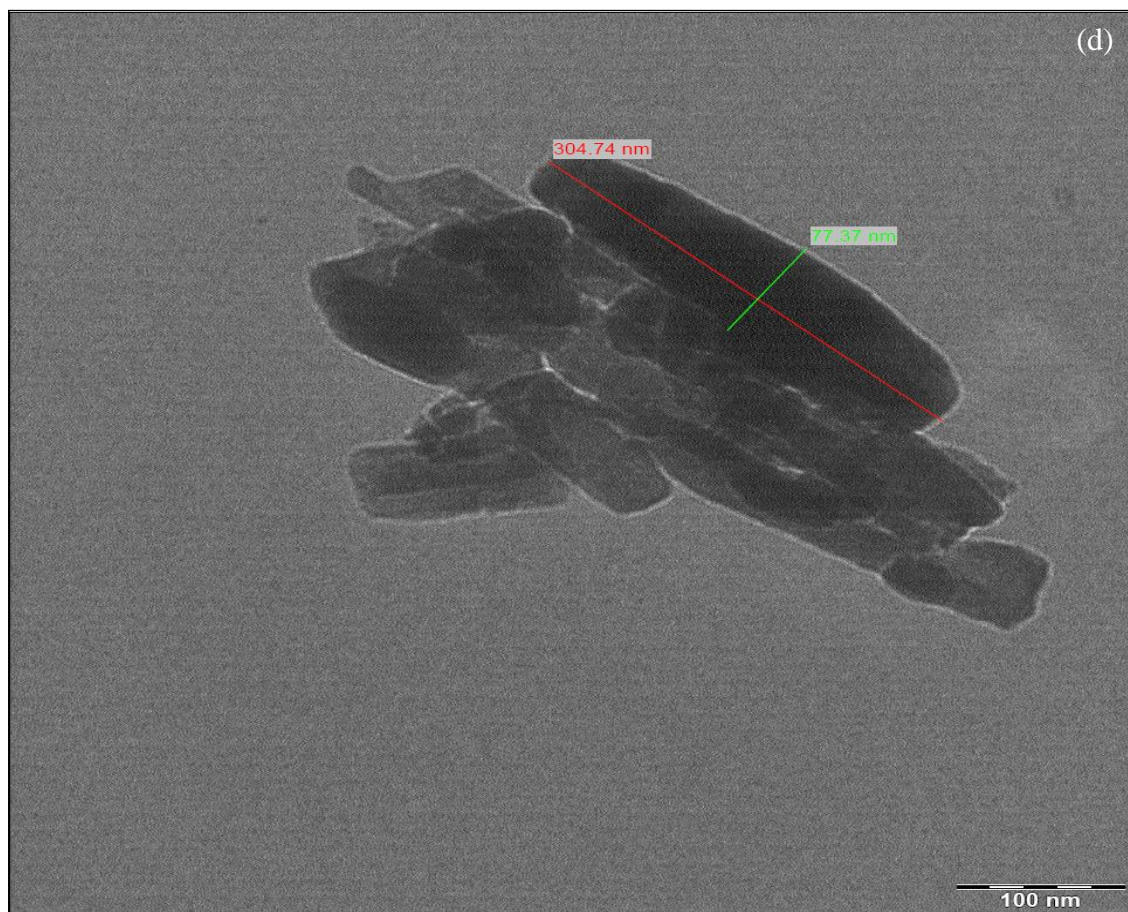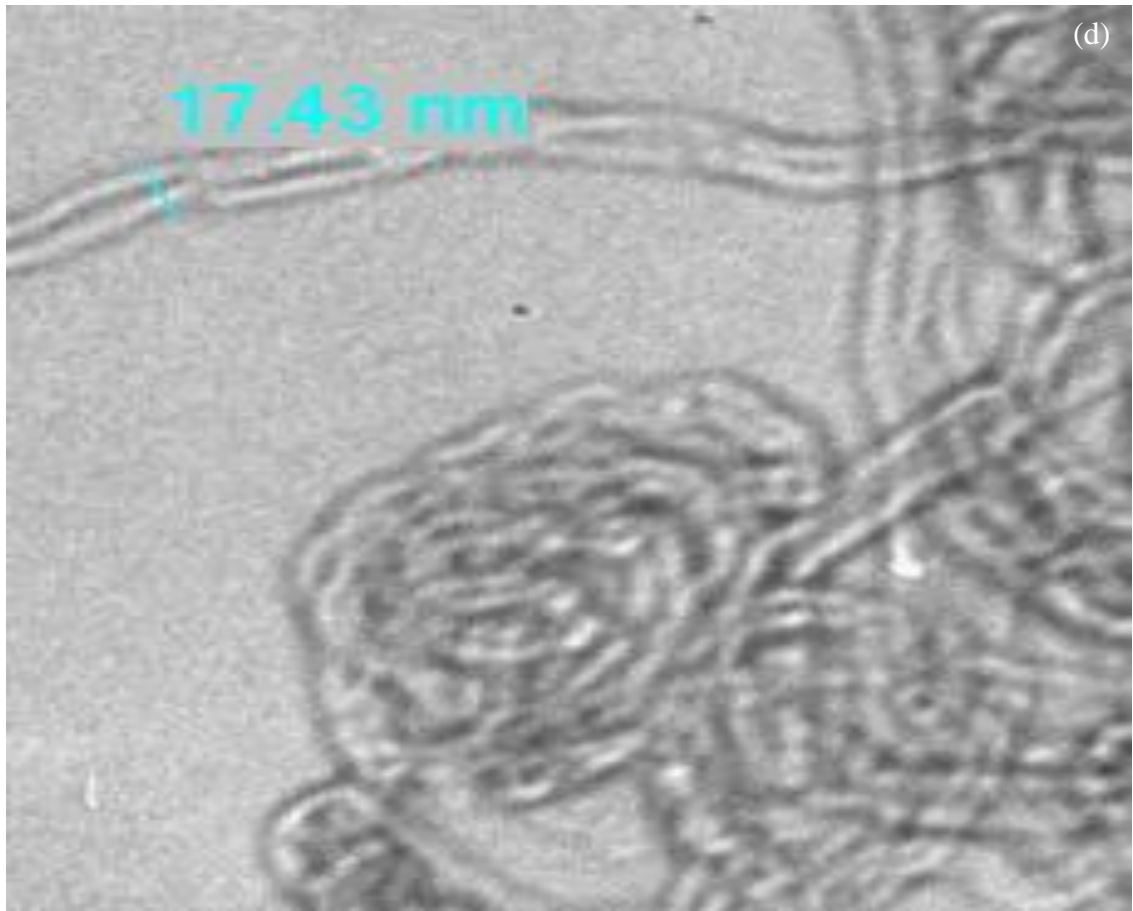LSecs : 15

(c)

(d)
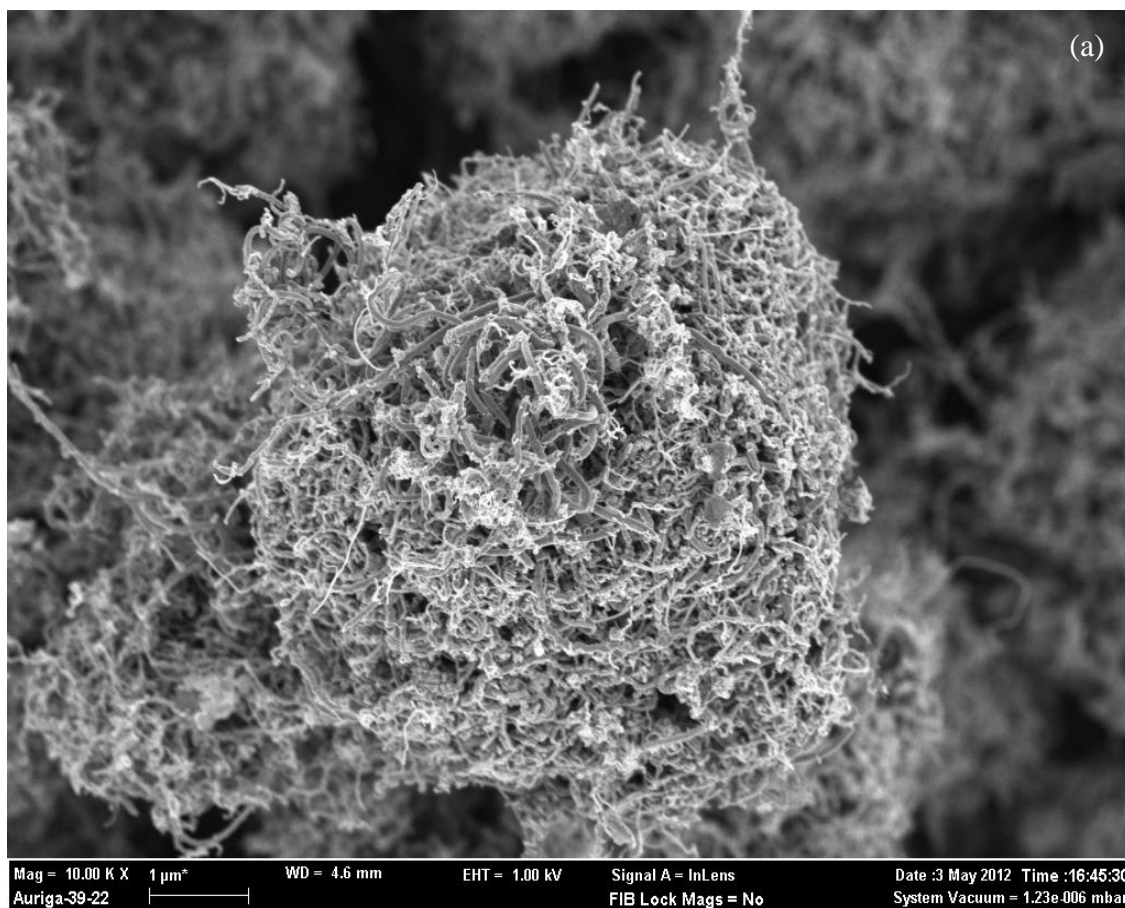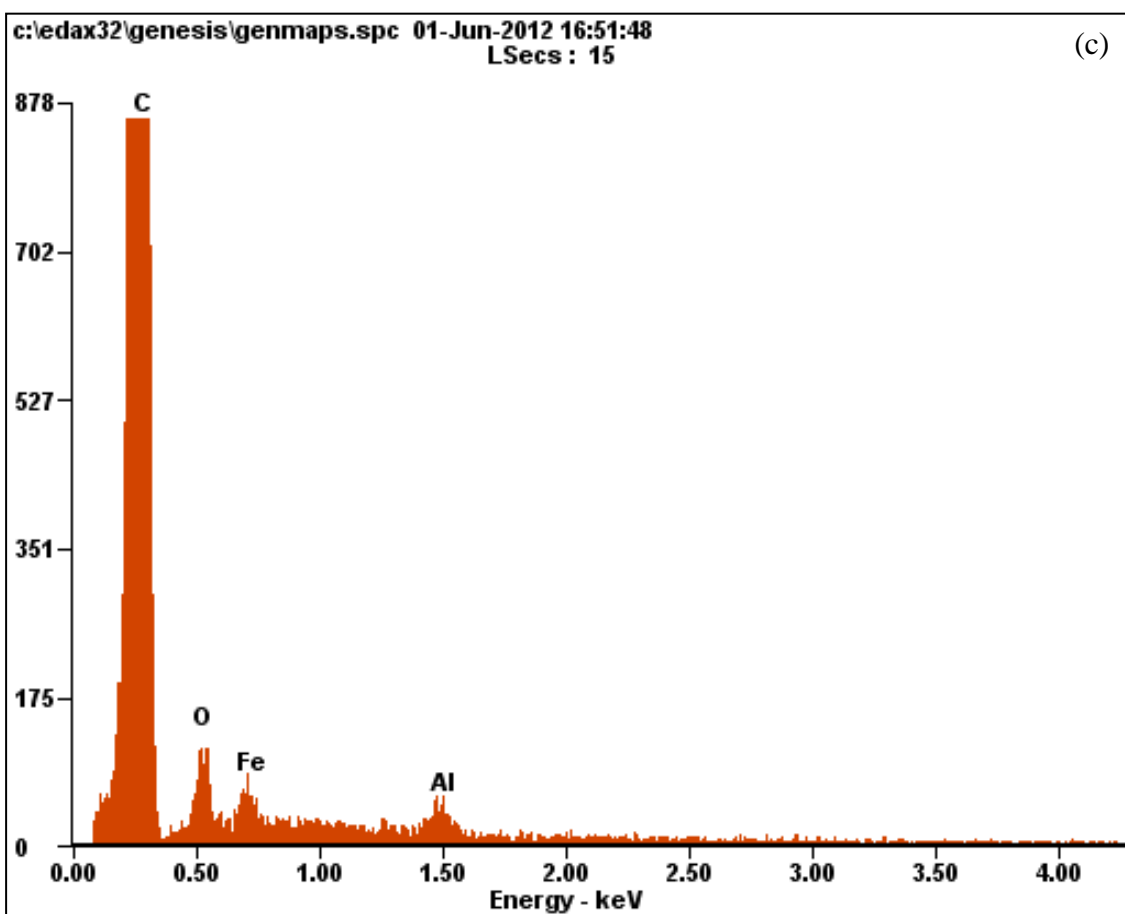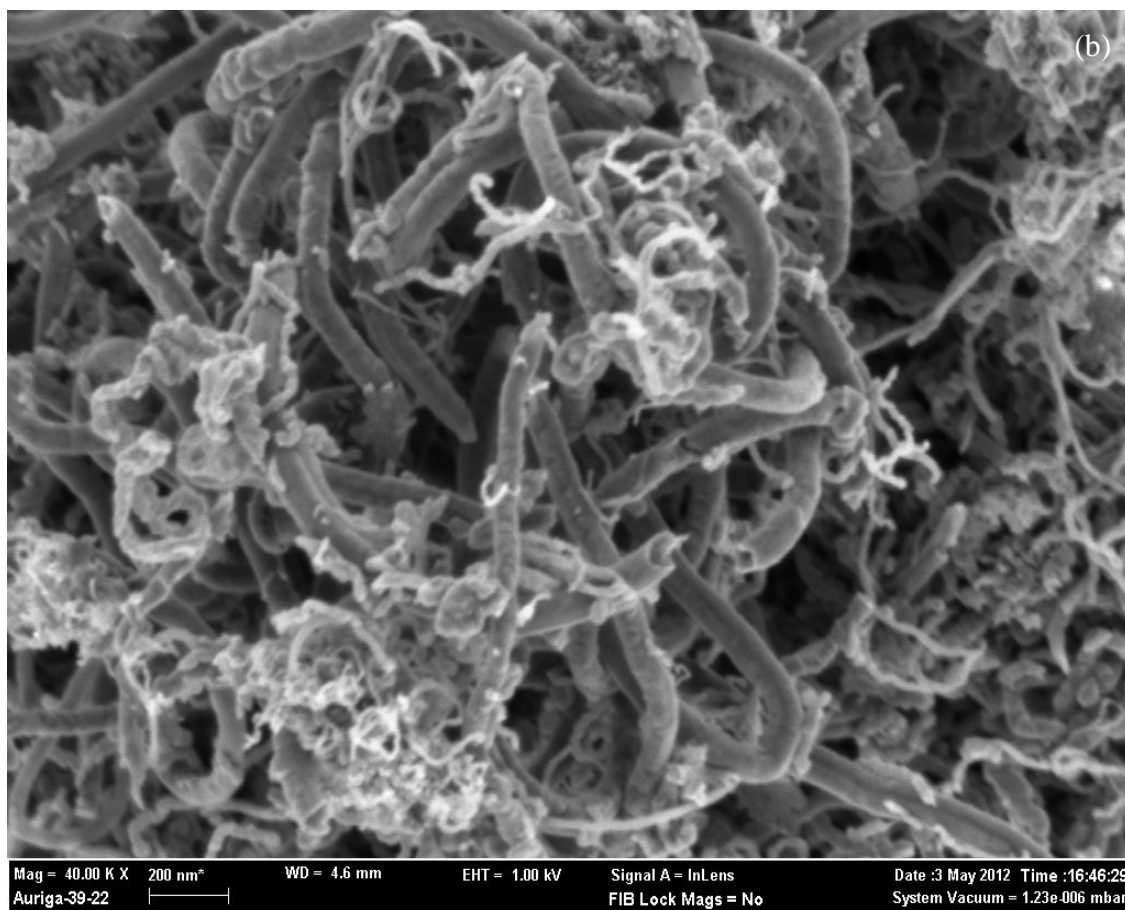
Figure 4.12: Results of Sample S11 (a) FESEM image at 10kX (b) FESEM image at

40kX (c) EDX spectrum (d) TEM image

4.3 Thermal studies of MnO_2 / MWCNT composites

Figures 4.13 – 4.23 show the TGA / DTG curves for all samples of MnO_2 / MWCNT composite. Tables 4.3 summarize the results. Based on the initial finding, the weight loss was started at 42 °C for the composites, similar to MWCNT control sample, S11. However, the control sample of MnO_2 (S10), the initial weight loss temperature is at 52 °C, about 10 °C higher than MWCNT and the composites. The initial weight loss of around 1.9% (max) from 40 °C to 150 °C is due to the evaporation of H_2O from the interlayer of the weak bonding in between H_2O and composites. From 150 °C to the decomposition temperature of the samples, around 500 °C, the weight loss at this region is caused by the loss of oxygen atoms from octahedral layer framework in relation to the partial reduction of Mn4+ to Mn3+ (Bok, 2006).

The decomposition temperatures show an increase pattern from S1 (484 °C) to S9 (533 °C). This is because the addition of more MnO_2 in mole with reduction in mole of MWCNT has caused the surface of the MWCNT to be coated with more MnO_2, which in return gives the composite a better thermal stability. This also explains the reduction in weight loss (%) from S1 to S9 as the surface of the MWCNT is protected from oxidization process which changes the MWCNT to CO_2 gas above 550 °C. The unprotected surface of the MWCNT as procured (S11) shows a drastic decrease of weight loss (%) as shown in Figure 4.23, above the decomposition temperature of 534 °C due to CO_2 gas formations.

This analysis shows that the presence of MnO$_2$ coating over MWCNT via solid state method has increased the thermal stability of the composite and also protects the MWCNT from being oxidized. A similar protection against oxygen and air oxidation by coating a thin, uniform and continuous carbide films has been reported for carbon fiber before (Piquero T, 1995).

Figure 4.13: TGA / DTG curves of sample S1

Figure 4.14: TGA / DTG curves of sample S2

Figure 4.15: TGA / DTG curves of sample S3
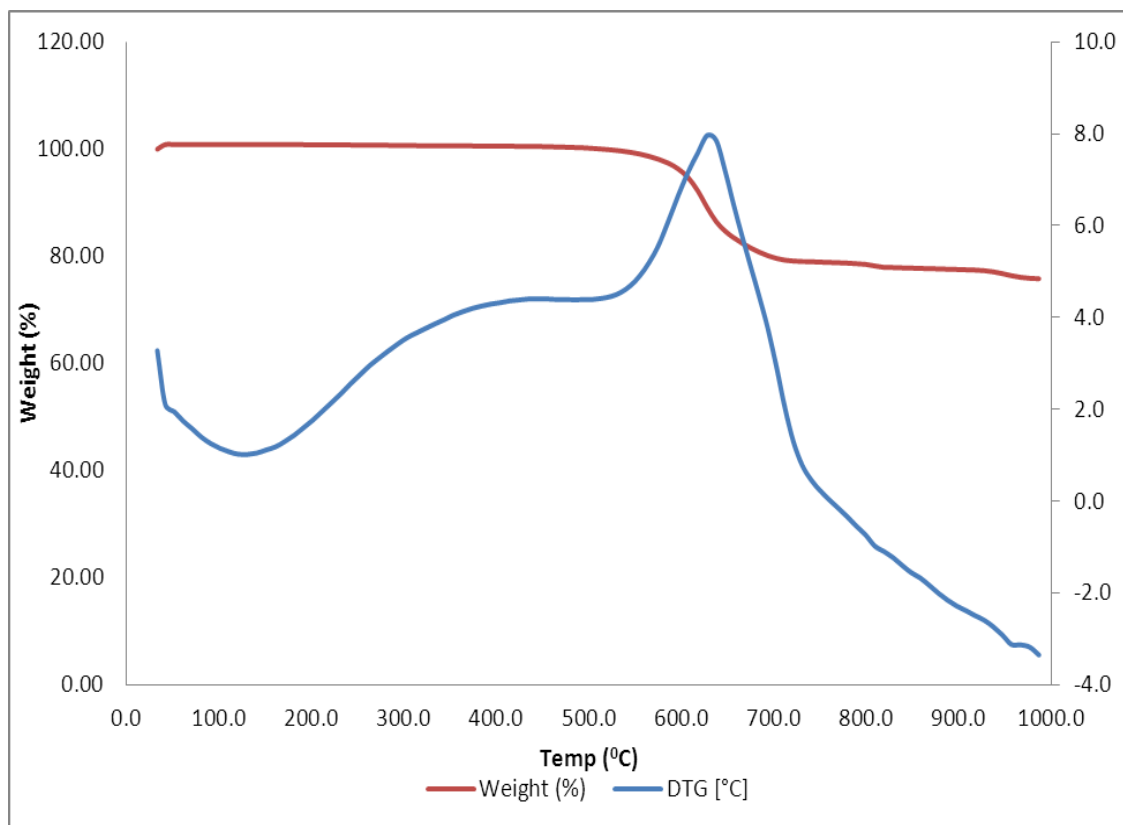
Figure 4.16: TGA / DTG curves of sample S4
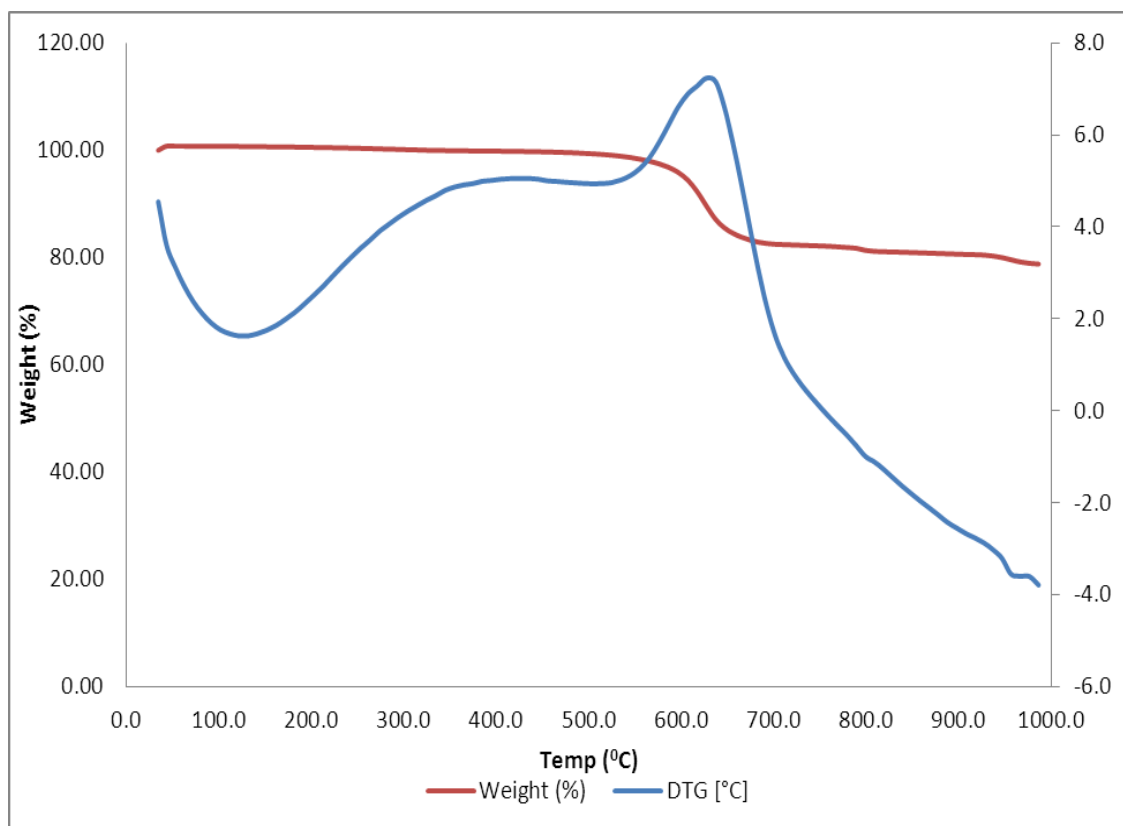
Figure 4.17: TGA / DTG curves of sample S5
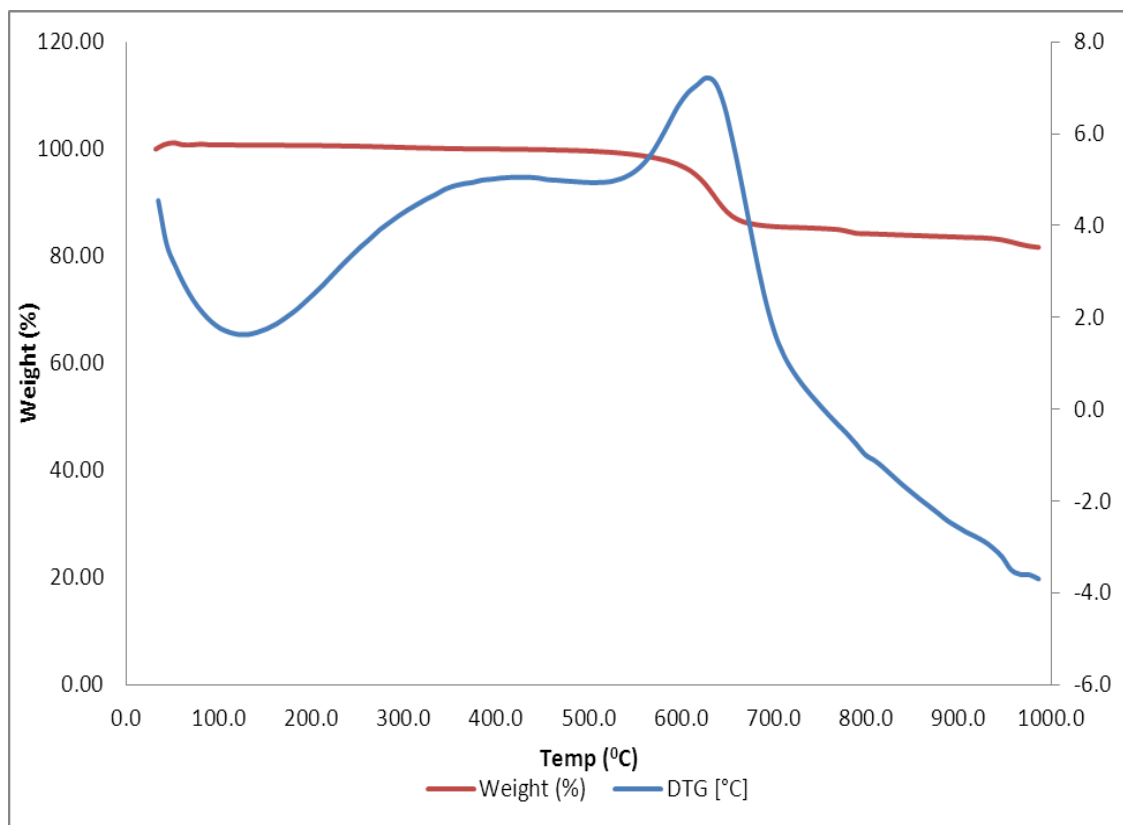
Figure 4.18: TGA / DTG curves of sample S6
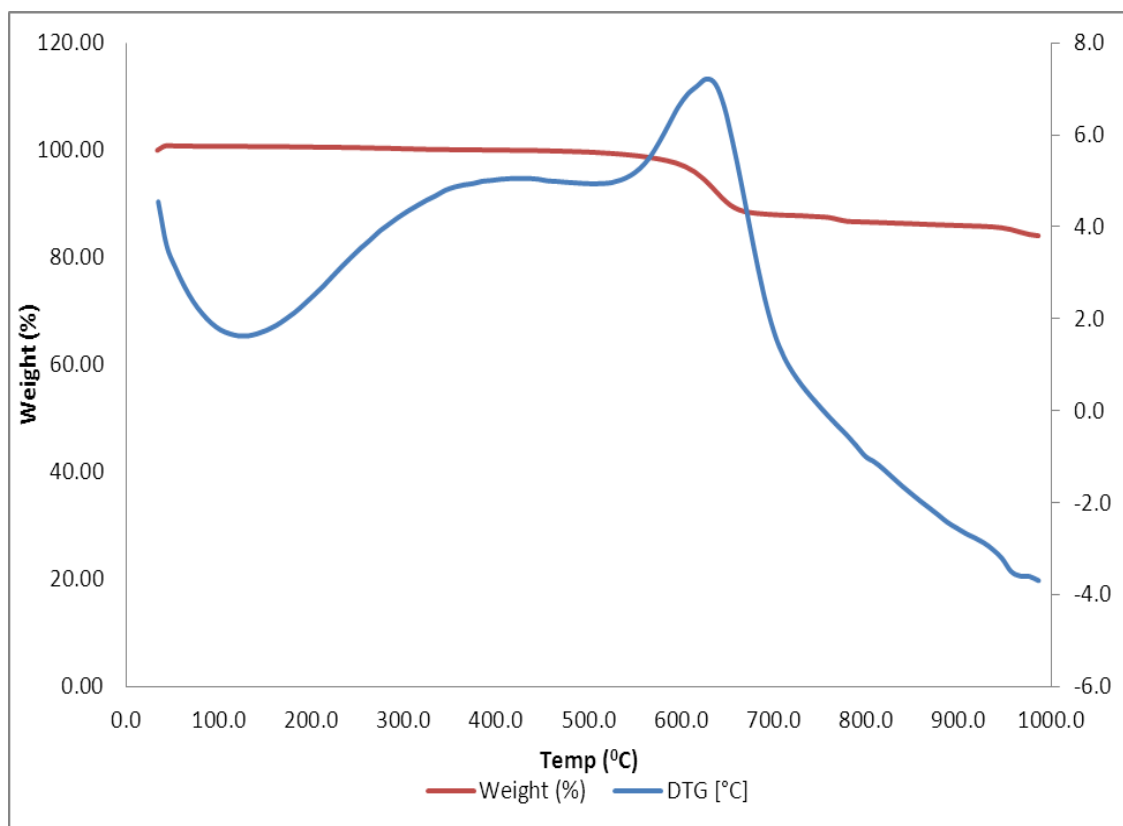
Figure 4.19: TGA / DTG curves of sample S7
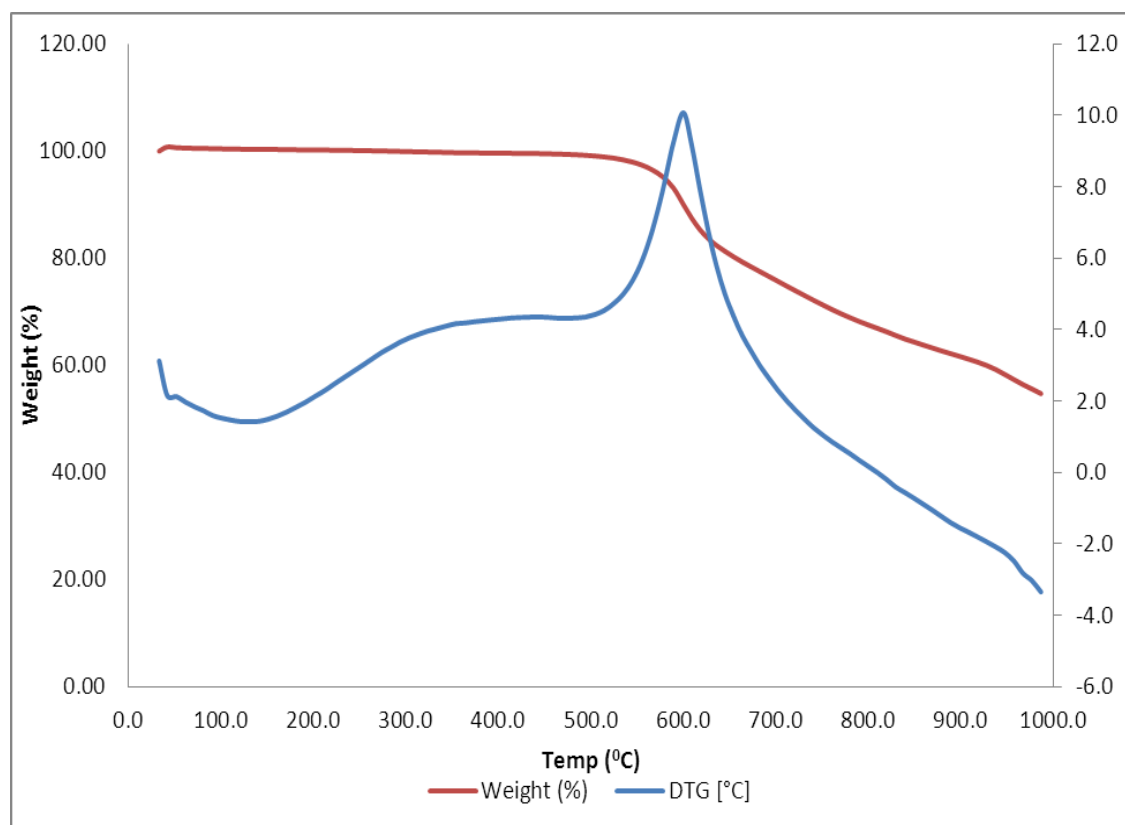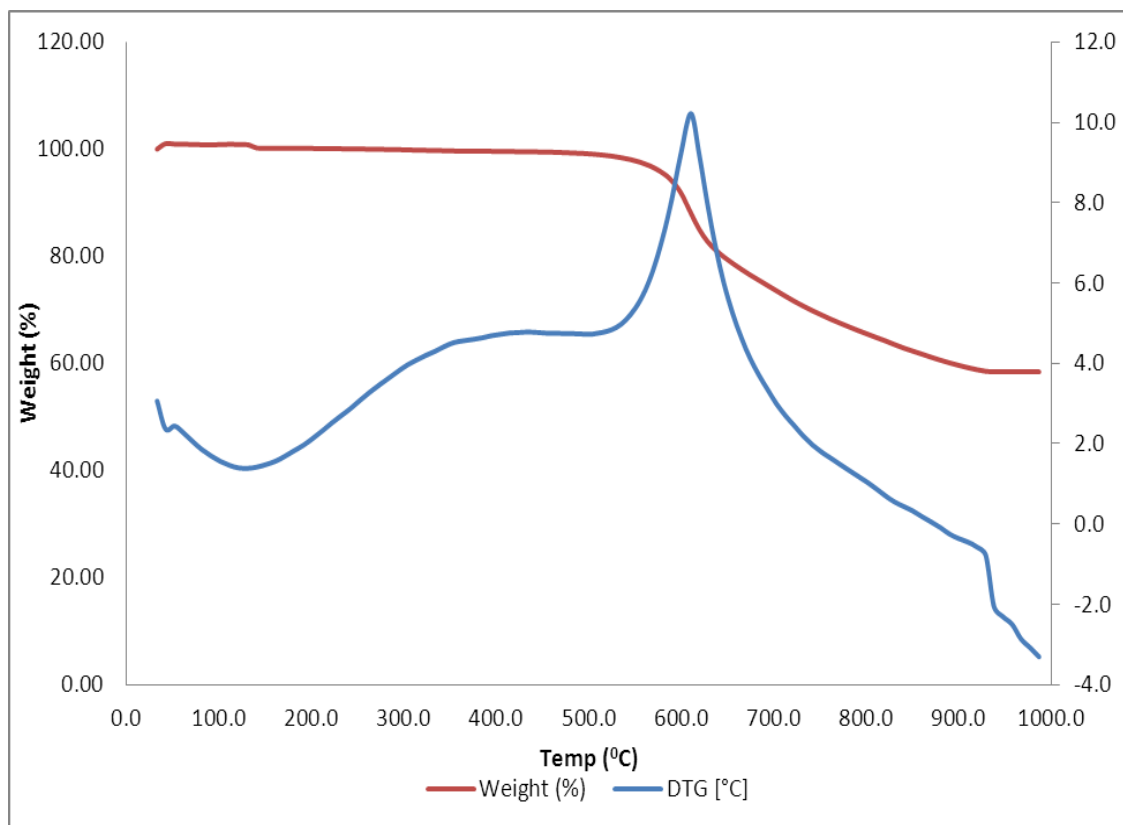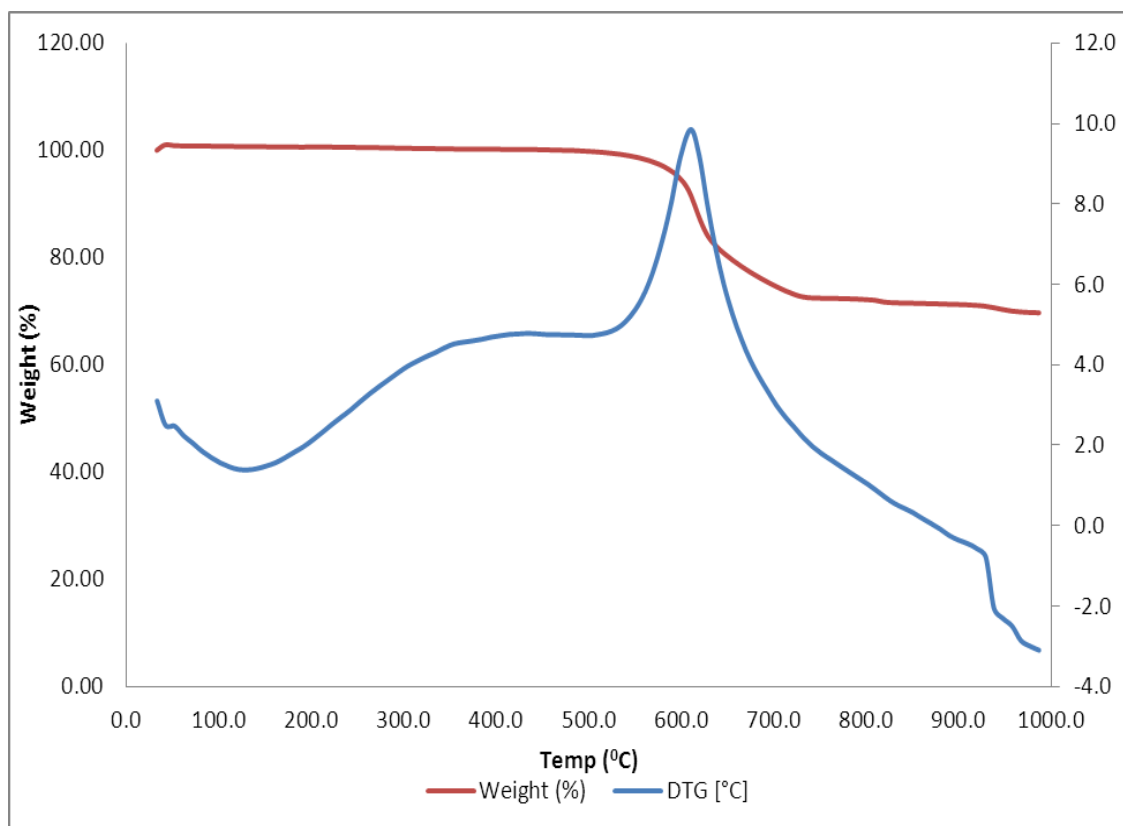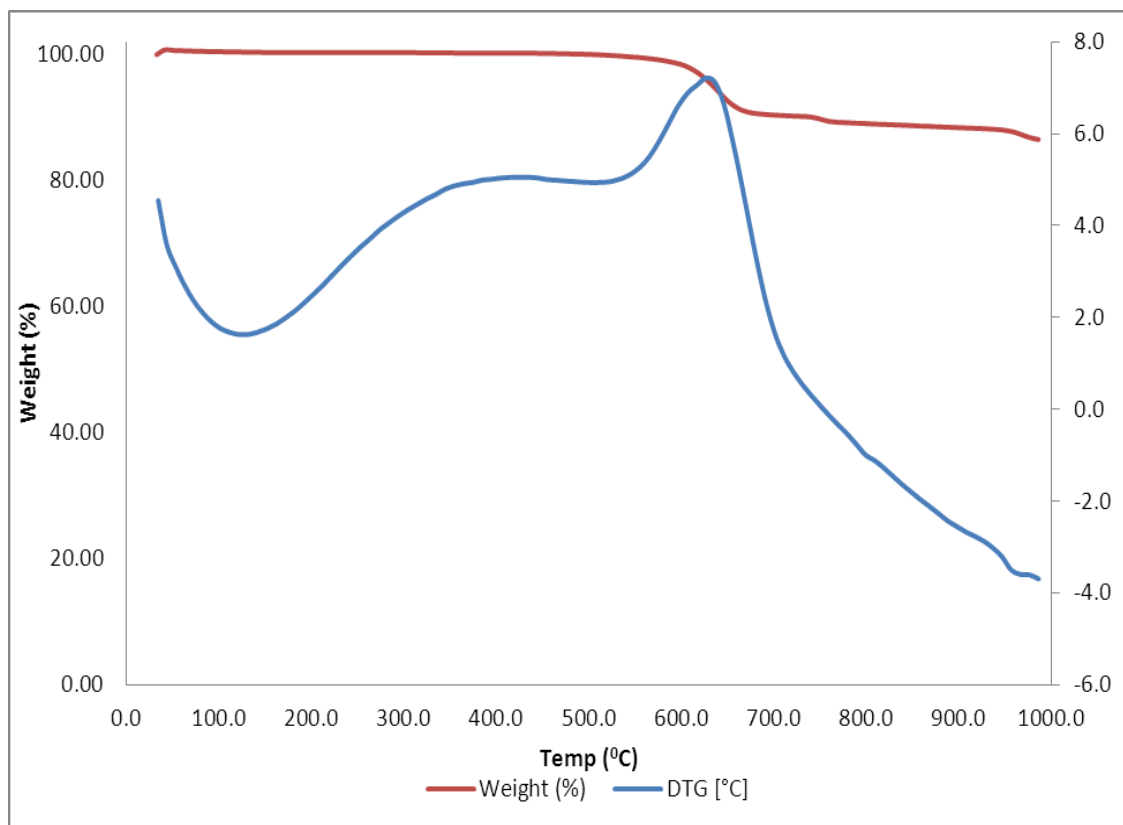
Figure 4.20: TGA / DTG curves of sample S8
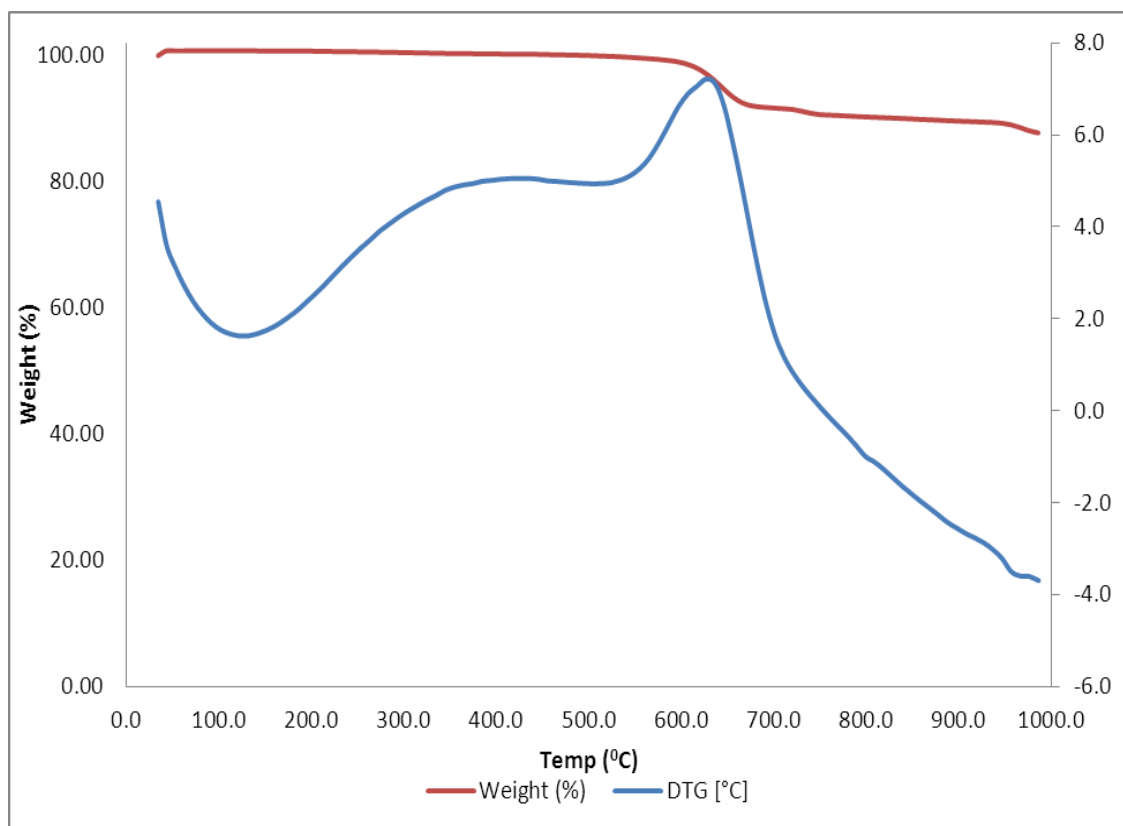
Figure 4.21: TGA / DTG curves of sample S9
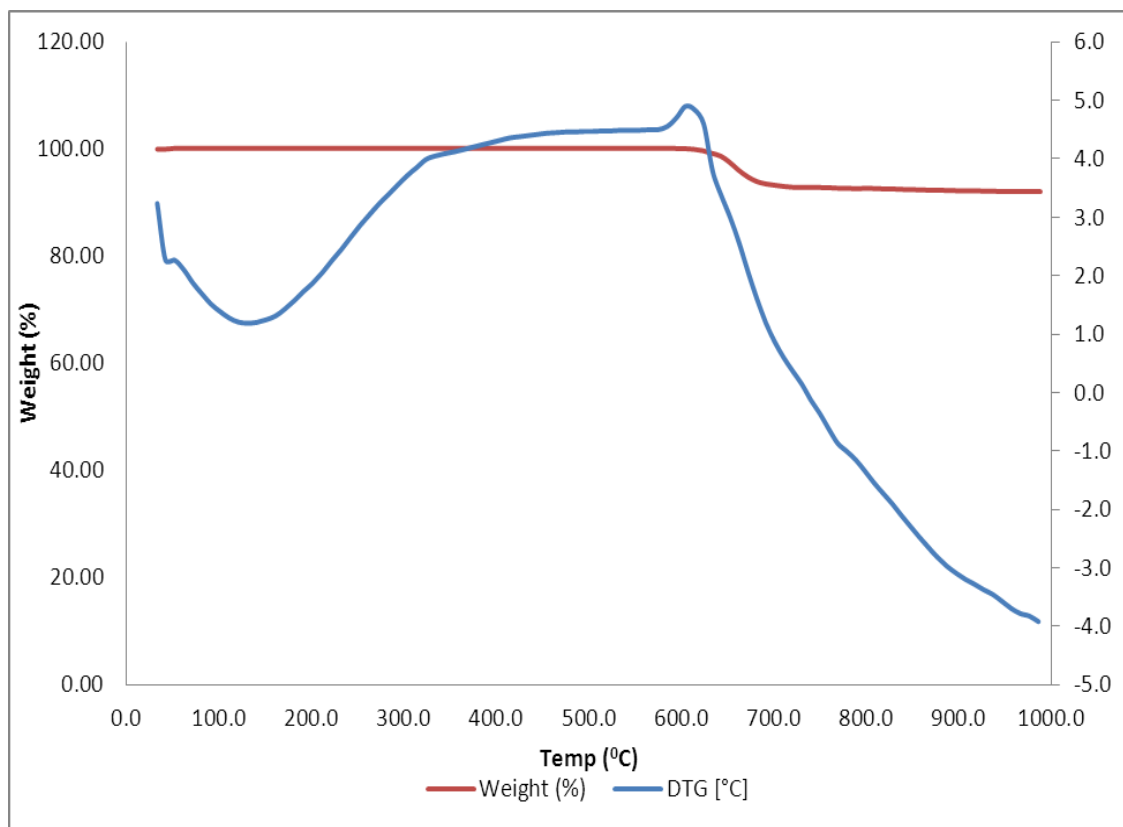
Figure 4.22: TGA / DTG curves of sample S10
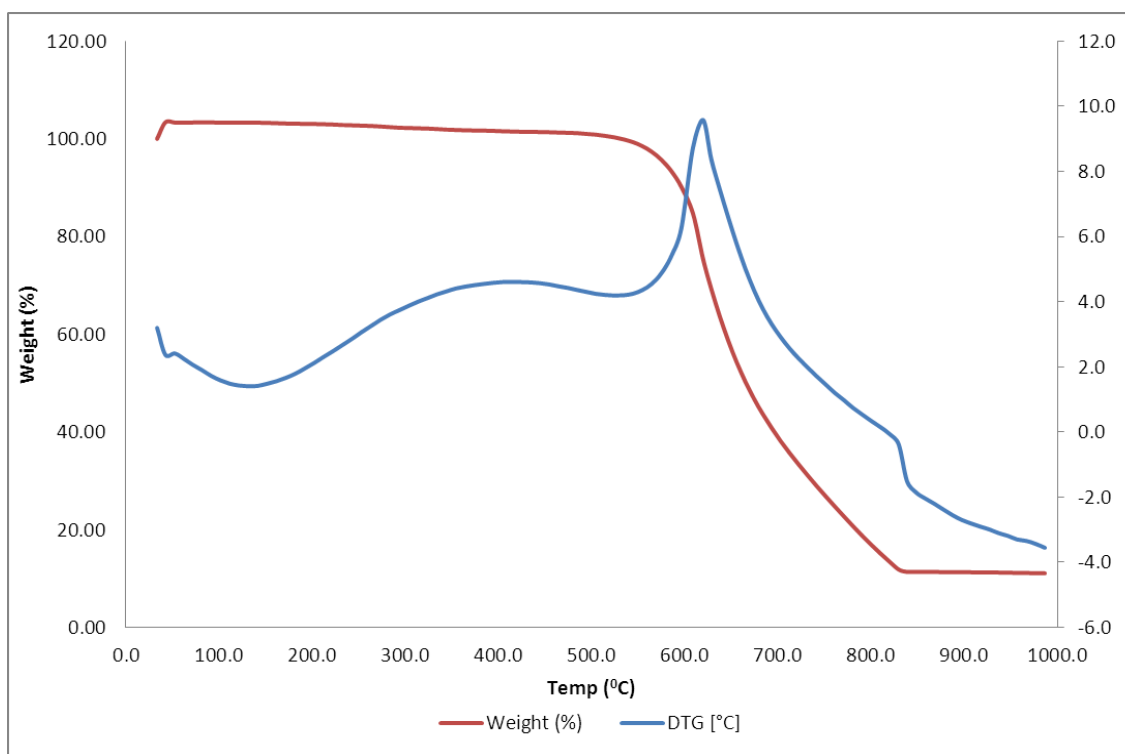
Figure 4.23: TGA / DTG curves of sample S11

Table 4.3: Percentage weight loss and specific temperature for all samples

Samples	Initial Weight Loss Temp. (^{o}C)	Weight Loss (%) (a)	Decom-position Temp. (^{o}C)	Weight Loss (%) (b)	Final Weight Temp. (^{o}C)	Final Weight Loss (%) (c)	Total Weight Loss (%) (a)+(b)+(c)
S1	42.2	1.46	484.3	18.03	645.0	25.73	45.22
S2	42.4	1.94	504.3	20.38	655.3	19.87	40.55
S3	42.0	1.44	505.7	20.32	655.9	9.75	31.51
S4	42.1	0.83	514.4	18.48	675.1	5.65	24.96
S5	43.6	1.69	525.0	16.60	701.6	3.57	21.86
S6	40.8	1.43	524.3	13.72	701.3	3.98	19.13
S7	42.3	1.41	524.4	11.43	700.9	3.68	16.52
S8	41.6	0.96	534.1	9.39	700.4	3.55	13.90
S9	42.9	0.91	533.9	8.13	700.6	3.59	12.63
S10	52	0.001	604.0	7.32	721.0	0.81	8.12
S11	42.4	3.48	534.2	88.05	829.6	0.78	92.31

CHAPTER FIVE

CONCLUSION AND FUTURE WORK

5.1 Conclusion

MnO_2 / MWCNT composite were synthesized and characterized via solid state technique in this research. The results from this study have proven that the old fashioned trituration process can be used to produce manganese dioxide (MnO_2) / multiwalled carbon nano tube (MWCNT) composites.

The FESEM / EDX / TEM studies of the composite have shown the addition of more MnO_2 into the composition ratio has increased the size of the composite due to the formation of the MnO_2 layer on the MWCNT. The diameters of the composite were ranging from 17 – 120 nm. The EDX results showed the content of MnO_2 was more than 72% wt with the lowest weight percent of MWCNT. The XRD studies shows the crystallite sizes of MnO_2 has increased from 60.71 to 90.71 nm, with increased MnO_2 ratio in the composite. The deposition of MnO_2 over MWCNT works as a shield to reduce the oxidation of MWCNT. This result is further supported by TGA studies, where increase in MnO_2 ratio has increased the thermal stability of the composite. The weight loss of the composite initially with 0.05 moles of MnO_2 was 45%, which later reduced to 12% with MnO_2 ratio of 0.45 moles in the composite composition.

In comparison to the constituent material, MWCNT, MnO_2 / MWCNT composite has a better thermal stability. MWCNT lost almost 92% of its weight after heating up to $950^{o}C$. However, in sample S9 with 0.45 mole of MnO_2 and 0.05 mole of MWCNT, the minimum weight lost was recorded at 12%. This shows the addition of MnO_2 has decreased the weight losses of the composite and thus increases its thermal stability.

5.2 Recommendation

Additional research to study the effects of using alternative solid state methods, such as ball mill, need to be carried out to understand the impact it causes to the MnO_2 / MWCNT composite, structurally and the effect of this structural change to the thermal stability of the composite. It is also recommended that further analysis to be made to understand the optical property as well as electrical characteristic of this composite under similar mole ratio composition, to find the optimum composition mixture for specific applications such as coatings for solar panels for optimum optical and thermal stability and for super capacitance ability.

REFERENCES

Ajayan *et el*. P.M., Schadler, L.S., Braun, P.V. (2003). Nano composite science and technology. *Wiley*.

Ajayan, P.M., Iijima S., and Ichihashi T. (1992). Growth Model for Carbon Nanotubes. *Physical Review Letters, 69*, 3100.

Bierdel, M., Buchholz S., Michele V., Mleczko L., Rudolf R., Voetz M., and Wolf A. (2007). *Phys. Stat. Sol., 244,* 3939-3943.

Baughman, R.H., Zakhidov, A.A., and De Heer, W.A., (2002), *Science,* pages 297, 787-792.

Chandra, R., Taneja, P., Ayuub, P., (1999). A simple method to synthesis single-crystalline manganese dioxide nanowires. *Nanostructural Materials, 4,* 505-512.

Daenen, M., de Fouw, R. D., Hamers B., Janssen P. G. A., Schouteden K., and Veld, M. A. J., (2003). The wondrous world of carbon nanotubes `A review of current carbon nanotube technologies'. Technische Universiteit Eindhoven, 1-96.

Dandan, Sang., Hongdong, Li., Shaoheng, Cheng., (2012). Growth and electron field emission of ZnO nanorods on diamond films", *Applied Surface Science*.

Devaraj, S. and Munichandraiah, N., (2007). Electrochemical Supercapacitor Studies of Nanostructured-MnO2 Synthesized by Microemulsion Method and the Effect of Annealing. *Journal of The Electrochemical Society, 154,* A80-A88.

Donald, R., Phule, P., (2003). *The Science of Engieering Materials, 4th edition.* University of Missouri – Rolla, Emeritus, University of Pittsburgh, 721-756.

Fan, Z., Chen, J., Wang, M., Cui, K., Zhou, H., Kuang, Y., (2006). *Preparation and characterization of manganese oxide/CNT composites as supercapacitive materials*. Diam Relat Mater,15, 1478–83.

Fan, Z., Chen, J. H., Zhang, B., Liu, B., Zhong, X. X., and Kuang, Y. F., (2008). *Diamond Relat. Mater., 17,* 1943.

Gaillot, AC., Lanson B., Drits, VA., (2005). *Chem Mater ,*17, 2959–75.

Guo, T., and Smalley R. E., (1995). Production of single-walled carbon nanotubes via laser vaporization technique." *Recent Advances in the Chemistry and Physics of Fullerenes and Related Materials,* 626-47.

Hibino, M., Kawaoka, H., Zhou, H., Honma, I., (2004). Rapid discharge performance of composite electrode of hydrated sodium manganese oxide and acetylene black. *Electrochim Acta ,49,* 5209–16.

Huang, Z.P., Xu, J.W., Ren, Z.F., Wang, J.H., Siegal, M.P., Provencio, P.N., (1998). Growth of large-scale well-aligned carbon nanotubes by plasma enhanced hot element chemical vapor deposition. *Appl. Phys. Lett.* 73, 3845–3847.

Huang, WJ., Chen, H., Zuo, JM., (2006). One-dimensional self-assembly of metallic Nano structures on single-walled carbon nanotube bundles, 2, 1418.

Iijima, S., (1991). *Nature,* 354, 56-58.

Jun, Yan., Zhuangjun, Fan., Tong, Wei., Jie, Cheng., Bo, Shao., Kai, Wang., Liping, Songs., Milin, Zhang., (2009). Carbon Nanotube / MnO_2 composites synthesized by microwave assisted method for supercapacitors with high power and energy densities. *Journal of Power Sources 194,* 1202 – 1207.

Journet, C., and Bernier, P., (1998). *Appl. Phys. A, 67*, 1-9.

Journet, C., Maser, W. K., Bernier, P., Loiseau A., delaChapelle M. L., Lefrant, S., Deniard, P., Lee, R., and Fischer, J. E. (1997). *Nature, 388,* 756-758.

Juan Xu., Yaomin, Zhao., Ling, Liu., Jie, Yang., Manming, Yan., Zhiyu, Jiang., (2006). High- performance supercapacitors of hydrous ruthenium oxide/mesoporous carbon composites*, 1-6*

Kawaoka, H., Hibino, M., Zhou, H., Honma, I., (2004). Sonochemical synthesis of amorphous manganese oxide coated on carbon and application to high power battery. *J Power Sources, 125,* 85–9.

Kilbride, B.E., Coleman J.N., Fraysse, J., Fournet, P., Cadek, M., Drury, A., Hutzler, S., Roth, S., Blau, W.J.,(2002), *Journal of Appl. Phys.2002*, 92(7), 4024-4030.

Kitiyanan, B., Alvarez, WE., Harwell, JH., Resasco, DE., (2000). Controlled production of single-wall carbon nanotubes by catalytic decomposition

of CO on bimetallic Co–Mo catalysts. *Chem Phys Lett , 317,* 497–503.

Lahi. E., Leahy R., Coleman N. J., and Blau W. J., (2006). *Carbon, 44,*1624-1652.

Lee, CY., Tsai, HM., Chuang, HJ., Li, SY., Lin, P., Tseng, TY., (2005). Characteristics and electrochemical performance of supercapacitors with manganese oxide- carbon nanotube nanocomposite electrodes. *J Electrochem Soc, 152,* A716–20.

Li, Zijiong., Wei, L., and Zhang, Y., (2008). *Appl. Surf. Sci., 254*, 5247-5251.

Li, J., Yang, Q. M., and Zhitomirskya, I.,(2008). *J. Power Sources, 185,* 1569.

Liang, C. L., Zhong K., Liu M., Jiang L., Liu S. K., Xing D. D., Li H. Y., Na Y., Zhao W. X., Tong Y. X., et al., (2010). *Nano-Micro Lett., 2,* 6.

Luo, Haiyang., Mingdeng Wei, Kemei Wei (2008). Formation of single-crystal γ-MnO2 nanowires at room temp. *Journal of Crystal Growth, 310*, 2738 – 2741.

Minghao, Sui., Sichu, Xing., Li, Sheng., Shuhang, Huang., Hongguang, Guo., (2012). Heterogeneous catalytic ozonation of ciprofloxacin in water with carbon nanotube supported manganese oxides as catalyst. *Journal of Hazardous Materials*, 227–228, 227–236.

Mingdeng, Wei., Yoshinari, Konishi., Haoshen, Zhou., Hideki, Sugihara., Hironori, Arakawa., (2005). Synthesis of single-crystal manganese dioxide nanowires by a soft chemical process. *Journal Nanotechnology,* 16, 245-249.

Nam, Ho-Seong., Yoon, Jae-Kook., Jang, Myoun Ko., Jong, Duk Kim., Electrochemicalcapacitors of flower-like and nanowire structured MnO$_2$ by a sonochemical method, Materials Chemistry and Physics, *Volume 123 Issue 1*, 1 September 2010, 331–336

Nikolaev, P., Bronikowski, M. J., Bradley, R. K., Rohmund, F., Colbert D. T., Smith, K. A., and Smalley, R. E.. (1999). *Chem. Phys. Lett., 313*, 91-97.

Pang, S.C., Chin, S.F., Ling, C.Y., (2012). Controlled Synthesis of Manganese Dioxide Nanostructures via a Facile Hydrothermal Route. *Journal of Nanomaterials Article ID 607870,* pages 7.

Pinero, Raymundo., E, Khomenko V, Frackowiak E, Beguin F.(2005)
Performance of manganese oxide/CNTs composites as electrodematerials for electrochemical capacitors. *J Electrochem Soc,152,* A229–35.

Pirlot, C., Williems, I., Fonseca, A., Nagy, J.B., Delhalle, J.,(2002). Preparation and characterization of carbon nano tube / polyacrylonitrile composites. *Advanced Engineering Materials*, Pirlot et el.

Piquero, T., Vincent, H., Vincent, C., Bouix J. (1995).
Influence of carbide coating on the oxidation behavior of carbon fibers. Journal of *Carbon, 33*, 455–467.

Pritchett, Ian., (2001). *The Building Conservation Directory*, "Wattle and Daub".

Poncharal, P. et al., *Science 283*, 1513 (1999).

Potter, R. and Rossman, G, (1979). Mineralogy of Manganese Dendrites and Coatings. *American Journal of Science, 35,* 243.

Ren, Z. F., Huang, Z. P., Xu, J. W., Wang, D. Z., Wen, J. G., and Wang, J. H..(1999). *Appl. Phys. Lett., 75*, 1086-1088.

Roch, A., Jost O., Schultrich B., and Beyer E., (2007). *Phys. Stat. Sol.*, *244*:3907-3910.

Qian, D., Wagner, G. J., Liu, W. K., Yu M.F., and Ruo, R. S., (2002). *Appl. Mech. Rev., 55,* 495-533.

Saito, Y., Nishikubo, K., Kawabata, K., and Matsumoto, T. J., (1996). *Appl. Phys., 80,* 3062-3067.

Sang, Bok Maa., Kyun, Young Ahn., Eun, Sung Lee., Ki, Hwan Oh., Kwang, Bum Kim., (2006). Synthesis and characterization of manganese dioxide spontaneously coated on carbon nanotubes. Department of Metallurgical Engineering, Yonsei University, 134 Shinchon-dong, Seodaemoon-gu, Seoul 120-749.

Subramanian, V., Zhu, H., Wei, B., (2006). Synthesis and electrochemical Characterizations of amorphous manganese oxide and single walled carbon nanotube composites as super capacitor electrode materials. *Electrochecommun, 8,* 827–32.

Thostenson, E. T., Renb, Z. F., and Choua, T. W., *Compos. Sci. Technol., 61:*1899-1912, 2001., 286:11-15, 2000.

Vikas Mittal, BASF SE, Polymer Research, Germany (2010). Polymer Nanotube Nano Composites, Synthesis Properties and Applications. *WILLEY, pg. 1 – 7, 45-47,* 345 – 350.

Wu, M., Snook, GA., Chen, GZ., Fray, DJ. (2004). Redox deposition of manganese oxide on graphite for supercapacitors. *Electrochem Commun ,6,* 499–504.

Xie, S., Li, W., Pan, Z., Chang, B., and Sun, L., (2000). Mater. Sci. Eng.

Yuan, Z.Y., Zhang, Z., Du, G., Ren, T.Z., & Su, B.L. (2003). A simple method to synthesise single-crystalline manganese oxide nanowires. *Journal Chemical Physics Letter, 378,* 349-353.

Wang, Y. H., Liu, H., Sun, X. L., and Zhitomirskya, I.,(2009). *Scr. Mater., 61,* 1079.

Wang, GX., Zhang, BL., Yu, ZL., Qu, MZ., (2005). Manganese oxide/MWNTs composite electrodes for supercapacitors. *Solid State Ionics, 176,* 69–74.

William, D. Calister,Jr., (1994). Materials Science and Engineering, An Introduction.*Wiley, 3rd Edition*, 514-538.

Xiangping, (2006). Zinc Oxide nanowires on carbon nanotubes. *Appl. Phys.Lett.*81, 2085.

Zhang, H., Cao, G. P., Wang, Z. Y., Yang, Y. S., Gu, Z. N.,(2008). *Nano Lett.,8,* 2664.

Zhao, D. D., Yang, Z., Kong, E. S. W., Xu, C. L., and Zhang, Y. F.,(2010). *J. Solid State Electrochem.*

Zhou, YK., He, BL., Zhang, FB., Li, HL., (2006). Hydrous manganese oxide/carbon nanotube composite electrodes for electrochemical capacitors. *J Soild State Electrochem 8,* 482–7.

Z. Shi, Y. Lian, F. H. Liao, X. Zhou, Z. Gu, Y. Zhang, and S. Iijima.(2000). *J. Phys. Chem. Solids, 61,* 1031-1036.

Internet References

http://www.centennialofflight.gov/essay/Evolution_of_Technology/composites/Tech40. htm (3.5.2012)

http://en.wikipedia.org/wiki/Nanocomposite (12.07.2012)

http://iopscience.iop.org/1402-4896/2010/T139/014008/:

http://www.nanoshel.com/nanoshel-catalog.php/Carbon%20Nano%20Tubes%20-%20Nanoshel/7

http://www.galleries.com/Pyrolusite (15.07.2012)

http://www.reade.com/Products/Nanowires/manganese_oxide_nanowire.html (18.11.11)

http://www.nano-ou.net/eduNanomaterials2.aspx

https://sites.google.com/site/cntcomposites/cost-and-production (22.08.2012)

http://webmineral.com/ (2005)

APPENDICES

A: Shows the Scherrer calculation for crystalline size of for γ-MnO$_2$ based on the highest peak at $2\theta = 28.50$º.

Sherrer Calculation \ Samples	S1	S2	S3	S4	S5	S6	S7	S8	S9	S10
2θ (degree)	28.5	28.5	28.5	28.5	28.5	28.5	28.5	28.5	28.5	28.5
θ (degree)	14.25	14.25	14.25	14.25	14.25	14.25	14.25	14.25	14.25	14.25
λ (nm)	0.15406	0.15406	0.15406	0.15406	0.15406	0.15406	0.15406	0.15406	0.15406	0.15406
I max	21211.65	24181.74	25034.07	25872.76	37542.57	37565.94	39096.23	58871.24	71324.46	57935.39
I max / 2	10605.83	12090.87	12517.04	12936.38	18771.29	18782.97	19548.12	29435.62	35662.23	28967.70
2B$_2$ @ 2θ (degree)	28.62	28.62	28.62	28.63	28.59	28.64	28.58	28.59	28.62	28.60
2B$_1$ @ 2θ (degree)	28.35	28.36	28.34	28.33	28.39	28.43	28.33	28.38	28.44	28.42
Δ β (rad) = 2B$_2$ - 2B$_1$	0.00471	0.00454	0.00489	0.00524	0.00349	0.00367	0.00436	0.00367	0.00314	0.00314
FWHM=β (rad) = Δ β (rad) / 2	0.00236	0.00227	0.00244	0.00262	0.00175	0.00183	0.00218	0.00183	0.00157	0.00157
Sherrer's Equation: t (nm) (thickness) = 0.9 λ / (β cos θ)	60.71	63.05	58.55	54.64	81.96	78.06	65.57	78.06	91.07	91.07

B: Shows the Scherrer calculation for crystallite size of for MWCNT based on the highest peak at 2θ of 25.8º.

| Sherrer Calculation \ Samples	S1	S2	S3	S4	S5	S6	S7	S8	S9	S11
2θ (degree)	25.8	25.8	25.8	25.8	25.8	25.8	25.8	25.8	25.8	25.8
θ (degree)	12.9	12.9	12.9	12.9	12.9	12.9	12.9	12.9	12.9	12.9
λ (nm)	0.15406	0.15406	0.15406	0.15406	0.15406	0.15406	0.15406	0.15406	0.15406	0.15406
I max	7200	4699	4350	3950	3826	3660	3878	4064	3732	28318.83
I max / 2	5475	4024.5	3800	3675	3613	3480	3714	3857	3616	16909.42
2B$_2$ @ 2θ (degree)	26.8	26.62	26.64	26.64	26.63	26.9	26.98	26.6	26.64	26.50
2B$_1$ @ 2θ (degree)	25.1	25.2	25.24	25.62	25.22	24.82	25.2	25.22	25.19	25.1
Δ β (rad) = 2B$_2$ - 2B$_1$	0.02967	0.02478	0.02443	0.01780	0.02461	0.03630	0.03107	0.02409	0.02531	0.02443
FWHM=β (rad) = Δ β (rad) / 2	0.01484	0.01239	0.01222	0.00890	0.01230	0.01815	0.01553	0.01204	0.01265	0.01222
Sherrer's Equation: t (nm) (thickness) = 0.9 λ / (β cos θ)	9.59	11.48	11.64	15.98	11.56	7.84	9.16	11.81	11.24	11.64

C: Results of EDX (next pages)

Microanalysis Report

Prepared for: *A.Vicneswaran*

Prepared by: *-*   *5/31/2012*

Sample - S1 (0.05 mole MnO_2 + 0.45 mole MWCNT)

c:\edax32\genesis\genmaps.spc 31-May-2012 17:12:39
LSecs : 17
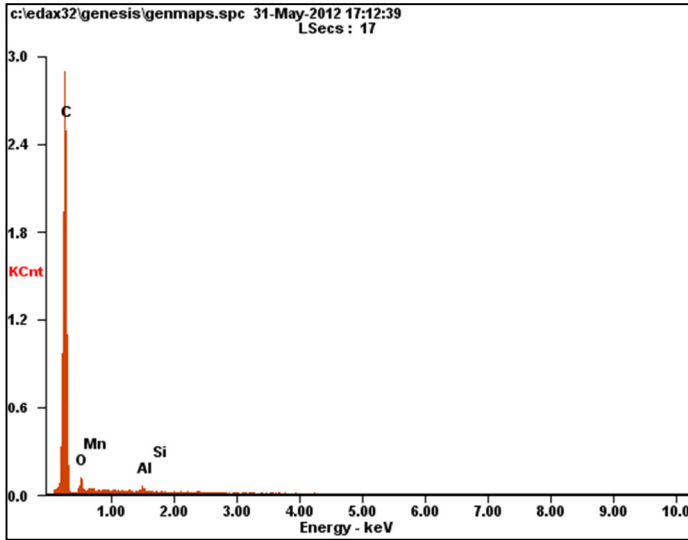
Element	Wt%	At%
CK	88.73	93.77
OK	05.08	04.03
MnL	02.83	00.65
AlK	01.57	00.74
SiK	01.79	00.81
Matrix	Correction	ZAF

Microanalysis Report

Prepared for: A.Vicneswaran

Prepared by: -   5/31/2012

EDAX **TSL**

advanced microanalysis solutions

AMETEK

Sample – S2 (0.10 mole MnO$_2$ + 0.40 mole MWCNT)

c:\edax32\genesis\genmaps.spc 31-May-2012 17:14:01
LSecs : 17
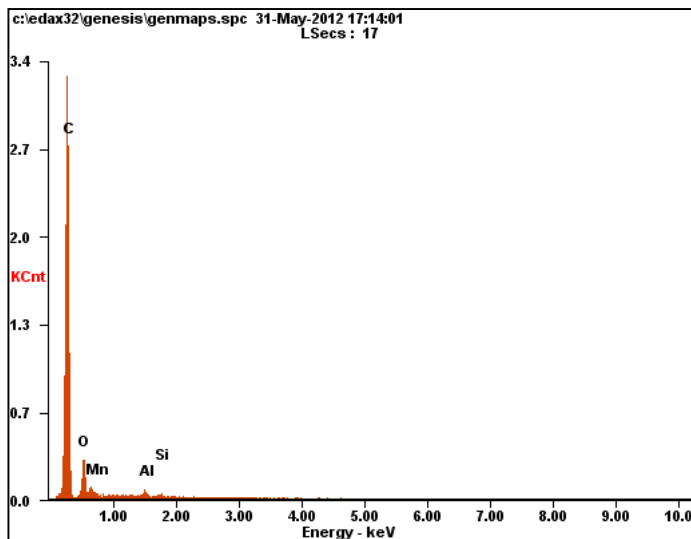
Element	Wt%	At%
CK	87.98	94.40
OK	03.83	03.09
MnL	05.70	01.34
AlK	02.10	01.00
SiK	00.38	00.18
Matrix	Correction	ZAF
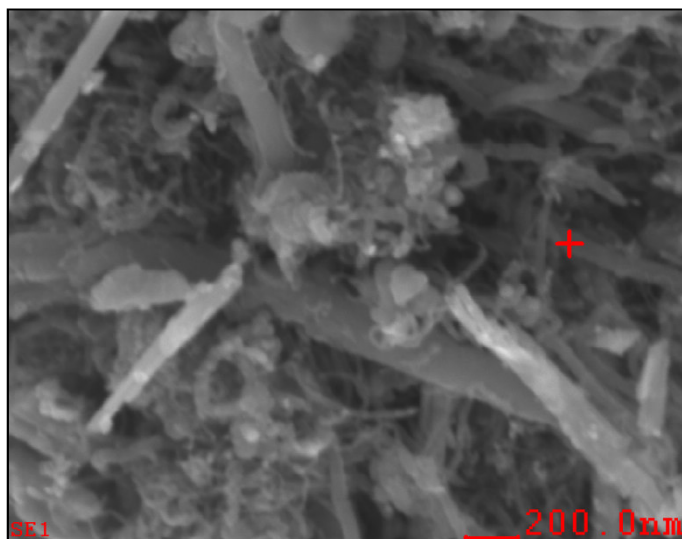
Microanalysis Report

Prepared for: *A.Vicneswaran*

Prepared by: *-*   *5/31/2012*

Sample – S3 (0.15 mole MnO$_2$ + 0.35 mole MWCNT)

c:\edax32\genesis\genmaps.spc 31-May-2012 17:36:58
LSecs : 17
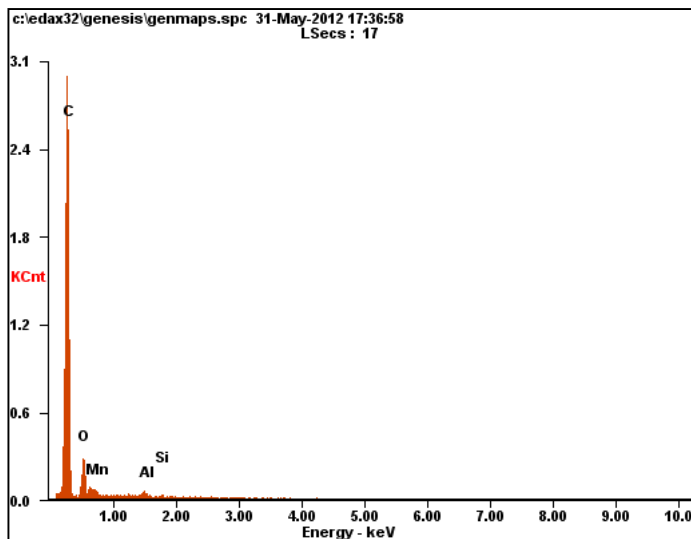
Element	Wt%	At%
CK	73.93	87.20
OK	08.28	07.33
MnL	14.39	03.71
AlK	02.27	01.19
SiK	01.14	00.57
Matrix	Correction	ZAF

Microanalysis Report

Prepared for: A.Vicneswaran

Prepared by: -   5/31/2012

EDAX TSL
advanced microanalysis solutions
AMETEK
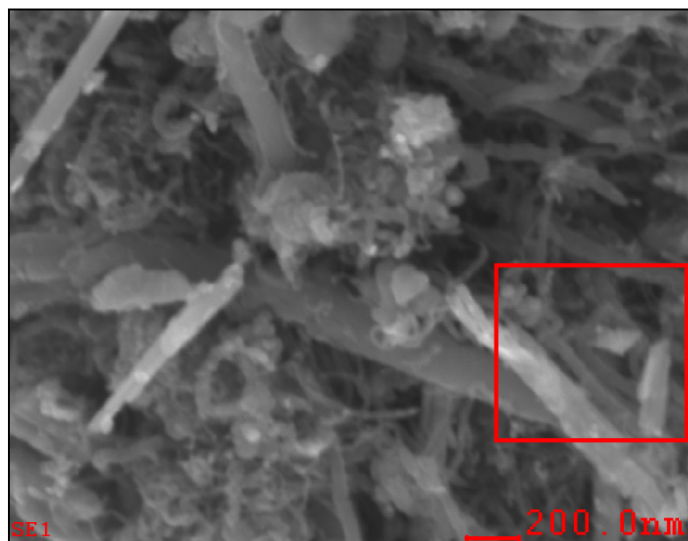
Sample – S4 (0.20 mole MnO₂ + 0.30 mole MWCNT)

c:\edax32\genesis\genmaps.spc 31-May-2012 17:57:22
LSecs : 12
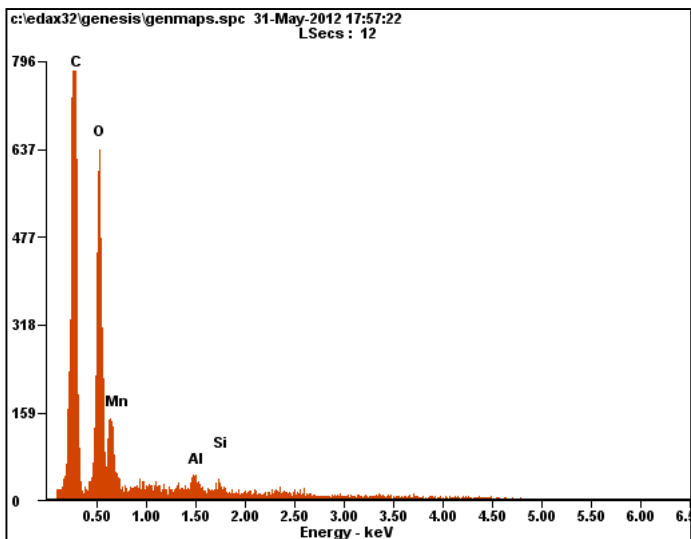
Element	Wt%	At%
CK	71.42	85.19
OK	09.81	08.78
MnL	14.45	03.77
AlK	02.51	01.33
SiK	01.81	00.92
Matrix	Correction	ZAF

Microanalysis Report

Prepared for: *A.Vicneswaran*

Prepared by: *-*   *6/1/2012*

EDAX TSL
advanced microanalysis solutions
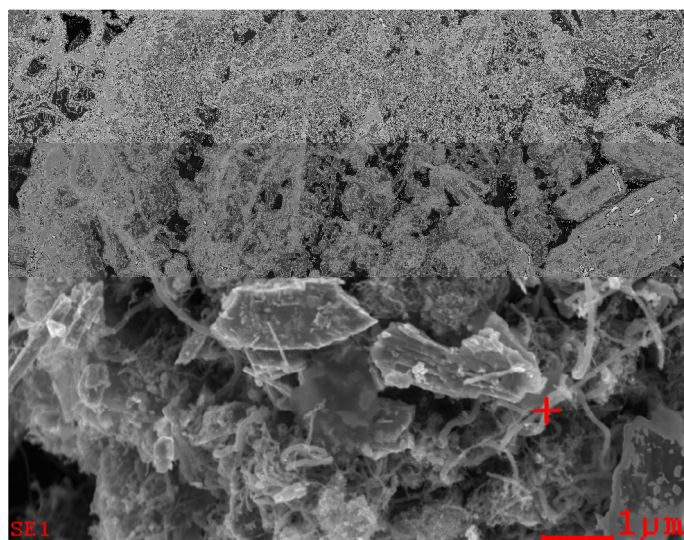AMETEK
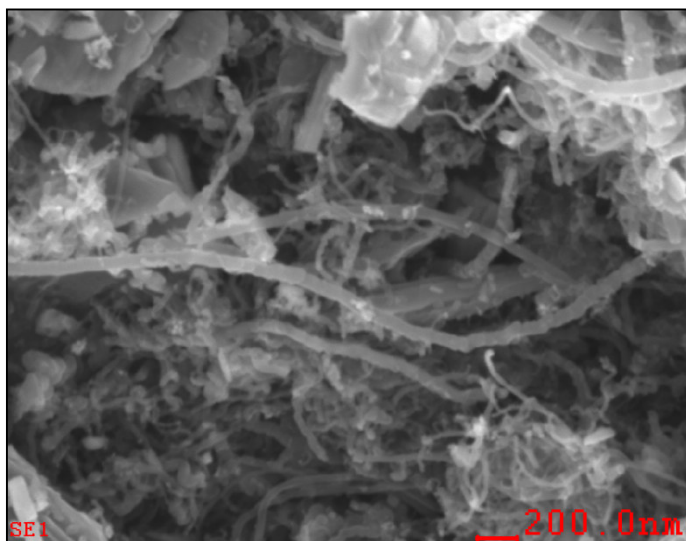
Sample – S5 (0.25 mole MnO₂ + 0.25 mole MWCNT)

c:\edax32\genesis\genmaps.spc 01-Jun-2012 18:08:26
LSecs : 5
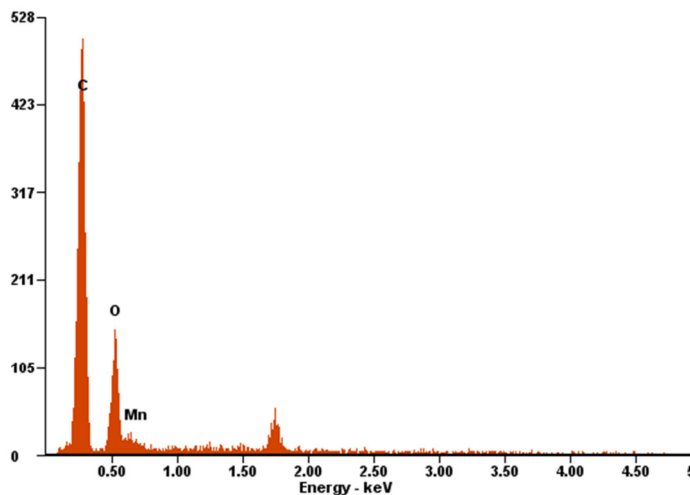
Element	Wt%	At%
CK	60.77	76.47
OK	19.02	17.97
MnL	20.21	05.56
Matrix	Correction	ZAF

Microanalysis Report

Prepared for: *A.Vicneswaran*

Prepared by: *-*   *6/1/2012*

Sample – S6 (0.30 mole MnO_2 + 0.20 mole MWCNT)

c:\edax32\genesis\genmaps.spc 01-Jun-2012 18:02:55
LSecs : 12
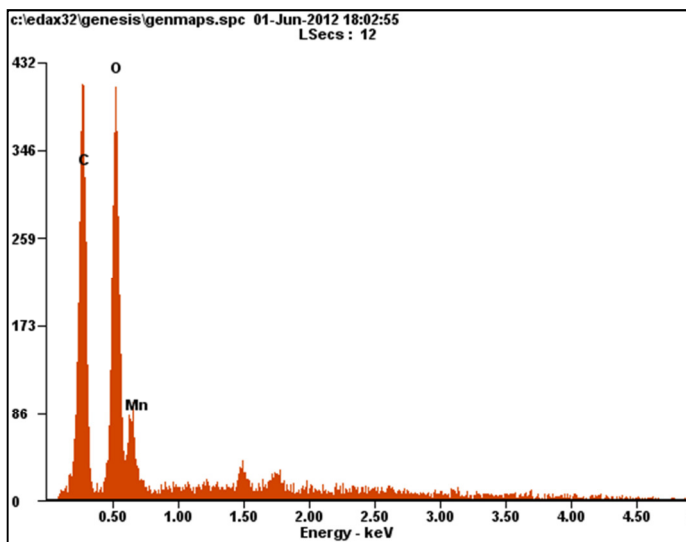
Element	Wt%	At%
CK	76.69	88.37
OK	09.39	08.13
MnL	13.92	03.51
Matrix	Correction	ZAF

Microanalysis Report

EDAX TSL
advanced microanalysis solutions
AMETEK®
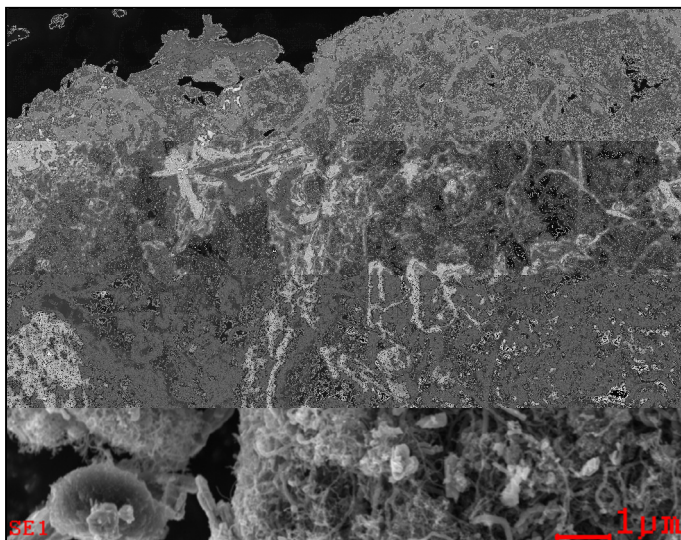
Sample – S7 (0.35 mole MnO$_2$ + 0.15 mole MWCNT)

c:\edax32\genesis\genmaps.spc 01-Jun-2012 17:39:34
LSecs : 5
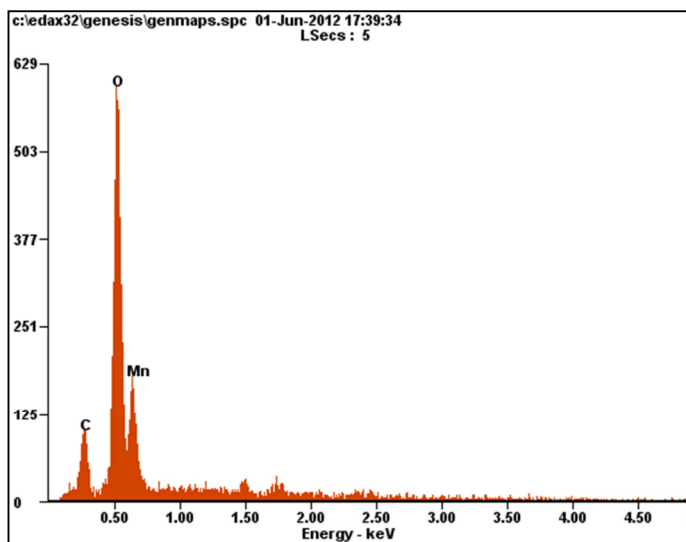
Element	Wt%	At%
CK	88.73	94.27
OK	05.51	04.40
MnL	05.75	01.34
Matrix	Correction	ZAF

Microanalysis Report

EDAX **TSL**
advanced microanalysis solutions
AMETEK
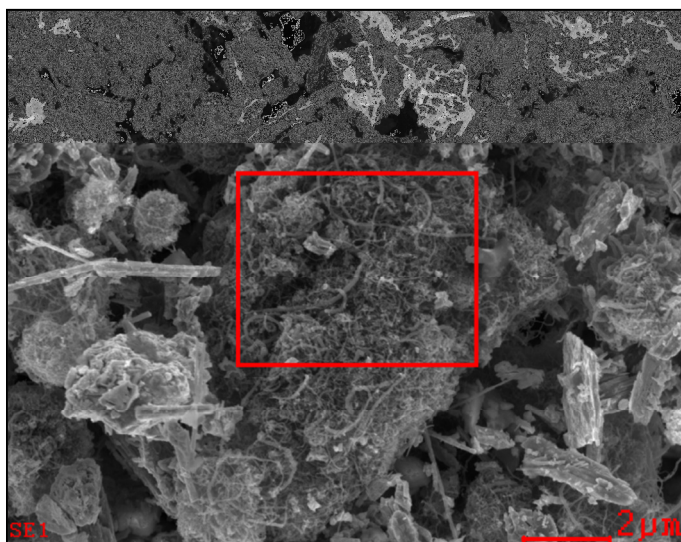
Prepared for: A.Vicneswaran

Prepared by: - *6/1/2012*

Sample – S8 (0.40 mole MnO$_2$ + 0.10 mole MWCNT)

c:\edax32\genesis\genmaps.spc 01-Jun-2012 17:22:38
LSecs : 17
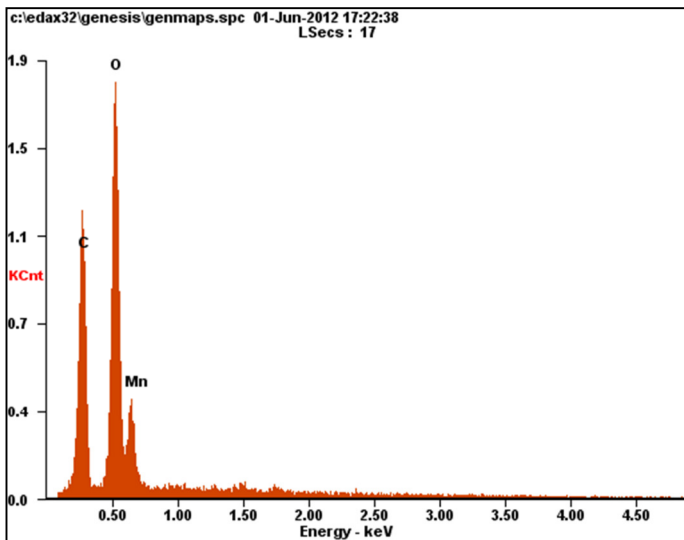
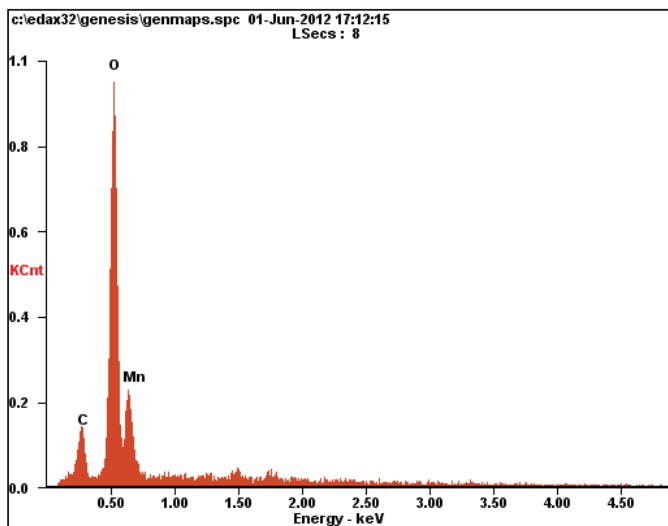| Element	Wt%	At%
CK	77.36	87.86
OK	10.78	09.19
MnL	11.86	02.95
Matrix	Correction	ZAF
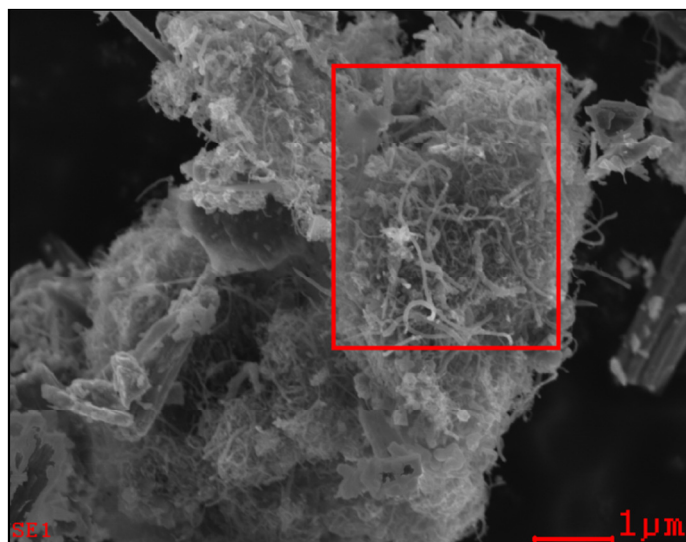
Microanalysis Report

Prepared for: A.Vicneswaran

Prepared by: Your Name Here 6/1/2012

Sample – S9 (0.45 mole MnO_2 + 0.05 mole MWCNT)

c:\edax32\genesis\genmaps.spc 01-Jun-2012 17:12:15
LSecs : 8

Element	Wt%	At%
CK	91.32	93.34
OK	08.68	06.66
Matrix	Correction	ZAF
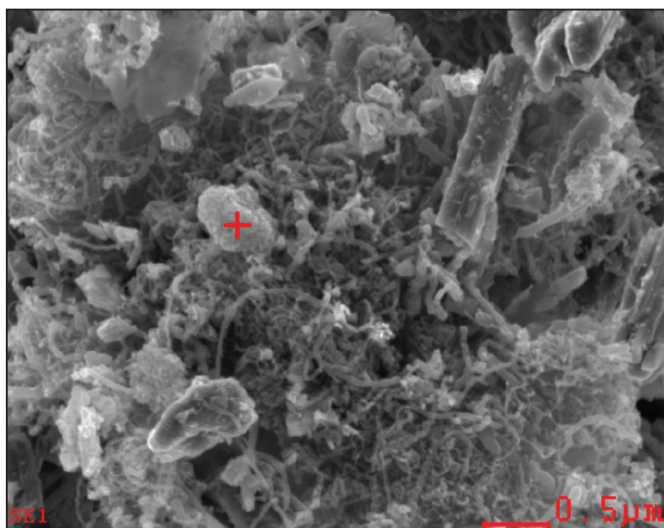
Microanalysis Report

Prepared for: A.Vicneswaran

Prepared by: - 5/31/2012

Sample – S10 (0.2 mole MnO₂)

c:\edax32\genesis\genmaps.spc 31-May-2012 12:49:28
LSecs : 9
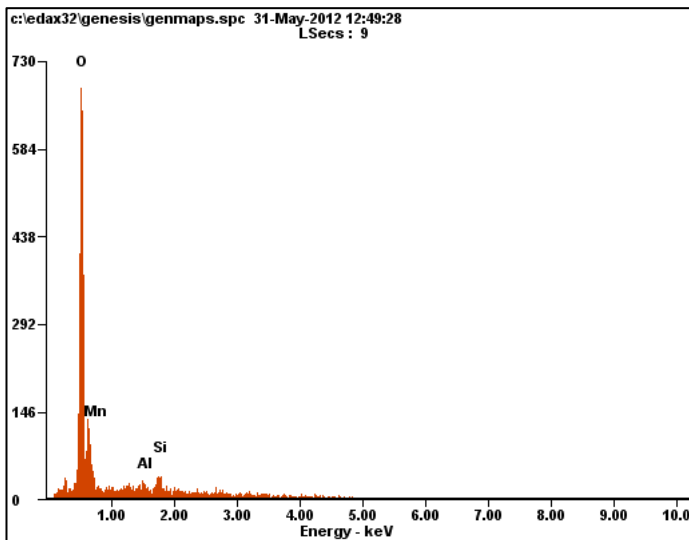
Element	Wt%	At%
OK	33.47	60.56
MnL	58.05	30.59
AlK	02.92	03.13
SiK	05.56	05.73
Matrix	Correction	ZAF
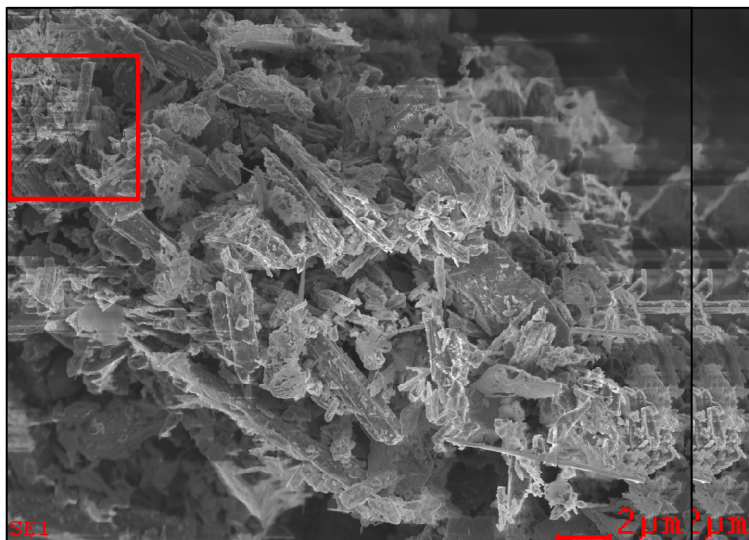
Microanalysis Report

Prepared for: *A.Vicneswaran*

Prepared by: *-*   *6/1/2012*

Sample – S11 (1 mole MWCNT)

c:\edax32\genesis\genmaps.spc 01-Jun-2012 16:51:48
LSecs : 15
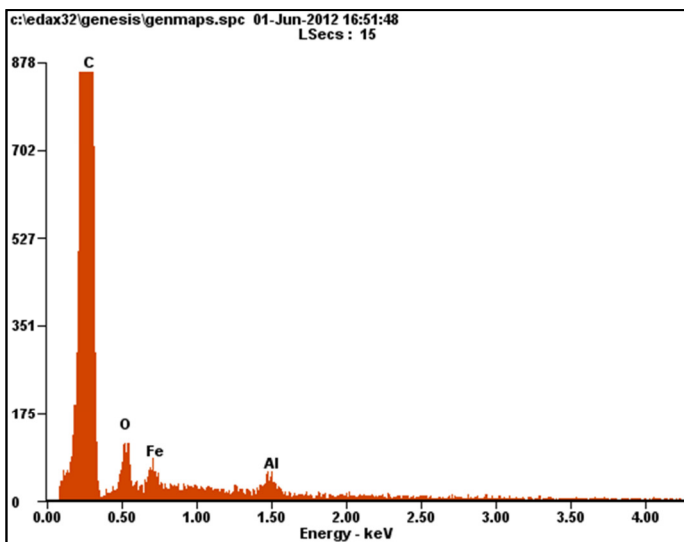
Element	Wt%	At%
CK	89.56	95.54
OK	02.67	02.14
FeL	05.57	01.28
AlK	02.21	01.05
Matrix	Correction	ZAF